Strain Localization and Failure Mechanics for Elastoplastic Damage Solids

J-Y. Wu
M. Cervera

Monograph CIMNE Nº-147, October 2014

Strain Localization and Failure Mechanics for Elastoplastic Damage Solids

J-Y. Wu
M. Cervera

Monograph CIMNE Nº-147, October 2014

International Center for Numerical Methods in Engineering
Gran Capitán s/n, 08034 Barcelona, Spain

INTERNATIONAL CENTER FOR NUMERICAL METHODS IN ENGINEERING
Edificio C1, Campus Norte UPC
Gran Capitán s/n
08034 Barcelona, Spain
www.cimne.com

First edition: October 2014

STRAIN LOCALIZATION AND FAILURE MECHANICS FOR ELASTOPLASTIC DAMAGE SOLIDS
Monograph CIMNE M147

ISBN: 978-84-943307-0-4
Depósito legal: B-23561-2014

Strain localization and failure mechanics for elastoplastic damage solids

Jian-Ying Wu

Department of Civil Engineering, South China University of Technology, 510041 Guangzhou, China.

Miguel Cervera

CIMNE, Technical University of Catalonia, Edificio C1, Campus Norte, Jordi Girona 1-3, 08034 Barcelona, Spain.

Abstract

This work investigates systematically strain localization and failure mechanics for elastoplastic damage solids. Two complementary methodologies, i.e., *traction-based discontinuities localized in an elastic solid* and *strain localization of a stress-based inelastic softening solid*, are addressed. In the former it is assumed *a priori* that the discontinuity (band) forms with a continuous stress field and along the known orientation. A traction-based failure criterion is introduced to characterize the discontinuity (band) and the orientation is determined from Mohr's maximization postulate. If the (apparent) displacement jumps are retained as independent variables, the strong/regularized discontinuity approaches follow, requiring constitutive models for both the bulk and discontinuity (band). Elimination of the displacement jumps at the material point level results in the embedded/smeared discontinuity approaches in which an overall inelastic constitutive model fulfilling the static constraint suffices. The second methodology is then adopted to check whether the assumed strain localization can occur and identify its consequences on the resulting approaches. The kinematic constraint guaranteeing stress boundedness/continuity upon strain localization is established for general inelastic softening solids. Application to a unified elastoplastic damage model naturally yields all the ingredients of a localized model for the discontinuity (band), justifying the first methodology. Two dual but not necessarily equivalent approaches, i.e., the traction-based elastoplastic damage model and the stress-based projected discontinuity model, are identified. The former is equivalent to the embedded/smeared discontinuity approaches, whereas in the later the discontinuity orientation and associated failure criterion, not given *a priori*, are determined consistently from the kinematic constraint. The *bi-directional* connections and equivalence conditions between the traction- and stress-based approaches are classified. Closed-form 2D results under plane stress condition are also given, with the classical Rankine, Mohr-Coulomb, von Mises and Drucker-Prager criteria analyzed as the illustrative examples. A generic failure criterion of either elliptic, parabolic or hyperbolic type, is then considered in a unified manner, resulting in many failure criteria frequently employed in practice.

Keywords:

Strain localization; localized failure; constitutive behavior; discontinuities; fracture; plasticity; damage.

October 14, 2014

1. Introduction

Overall responses of inelastic softening solids are characterized by strain localization, i.e. a manifestation of concentration of micro-structural defects. Depending on the material interested, the phenomena resulting from strain localization may be diverse: dislocations of order of microns in crystal metals, cracks of order of millimeters in concrete, and shear bands of order ranging from millimeters to kilometers in granular and geological problems. From the structural point of view these localization band may be regarded as a fracture surface of small or even negligible width compared to the length scale of the structure. Structural collapse is often induced by formation of such localization bands. Therefore, it is of utmost significance to evaluate (residual) structural safety once strain localization occurs, and to prevent potential catastrophic collapse caused by localized failure. However, despite the recent progresses made, the modeling of strain localization and subsequent structural collapse still remains a challenging issue.

Strain localization inevitably induces strain/displacement discontinuities, hindering the applicability of classical continuum mechanics. With respect to the strategies for the approximation of such discontinuities and resulting consequences on material or structural responses, different approaches have been proposed ever since the pioneering work of Ngo and Scordelis [35] and Rashid [50]. Generally speaking, existing approaches can be classified into the nonlinear fracture mechanics based discontinuous models or the generalized continuum mechanics based continuous models. In the computational context, they correspond to the discrete and smeared discontinuity methods, respectively.

In the discontinuous (discrete) approach strain/displacement jumps are explicitly accounted for by embedding the discontinuities into a solid matrix along preferred orientations. It is generally assumed that energy dissipation mechanisms are localized into the discontinuities while the bulk remains elastic. The traction continuity condition is imposed between them. The overall inelastic behavior is of anisotropy by construction. To characterize the dissipative behavior lumped in the discontinuities, vectorial traction-based cohesive models furnished with the fracture energy are introduced. Generally, displacement discontinuities are regarded as zero-width failure surfaces characterized by tractions vs. displacement jumps [3, 4, 17, 22]. Alternatively, strain discontinuities across the localized band with a finite width can be represented in terms of tractions vs. inelastic deformations (i.e., apparent displacement jumps normalized with respect to the bandwidth) [9, 10]. Depending on the recoverable/irreversible properties of the discontinuities, traction-based cohesive models of either plastic [7, 62, 66], damage [1, 2, 24] or combined plastic-damage [67, 70] type can be established.

Contrariwise, the continuous approach relies on the introduction of a generalized continuum, so that stress-based constitutive models with regularized softening regime can be used. In this approach, the strain/displacement discontinuities are regularized (smeared) so that the classical concepts of (average) stress and strain still apply. It is no longer necessary to make distinction between the elastic bulk and the inelastic localization band. But rather, the overall nonlinear behavior of the weakened medium is described by generalized constitutive laws in terms of stress vs. strain tensors equipped with softening internal variables. In this way, plasticity and damage mechanics or their combination [15, 25] can be employed to develop appropriate inelastic constitutive laws. Induced anisotropy can be considered

either theoretically [19, 31, 70] or in the computational context [12, 13]. Furthermore, to guarantee objectivity of the energy dissipated during the fracture process, the softening regime has to be regularized with respect to the length scale of localization band. The fracture energy – a material property measuring the dissipation per fracture surface, and an appropriately identified localization band width [5, 38], are fundamental ingredients for this purpose.

In the traction-based approached for the modeling of localized failure in solids, a crucial step is to determine the discontinuity orientation. This is a non-trivial goal for a new or propagating discontinuity whose orientation is not pre-defined or known *a priori*. To this end, *ad hoc* strategies have to be introduced, usually in an heuristic manner. For instance, the maximum tensile stress (i.e., Rankine) criterion is often adopted for mode I failure in quasi-brittle materials. For more general cases, selecting the discontinuity orientation according to some makeshift condition and fixing it afterwards becomes a superimposed condition on the material behavior. Fortunately, the occurrence of necessary requisites for a certain type of failure to be initiated during the whole deformation process in inelastic solids provides useful information. In this aspect, the pioneering works by Hill [20, 21], Thomas [64] and Rice [51, 57] have been widely adopted in the literature. The necessary conditions for discontinuous bifurcation and strain localization of elastoplastic materials were identified and formulations for the orientation of shear bands were obtained; see [58] and the references therein. Discontinuous bifurcation analysis, based on the assumption of linear comparison solid (inelastic loading state both inside and outside the localization band) and the traction continuity condition, has now become the standard tool to analyze propagation of strain or weak discontinuities.

For strong discontinuities in solids with strain softening regimes, there is no consensus for the determination of the discontinuity orientation. For instance, Simó et al. [61] and Oliver [39] suggested using the discontinuous bifurcation condition with perfect (null) softening/hardening modulus to determine the discontinuity orientation. This necessary discontinuous bifurcation condition in general does not guarantee the occurrence of strong discontinuities [40, 41]. To remedy this problem, a variable band width model was proposed in the last reference, so that weak discontinuities can evolve smoothly to a strong one at a later stage. However, for strain localization to occur in a softening solid and develop eventually into a fully softened discontinuity at the final stage of the deformation process, material points inside the discontinuity (band) undergo inelastic loading while those outside it unload elastically. That is, the actual loading state is not consistent with the assumption of linear comparison solids. Therefore, the limit decohesion cannot be guaranteed in general cases and stress locking occurs due to the mis-prediction of the discontinuity orientation. Furthermore, due to the singular strain field associated with displacement discontinuities, traction continuity alone is not sufficient to guarantee physically meaningful results, but rather, stress boundedness also has to be invoked [39–42, 61]. Noticing this fact, Cervera et al. [11] recently used the kinematic compatibility condition resulting from stress boundedness to determine the discontinuity orientation, so that the stress locking-free property can be guaranteed for a fully softening discontinuity. The analytical results, obtained for von Mises (J_2) plastic materials in the cases of plane stress and plane strain, were validated by numerical simulations.

Failure criterion is another indispensable ingredient for the modeling of localized failure in solids. It defines an elastic domain outside which nonlinear energy dissipation mechanisms are active. In discontinuous approaches a

traction-based failure criterion is in general adopted. For mode-I failure a trivial Rankine criterion can be employed. For mixed mode failure, the simple linear Mohr-Coulomb criterion is in general insufficient and more complex function has to be introduced, usually in an *ad hoc* manner. For instance, either elliptical [6, 24, 49, 70], parabolic [33, 36] or hyperbolic [7, 14, 34, 66] function has been postulated in the literature to describe mixed-mode failure in quasi-brittle materials. However, the involved parameters are essentially mesoscopical entities hard to be determined from rather limited experimental tests. This shortcoming restrains heavily the application of traction-based discontinuous approaches. On the other hand, situations are totally different for the continuous approaches. Large quantities of stress-based failure criteria have been suggested based on triaxial test data, especially for concrete-like quasi-brittler materials [15].

Traction-based discontinuity methods and stress-based material models with regularized softening regime both have been widely adopted for the modeling of localized failure in solids, though they are motivated from different methodologies and usually regarded as unconnected ones. It would be of great significance to establish a solid theoretical connection between results obtained from strain localization analysis of stress-based inelastic materials and from traction-based discontinuities localized into the elastic matrix. Such a correspondence will serve as a guidance how to select an appropriate approach when modeling localized failure in solids. Furthermore, it will also bridge the gap in identifying those mesoscopic parameters involved in the traction-based failure criterion from the easily obtained macroscopic properties of materials. In the literature, some attempts have been made to link them each other. For instance, Oliver and coworkers [40–44] derived the traction-based discontinuity models by projecting inelastic stress-based constitutive laws onto the discontinuity orientation. They managed deriving in closed-form the traction-based failure criterion for the isotropic damage model in total form [42–44]. Except for the Rankine and plane strain von Mises criteria [40, 41], stress-based plastic and plastic-damage models with general failure criterion have not been sufficiently accounted for. More importantly, the discontinuity orientation is determined through the discontinuous bifurcation condition. Accordingly, the resulting traction-based discontinuity model is in general inconsistent with the original stress-based counterpart and some mismatches are observed in the discontinuity kinematics [44, 45].

Recent investigations [68, 69] show that upon strain localization the stress field not only is bounded, but also is continuous, providing only the discontinuity modes caused by relative rigid body motions (translations and rotations) are considered [67]. Satisfaction of such a stress boundedness/continuity condition upon strain localization not only allows the formation of a fully softened discontinuity, but also establishes a bridge connecting the stress- and traction-based approaches motivated from rather different viewpoints. This work is to make further contributions to the above topics. Two complementary methodologies, i.e., *traction-based discontinuities localized in an elastic solid* and *strain localization of a stress-based inelastic solid*, are presented. Both strong and regularized discontinuities are considered. Regarding the strategies dealing with the orientation and failure criterion of the discontinuity, the connections and in particularly, the equivalence conditions, between traction- and stress-based approaches are investigated systematically. Compared to the existing literature, the theoretical connections are *bi-directional*, making it possible to bridge the gaps between the stress- and traction-base approaches. For instance, the proposed strain localization approach directly

motivates the necessary modifications to be made to the stress-based failure criterion, so that strain localization can occur under some unfavorable stress states while maintaining its equivalence to the corresponding traction-based counterpart.

This paper is organized as follows. After this introduction, the kinematics and governing equations of localized failure in solids are briefly presented in Section 2. Within the first methodology of discontinuities localized in an elastic solid, several traction-based approaches are discussed in Section 3. To justify the first methodology, an alternative one, i.e., strain localization of a stress-based inelastic solid, is then considered in Section 4. The kinematic constraint guaranteeing the stress boundedness/continuity condition is derived for general inelastic softening solids and applied to a unified elastoplastic damage model. Two dual (formally identical) but not necessarily equivalent approaches, i.e., the traction-based elastoplastic damage model and the stress-based projected discontinuity model, are identified. Section 5 addresses the *bi-directional* connections, in particular, the equivalence conditions, between the aforementioned traction- and stress-based approaches. In Section 6 closed-form results in plane stress condition are given, and the classical Rankine, Mohr-Coulomb, von Mises (J_2) and Drucker-Prager failure criteria are analyzed as prototype examples. Section 7 addresses the application to a generic stress-based failure criterion from which many traction-based counterparts widely employed in practice are recovered as the particular cases. Some relevant conclusions are drawn in Section 8. For the sake of completeness, two appendices are also attached to close this paper.

Notation. Compact tensor notation is used in this paper as far as possible. As a general rule, scalars are denoted by italic light-face Greek or Latin letters (e.g. a or λ); vectors and second-order tensors are signified by italic boldface minuscule and majuscule letters like $\boldsymbol{a}$ and $\boldsymbol{A}$, respectively. Fourth-order tensors are identified by blackboard-bold majuscule characters (e.g. $\mathbb{A}$). Symbols $\boldsymbol{I}$ and $\mathbb{I}$ represent the second-order and symmetric fourth-order identity tensors, respectively. Superscripts '$^{\mathrm{T}}$' and '$^{\mathrm{sym}}$' indicate the transposition and symmetrization operations, respectively. The inner products with single and double contractions are denoted by '$\cdot$' and ':', respectively. The dyadic product '$\otimes$' and the symmetrized Kronecker product $\overline{\otimes}$ are defined as

$$\big(\boldsymbol{A}\otimes\boldsymbol{B}\big)_{ijkl}=A_{ij}B_{kl},\qquad \big(\boldsymbol{A}\,\overline{\otimes}\,\boldsymbol{B}\big)_{ijkl}=\frac{1}{2}\big(A_{ik}B_{jl}+A_{il}B_{jk}\big)$$

2. General formulation of localized failure in solids

Let us consider the domain $\Omega\subset\mathbb{R}^{n_{\mathrm{dim}}}$ ($n_{\mathrm{dim}}=1,2,3$) shown in Fig. 1. It is occupied by a solid with reference position vector $\boldsymbol{x}\in\mathbb{R}^{n_{\mathrm{dim}}}$. The boundary is denoted by $\Gamma\subset\mathbb{R}^{n_{\mathrm{dim}}-1}$, with an external unit normal vector $\boldsymbol{n}^*$. Deformations of the solid are characterized by the displacement field $\boldsymbol{u}:\Omega\to\mathbb{R}^{n_{\mathrm{dim}}}$ and the infinitesimal strain field $\boldsymbol{\epsilon}:=\nabla^{\mathrm{sym}}\boldsymbol{u}$, with $\nabla(\cdot)$ being the spatial gradient operator. The solid is subjected to a distributed body force $\boldsymbol{b}^*:\Omega\to\mathbb{R}^{n_{\mathrm{dim}}}$ per unit volume. Surface tractions $\boldsymbol{t}^*:\Gamma_t\to\mathbb{R}^{n_{\mathrm{dim}}}$ and displacements $\boldsymbol{u}^*:\Gamma_u\to\mathbb{R}^{n_{\mathrm{dim}}}$ are imposed on the disjoint and complementary parts $\Gamma_t\subset\Gamma$ and $\Gamma_u\subset\Gamma$ of the boundary Γ, respectively.

At the early stage of the deformation process, standard compatibility relations of a continuum medium apply. That is, both the displacement and strain fields are continuous and regular (bounded). Upon satisfaction of a specific

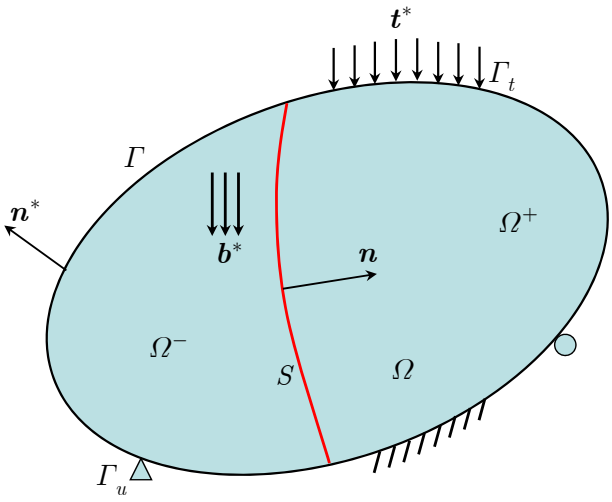

Figure 1: Problem setting in an elastic solid medium with an internal discontinuity

criterion, strain localization occurs, inevitably inducing strain/displacement jumps. To approximate these jumps, a strong discontinuity or a regularized one may be introduced. In either case, the standard kinematics no longer applies and is replaced by Maxwell's compatibility condition.

2.1. Kinematics of discontinuities

Displacement jumps can be described by a strong discontinuity. As depicted in Fig. 2(a), the strong discontinuity $\mathcal{S}$ splits the solid Ω into two parts Ω^+ and Ω^-, located "ahead of" and "behind" $\mathcal{S}$, respectively, in such a way that $\Omega^+ \cup \Omega^- \cup \mathcal{S} = \Omega$. The discontinuity orientation characterized by a unit normal vector $\boldsymbol{n}$, pointing from Ω^- to Ω^+ and fixed along time (i.e., $\dot{\boldsymbol{n}} = \boldsymbol{0}$); see Appendix A for the details. The strong discontinuity $\mathcal{S}$ causes displacement jumps $\boldsymbol{w} := \boldsymbol{u}(\boldsymbol{x} \in \Omega^+ \cap \mathcal{S}) - \boldsymbol{u}(\boldsymbol{x} \in \Omega^- \cap \mathcal{S})$ across it. In this case, the displacement field $\boldsymbol{u}(\boldsymbol{x})$ is expressed as

$$\boldsymbol{u}(\boldsymbol{x}) = \bar{\boldsymbol{u}}(\boldsymbol{x}) + \mathscr{H}_{\mathcal{S}}(\boldsymbol{x})\, \hat{\boldsymbol{u}}(\boldsymbol{x}) \tag{2.1a}$$

so that the strain field $\boldsymbol{\epsilon}(\boldsymbol{x})$ is given by

$$\boldsymbol{\epsilon}(\boldsymbol{x}) := \nabla^{\text{sym}}\boldsymbol{u}(\boldsymbol{x}) = \nabla^{\text{sym}}\bar{\boldsymbol{u}}(\boldsymbol{x}) + \big(\boldsymbol{w} \otimes \boldsymbol{n}\big)^{\text{sym}}\, \delta_{\mathcal{S}}(\boldsymbol{x}) \tag{2.1b}$$

where $\bar{\boldsymbol{u}}(\boldsymbol{x})$ denotes the continuous part of the displacement field; $\mathscr{H}_{\mathcal{S}}(\boldsymbol{x})$ is Heaviside function defined at the interface $\mathcal{S}$, i.e., $\mathscr{H}_{\mathcal{S}}(\boldsymbol{x}) = 0$ if $\boldsymbol{x} \in \Omega^- \cup \mathcal{S}$ and $\mathscr{H}_{\mathcal{S}}(\boldsymbol{x}) = 1$ otherwise; $\delta_{\mathcal{S}}(\boldsymbol{x})$ denotes Dirac-delta at the discontinuity $\mathcal{S}$. By construction, the relative displacement field $\hat{\boldsymbol{u}}(\boldsymbol{x}) : \Omega \to \mathbb{R}^{n_{\text{dim}}}$, satisfying the property $\hat{\boldsymbol{u}}(\boldsymbol{x} \in \mathcal{S}) = \boldsymbol{w}$, describes how the part Ω^+ moves as a relative rigid body (e.g. translations and rotations) with respect to the other one Ω^-; see Wu [67]. Accordingly, though the relative displacement field $\hat{\boldsymbol{u}}(\boldsymbol{x})$ itself is not necessarily constant, its contribution to the strain field vanishes, i.e., $\nabla^{\text{sym}}\hat{\boldsymbol{u}}(\boldsymbol{x}) = \boldsymbol{0}$. If only relative rigid body translations are considered, the relative displacement field $\hat{\boldsymbol{u}}(\boldsymbol{x})$ is constant and coincident with the displacement jump $\boldsymbol{w}$.

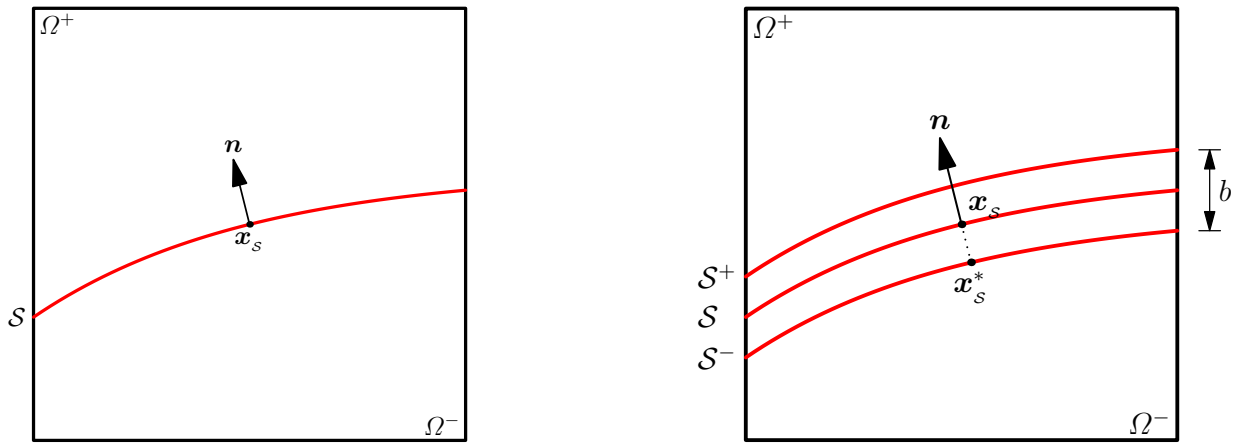

(a) Strong discontinuity

(b) Regularized discontinuity

Figure 2: Strong and regularized discontinuities in a solid

The unbounded strain field (2.1b) resulting from the discontinuous displacement field (2.1a) can be regularized over a discontinuity band $\mathcal{B}$ of finite width b. Here, the width b is not a physical length but a regularization parameter which can be made as small as desired. As shown in Fig. 2(b), the regularized discontinuity (or discontinuity band) $\mathcal{B}$ is delimited by two surfaces $\mathcal{S}^+$ and $\mathcal{S}^-$ parallel to the discontinuity $\mathcal{S}$, i.e., $\Omega^+ \cup \Omega^- \cup \mathcal{B} = \Omega$. In this case, the displacement field $\boldsymbol{u}(\boldsymbol{x})$ is continuous, with an apparent displacement jump $\boldsymbol{w} := \boldsymbol{u}(\boldsymbol{x} \in \Omega^+ \cap \mathcal{S}^+) - \boldsymbol{u}(\boldsymbol{x} \in \Omega^- \cap \mathcal{S}^-)$ across the discontinuity band $\mathcal{B}$. Accordingly, the $\mathcal{C}^0$-continuous displacement field $\boldsymbol{u}(\boldsymbol{x})$ can be expressed as

$$\boldsymbol{u}(\boldsymbol{x}) = \bar{\boldsymbol{u}}(\boldsymbol{x}) + \mathscr{H}_{\mathcal{B}}(\boldsymbol{x})\, \hat{\boldsymbol{u}}(\boldsymbol{x}) \tag{2.2a}$$

and the singular strain field (2.1b) is regularized as

$$\boldsymbol{\epsilon}(\boldsymbol{x}) = \nabla^{\text{sym}} \bar{\boldsymbol{u}}(\boldsymbol{x}) + \big(\boldsymbol{e} \otimes \boldsymbol{n}\big)^{\text{sym}}\, \Xi_{\mathcal{B}}(\boldsymbol{x}) \tag{2.2b}$$

where the inelastic deformation vector $\boldsymbol{e} := \boldsymbol{w}/b$ is defined as the apparent displacement jump $\boldsymbol{w}$ normalized with respect to the band width b; $\mathscr{H}_{\mathcal{B}}(\boldsymbol{x})$ is a regularized ramp function defined as $\mathscr{H}_{\mathcal{B}}(\boldsymbol{x}) = 0$ if $\boldsymbol{x} \in \Omega^-$, $\mathscr{H}_{\mathcal{B}}(\boldsymbol{x}) = \frac{1}{b}\big(\boldsymbol{x} - \boldsymbol{x}^*\big) \cdot \boldsymbol{n}$ if $\boldsymbol{x} \in \mathcal{B}$ and $\mathscr{H}_{\mathcal{B}}(\boldsymbol{x}) = 1$ otherwise, with $\boldsymbol{x}^*$ being the spatial coordinates of point $\boldsymbol{x}$ projected along the direction $-\boldsymbol{n}$ to the surface $\mathcal{S}^-$; $\Xi_{\mathcal{B}}(\boldsymbol{x})$ denotes the collocation function within the discontinuity band $\mathcal{B}$, i.e., $\Xi_{\mathcal{B}}(\boldsymbol{x}) = 1$ if $\boldsymbol{x} \in \mathcal{B}$ and $\Xi_{\mathcal{B}}(\boldsymbol{x}) = 0$ otherwise.

In summary, the strong discontinuity $\mathcal{S}$ induces a discontinuous displacement field $\boldsymbol{u}(\boldsymbol{x})$ and a singular (unbounded) strain field $\boldsymbol{\epsilon}(\boldsymbol{x})$; see Fig. 3(a). Contrariwise, as shown in Fig. 3(b), the kinematic of a regularized discontinuity is characterized by a continuous displacement field $\boldsymbol{u}(\boldsymbol{x})$ and a regular (bounded) strain field $\boldsymbol{\epsilon}(\boldsymbol{x})$.

Remark 2.1 As the discontinuity band width b tends to zero, it follows that

$$\lim_{b\to 0} \mathscr{H}_{\mathcal{B}}(\boldsymbol{x}) = \mathscr{H}_{\mathcal{S}}(\boldsymbol{x}), \qquad \lim_{b\to 0} \frac{1}{b}\Xi_{\mathcal{B}}(\boldsymbol{x}) = \delta_{\mathcal{S}}(\boldsymbol{x}), \qquad \lim_{b\to 0} \boldsymbol{e}\,\Xi_{\mathcal{B}}(\boldsymbol{x}) = \boldsymbol{w}\delta_{\mathcal{S}}(\boldsymbol{x}) \tag{2.3}$$

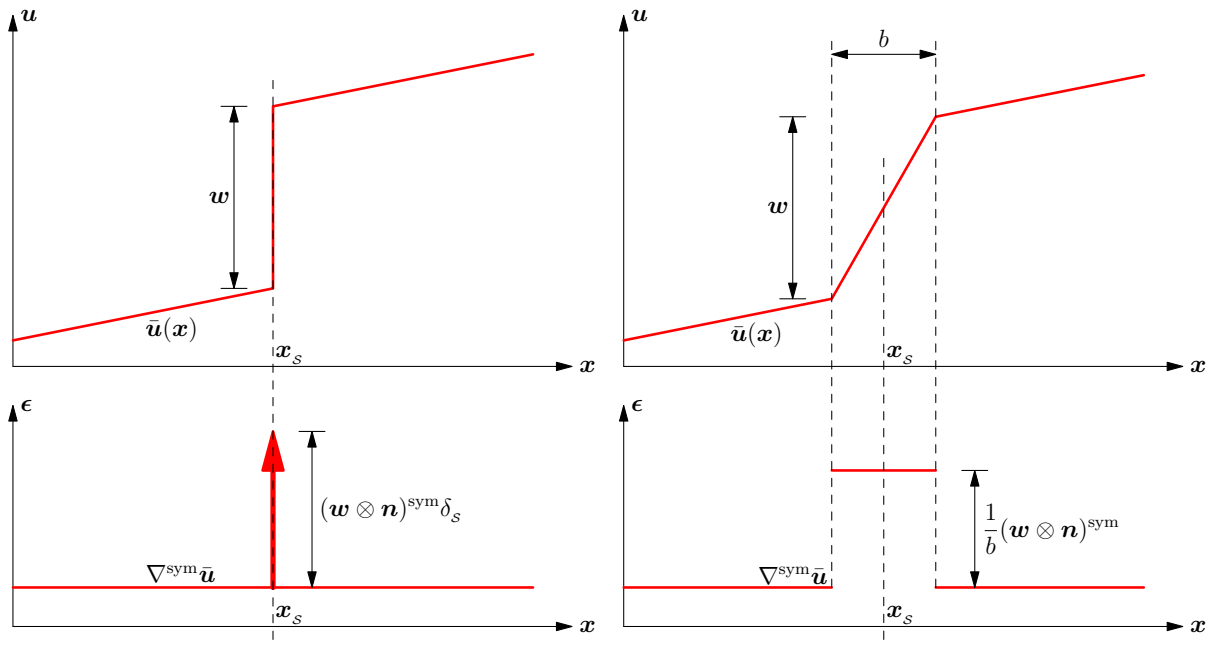

(a) Displacement/strain fields around a strong discontinuity (b) Displacement/strain fields around a regularized discontinuity

Figure 3: Kinematics of strong/regularized discontinuities

That is, the strong discontinuity can be regarded as the limit of a regularized one, with a vanishing band width $b \to 0$. Reciprocally, a discontinuity band can be regarded as the convenient regularization of a strong discontinuity. □

Remark 2.2 For either the strong or regularized discontinuity, the strain field $\boldsymbol{\epsilon}(\boldsymbol{x})$ remains continuous across it, i.e.,

$$\boldsymbol{\epsilon}_s^+ = \boldsymbol{\epsilon}_s^- = \boldsymbol{\epsilon}_s^\pm \tag{2.4}$$

where $\boldsymbol{\epsilon}_s^+ := \boldsymbol{\epsilon}(\boldsymbol{x} \in \Omega^+ \cap \mathcal{S}^+)$ and $\boldsymbol{\epsilon}_s^- := \boldsymbol{\epsilon}(\boldsymbol{x} \in \Omega^- \cap \mathcal{S}^-)$ represent the strains "ahead of" the surface $\mathcal{S}^+$ and "behind" the surface $\mathcal{S}^-$, respectively. Therefore, in this work no distinction is made between $\boldsymbol{\epsilon}_s^+$ and $\boldsymbol{\epsilon}_s^-$, and are both denoted by $\boldsymbol{\epsilon}_s^\pm$. Contrariwise, the strain $\boldsymbol{\epsilon}_\mathcal{S} := \boldsymbol{\epsilon}(\boldsymbol{x} \in \mathcal{S})$ at the discontinuity (band) exhibits a jump with respect to the strain $\boldsymbol{\epsilon}_s^\pm$ outside it, which verifies Maxwell's compatibility condition

$$[\![\boldsymbol{\epsilon}]\!] := \boldsymbol{\epsilon}_\mathcal{S} - \boldsymbol{\epsilon}_s^\pm = \big(\boldsymbol{e} \otimes \boldsymbol{n}\big)^{\text{sym}} = \frac{1}{b}\big(\boldsymbol{w} \otimes \boldsymbol{n}\big)^{\text{sym}} \tag{2.5}$$

The strain jump $[\![\boldsymbol{\epsilon}]\!]$ is inversely proportional to b for a regularized discontinuity (or unbounded for a strong one). □

2.2. *Governing equations*

Restricting the discussion to quasi-static loading, the governing equations of the above problem are expressed as

$$\begin{array}{lll} \text{Balance of linear momentum:} & \nabla \cdot \boldsymbol{\sigma} + \boldsymbol{b}^* = \boldsymbol{0} & \text{in } \Omega \backslash \mathcal{S} \\ \text{Traction continuity condition:} & \boldsymbol{\sigma}_s^+ \cdot \boldsymbol{n} = \boldsymbol{\sigma}_s^- \cdot \boldsymbol{n} = \boldsymbol{t} & \text{in } \mathcal{S} \end{array} \tag{2.6}$$

subjected to the following boundary conditions

$$\begin{aligned} &\text{Traction boundary condition:} && \boldsymbol{\sigma}\cdot\boldsymbol{n}^{*}=\boldsymbol{t}^{*} && \text{in } \Gamma_t \\ &\text{Displacement boundary condition:} && \boldsymbol{u}=\boldsymbol{u}^{*} && \text{in } \Gamma_u \end{aligned} \tag{2.7}$$

where the second-order tensor $\boldsymbol{\sigma} : \Omega\backslash\mathcal{S} \rightarrow \mathbb{R}^{n_{\text{dim}}\times n_{\text{dim}}}$ denotes the stress field in the bulk $\Omega\backslash\mathcal{S} = \Omega^{+}\cup\Omega^{-}$, with $\boldsymbol{\sigma}^{+}_{\mathcal{S}} := \boldsymbol{\sigma}(\boldsymbol{x}\in\Omega^{+}\cap\mathcal{S})$ and $\boldsymbol{\sigma}^{-}_{\mathcal{S}} := \boldsymbol{\sigma}(\boldsymbol{x}\in\Omega^{-}\cap\mathcal{S})$ being the stresses "ahead of" and "behind" the interface $\mathcal{S}$, respectively; the vector $\boldsymbol{t} : \mathcal{S}\rightarrow\mathbb{R}^{n_{\text{dim}}}$ represents the cohesive tractions transferred across the discontinuity $\mathcal{S}$.

3. Discontinuities localized in elastic solids

Once strain localization occurs, it is generally assumed that the bulk material remains elastic during the whole deformation process and all inelastic behavior is localized within the discontinuity (band). This is methodology considered in this section, i.e., inelastic discontinuities localized in elastic solids along preferred orientation.

3.1. General framework

Confining the discussion to a purely mechanical theory, the second law of thermodynamics requires that

$$\int_{\Omega}\mathscr{D}\,\mathrm{d}\Omega = \int_{\Omega}\left(\boldsymbol{\sigma}:\dot{\boldsymbol{\epsilon}}-\dot{\psi}\right)\mathrm{d}\Omega \geq 0 \tag{3.1}$$

with the (local form) energy dissipation $\mathscr{D}$ per unit volume defined as

$$\mathscr{D} := \boldsymbol{\sigma}:\dot{\boldsymbol{\epsilon}}-\dot{\psi}\geq 0 \tag{3.2}$$

where $\boldsymbol{\sigma}$ and $\boldsymbol{\epsilon}$ denote the second-order stress and strain tensors, respectively; ψ is the free energy density function of the material; $\dot{()}$ represents the rate with respect to the (pseudo-) time. As the strain field in the solid Ω is non-uniform upon strain localization, the global form (3.1), instead of the local counterpart (3.2), is employed to establish consistent constitutive laws for both the bulk and discontinuity (band).

Upon the methodology of inelastic discontinuities localized in elastic solids, the strain field $\boldsymbol{\epsilon}(\boldsymbol{x})$ is expressed as

$$\boldsymbol{\epsilon}(\boldsymbol{x}) = \boldsymbol{\epsilon}^{\text{e}}(\boldsymbol{x}) + \boldsymbol{\epsilon}^{\text{in}}(\boldsymbol{x}) \tag{3.3}$$

where $\boldsymbol{\epsilon}^{\text{e}}(\boldsymbol{x}) = \nabla^{\text{sym}}\bar{\boldsymbol{u}}(\boldsymbol{x})$ represents the elastic strain field; the inelastic strain field $\boldsymbol{\epsilon}^{\text{in}}(\boldsymbol{x})$ is given by

$$\boldsymbol{\epsilon}^{\text{in}}(\boldsymbol{x}) = \left(\boldsymbol{w}\otimes\boldsymbol{n}\right)^{\text{sym}}\delta_{\mathcal{S}}(\boldsymbol{x}) \qquad \text{or} \qquad \boldsymbol{\epsilon}^{\text{in}}(\boldsymbol{x}) = \left(\boldsymbol{e}\otimes\boldsymbol{n}\right)^{\text{sym}}\Xi_{\mathcal{B}}(\boldsymbol{x}) \tag{3.4}$$

localized within the discontinuity (band).

Similarly, the free energy density $\psi(\boldsymbol{x})$ is also split into an elastic part $\psi^{\text{e}}(\boldsymbol{x})$ and a localized inelastic one $\psi^{\text{in}}(\boldsymbol{x})$

$$\psi(\boldsymbol{x}) = \psi^{\text{e}}(\boldsymbol{x}) + \psi^{\text{in}}(\boldsymbol{x}) \tag{3.5}$$

where the elastic free energy density $\psi^{\mathrm{e}}(\boldsymbol{x})$ is expressed as a quadratic function, i.e.,

$$\psi^{\mathrm{e}}(\boldsymbol{x}) = \frac{1}{2}\,\boldsymbol{\epsilon}^{\mathrm{e}}(\boldsymbol{x}) : \mathbb{E}^{0} : \boldsymbol{\epsilon}^{\mathrm{e}}(\boldsymbol{x}) \tag{3.6}$$

with $\mathbb{E}^{0}$ being the fourth-order elasticity tensor. The inelastic free energy density $\psi^{\mathrm{in}}(\boldsymbol{x})$, independent of the elastic strain tensor $\boldsymbol{\epsilon}^{\mathrm{e}}(\boldsymbol{x})$, is discussed later according to the singular or regularized kinematics.

Making use of standard arguments, one arrives at

$$\boldsymbol{\sigma}(\boldsymbol{x}) = \frac{\partial \psi^{\mathrm{e}}}{\partial \boldsymbol{\epsilon}^{\mathrm{e}}} = \mathbb{E}^{0} : \boldsymbol{\epsilon}^{\mathrm{e}}(\boldsymbol{x}), \qquad \boldsymbol{\epsilon}^{\mathrm{e}}(\boldsymbol{x}) = \mathbb{C}^{0} : \boldsymbol{\sigma}(\boldsymbol{x}) \tag{3.7}$$

or equivalently, in rate form

$$\dot{\boldsymbol{\sigma}}(\boldsymbol{x}) = \mathbb{E}^{0} : \dot{\boldsymbol{\epsilon}}^{\mathrm{e}}(\boldsymbol{x}), \qquad \dot{\boldsymbol{\epsilon}}^{\mathrm{e}}(\boldsymbol{x}) = \mathbb{C}^{0} : \dot{\boldsymbol{\sigma}}(\boldsymbol{x}) \tag{3.8}$$

with the fourth-order elastic compliance tensor $\mathbb{C}^{0} := \left(\mathbb{E}^{0}\right)^{-1}$. Note that the constitutive relations (3.7) and (3.8), together with the kinematic decomposition (3.3), hold for both the elastic bulk and the discontinuity (band).

Furthermore, the inelastic behavior of the discontinuity (band) is constrained additionally by the second law of thermodynamics (3.1), i.e.,

$$\int_{\Omega} \mathscr{D}\, \mathrm{d}\Omega = \int_{\Omega} \left(\boldsymbol{\sigma} : \dot{\boldsymbol{\epsilon}}^{\mathrm{in}} - \dot{\psi}^{\mathrm{in}}\right) \mathrm{d}\Omega \geq 0 \tag{3.9}$$

Once the inelastic free energy density function ψ^{in} is defined, a consistent (regularized) cohesive model, characterized by a specific traction-based failure criterion, can be established for the discontinuity (band).

Remark 3.1 As the inelastic strains $\boldsymbol{\epsilon}^{\mathrm{in}}$ are localized completely within the discontinuity (band), the elastic strain field $\boldsymbol{\epsilon}^{\mathrm{e}}$ is continuous in the entire solid. It follows from the constitutive relations (3.7) that, ***though the strain field may be discontinuous or even singular, the resulting stress filed is continuous across the discontinuity (band)***, i.e.,

$$\boxed{\boldsymbol{\sigma}_{\mathcal{S}}^{+} = \boldsymbol{\sigma}_{\mathcal{S}}^{-} = \boldsymbol{\sigma}_{\mathcal{S}}} \tag{3.10}$$

for the stress $\boldsymbol{\sigma}_{\mathcal{S}} := \boldsymbol{\sigma}(\boldsymbol{x} \in \mathcal{S})$ at the discontinuity (band). This conclusion, applicable for both strong and regularized discontinuities, is exactly the *stress continuity condition* upon strain localization in inelastic softening solids; see Section 4.1 for the details. In this case, the traction continuity condition $(2.6)_2$, which describes the relation between the bulk stresses $\boldsymbol{\sigma}_{\mathcal{S}}^{+} = \boldsymbol{\sigma}_{\mathcal{S}}^{-}$ and tractions $\boldsymbol{t}$ transferred by the discontinuity (band), coincides with the classical static constraint at the material level, i.e.,

$$\boldsymbol{t} = \boldsymbol{\sigma}_{\mathcal{S}} \cdot \boldsymbol{n}, \qquad \dot{\boldsymbol{t}} = \dot{\boldsymbol{\sigma}}_{\mathcal{S}} \cdot \boldsymbol{n} \tag{3.11}$$

where the material character $\dot{\boldsymbol{n}} = \boldsymbol{0}$ has been considered. The static constraint is employed in the embedded/smeared crack models [2, 55] and traction-based elastoplastic damage models [70] discussed later in this work. □

Remark 3.2 Calling for the relations (3.1) and (3.5), the external energy supplied to the solid during whole failure process is evaluated as

$$W := \int_{\Omega}\int_{0}^{\infty} \boldsymbol{\sigma} : \dot{\boldsymbol{\epsilon}}\, \mathrm{d}T\, \mathrm{d}\Omega = \int_{\Omega}\int_{0}^{\infty} \left(\dot{\psi}^{\mathrm{in}} + \mathscr{D}\right) \mathrm{d}T\, \mathrm{d}\Omega \tag{3.12}$$

where the result $\int_{0}^{\infty} \dot{\psi}^{\mathrm{e}}\, \mathrm{d}T = 0$ has been considered for the time $T \in [0, \infty]$ and the state variable ψ^{e}. □

3.2. Failure criterion and orientation of the discontinuity (band)

To characterize the discontinuity (band), a *traction-based* failure criterion $\hat{f}(\boldsymbol{t}, q) \leq 0$, is introduced. Without loss of generality, let us consider the homogeneous failure function $\hat{f}(\boldsymbol{t}, q)$ of degree $M \geq 1$, i.e.,

$$\hat{f}(\boldsymbol{t}, q) = \frac{1}{M}\big(\partial_{\boldsymbol{t}} \hat{f} \cdot \boldsymbol{t} + \partial_q \hat{f} \cdot q\big) = \frac{1}{M}\big(\hat{\boldsymbol{\gamma}} \cdot \boldsymbol{t} - \hat{h} \cdot q\big) \leq 0 \tag{3.13}$$

where $q(\cdot)$ denotes the cohesive strength of the discontinuity (band), dependent on a displacement-like internal variable $\tilde{\kappa}$ (or a strain-like one κ); the derivatives $\hat{\boldsymbol{\gamma}}$ and $\hat{h}$ are expressed as

$$\hat{\boldsymbol{\gamma}} := \frac{\partial \hat{f}}{\partial \boldsymbol{t}}, \qquad \hat{h} := -\frac{\partial \hat{f}}{\partial q} \tag{3.14}$$

As will be clear, the vector $\boldsymbol{\gamma}$ characterizes the evolution laws of the inelastic discontinuity (band).

The above failure criterion $\hat{f}(\boldsymbol{t}, q) \leq 0$ is expressed in terms of the traction $\boldsymbol{t} = \boldsymbol{\sigma} \cdot \boldsymbol{n}$ (hereafter the subscript '$_{\mathcal{S}}$' associated with $\boldsymbol{\sigma}_{\mathcal{S}}$ is dropped for brevity), or equivalently, of the stress tensor $\boldsymbol{\sigma}$ and the normal vector $\boldsymbol{n}$ of the discontinuity (band). With the local orthogonal base vectors $(\boldsymbol{n}, \boldsymbol{m}, \boldsymbol{p})$ introduced in Eqs. (A.2), the tractions $\boldsymbol{t}(\boldsymbol{\theta})$ acting on the surface with normal vector $\boldsymbol{n}(\boldsymbol{\theta})$ can be expressed as Eqs. (A.3) and (A.4), in terms of the principal stresses σ_i and the characteristic angles $\boldsymbol{\theta}$. Accordingly, the discontinuity orientation $\boldsymbol{n}$ has to be determined, usually in an heuristic manner (e.g., along the major principal stress for mode-I fracture) which might be insufficient for general cases. Owing to the static constraint (3.11), Mohr's maximization postulate [32] is adopted in this work for a given traction-based failure criterion $\hat{f}(\boldsymbol{t}, q) \leq 0$. That is, a discontinuity is initiated on the orientation upon which the tractions $\boldsymbol{t}(\boldsymbol{\theta}^{\mathrm{cr}})$ maximize the failure function $\hat{f}\big[\boldsymbol{t}(\boldsymbol{\theta}), q\big]$, i.e.,

$$\hat{\boldsymbol{\theta}}^{\mathrm{cr}} = \arg\max \hat{f}\big[\boldsymbol{t}(\boldsymbol{\theta}), q\big] \qquad \forall \boldsymbol{\theta} \tag{3.15}$$

where the characteristic angles $\hat{\boldsymbol{\theta}}^{\mathrm{cr}}$ define the discontinuity orientation. The corresponding stationarity condition reads

$$\left.\frac{\partial \hat{f}}{\partial \boldsymbol{\theta}}\right|_{\hat{\boldsymbol{\theta}}^{\mathrm{cr}}} = \left(\hat{\boldsymbol{\gamma}} \cdot \frac{\partial \boldsymbol{t}}{\partial \boldsymbol{\theta}}\right)_{\hat{\boldsymbol{\theta}}^{\mathrm{cr}}} = \left(\hat{\gamma}_n \frac{\partial t_n}{\partial \boldsymbol{\theta}} + \hat{\gamma}_m \frac{\partial t_m}{\partial \boldsymbol{\theta}} + \hat{\gamma}_p \frac{\partial t_p}{\partial \boldsymbol{\theta}}\right)_{\hat{\boldsymbol{\theta}}^{\mathrm{cr}}} = \boldsymbol{0} \tag{3.16}$$

together with a negative definite Hessian matrix

$$\boldsymbol{\theta}^* \cdot \left.\frac{\partial^2 \hat{f}}{\partial \boldsymbol{\theta}^2}\right|_{\hat{\boldsymbol{\theta}}^{\mathrm{cr}}} \cdot \boldsymbol{\theta}^* < 0 \qquad \forall \boldsymbol{\theta}^* \tag{3.17}$$

where the local Cartesian components $(\hat{\gamma}_n, \hat{\gamma}_m, \hat{\gamma}_p)$ of the vector $\hat{\boldsymbol{\gamma}}$ are expressed as

$$\hat{\gamma}_n = \frac{\partial \hat{f}}{\partial t_n}, \qquad \hat{\gamma}_m = \frac{\partial \hat{f}}{\partial t_m}, \qquad \hat{\gamma}_p = \frac{\partial \hat{f}}{\partial t_p} \tag{3.18}$$

Recalling the traction components (A.4), the stationarity condition (3.16) results in a set of nonlinear equations so that the discontinuity angles $\hat{\boldsymbol{\theta}}^{\mathrm{cr}}$ can be solved. Note that, providing the solution exists, it depends only on the given traction-based failure criterion and the stress state.

Remark 3.3 For an active discontinuity (band), it follows that

$$\hat{f}(\boldsymbol{t}, q) = 0 \qquad \Longrightarrow \qquad \hat{\boldsymbol{\gamma}} \cdot \boldsymbol{t} = \hat{h} \cdot q \tag{3.19}$$

This relation will be used later in evaluation of the energy dissipation and fracture energy. □

3.3. Strong/regularized discontinuity approaches

With respect to the strategies dealing with the kinematic unknowns $\boldsymbol{w}$ (or $\boldsymbol{e} := \boldsymbol{w}/b$), two approaches can be identified from the methodology of inelastic discontinuities localized in elastic solids. Either the singular kinematics (2.1) or the regularized one (2.2) can be incorporated in both approaches.

Let us first consider the *strong/regularized discontinuity approaches* in which the kinematic unknowns $\boldsymbol{w}$ (or $\boldsymbol{e}$) associated to the discontinuity (band) are retained as independent variables. With the singular kinematics (2.1), the governing equations (2.6) and the traction boundary condition $(2.7)_1$ can be cast as: Find $\boldsymbol{u} \in \mathscr{U}$ such that [30]

$$\int_{\Omega} \nabla^{\text{sym}} \delta\bar{\boldsymbol{u}} : \boldsymbol{\sigma} \, \mathrm{d}\Omega + \int_{\mathcal{S}} \delta\boldsymbol{w} \cdot \boldsymbol{t} \, \mathrm{d}\mathcal{S} = \int_{\Omega} \delta\boldsymbol{u} \cdot \boldsymbol{b}^* \, \mathrm{d}\Omega + \int_{\Gamma_t} \delta\boldsymbol{u} \cdot \boldsymbol{t}^* \, \mathrm{d}\Gamma \qquad \forall \delta\boldsymbol{u} \in \mathcal{V} \tag{3.20}$$

where the trial function $\boldsymbol{u} \in \mathscr{U}$ and its variation $\delta\boldsymbol{u} \in \mathcal{V}$ are chosen from the spaces

$$\mathscr{U} := \left\{ \boldsymbol{u} \middle| \boldsymbol{u} = \bar{\boldsymbol{u}} + \mathscr{H}_{\mathcal{S}} \, \hat{\boldsymbol{u}};\ \boldsymbol{u} = \boldsymbol{u}^* \text{ in } \Gamma_u;\ \hat{\boldsymbol{u}} = \boldsymbol{w} \text{ in } \mathcal{S} \right\} \tag{3.21a}$$

$$\mathcal{V} := \left\{ \delta\boldsymbol{u} \middle| \delta\boldsymbol{u} = \delta\bar{\boldsymbol{u}} + \mathscr{H}_{\mathcal{S}} \, \delta\hat{\boldsymbol{u}};\ \delta\boldsymbol{u} = \boldsymbol{0} \text{ in } \Gamma_u;\ \delta\hat{\boldsymbol{u}} = \delta\boldsymbol{w} \text{ in } \mathcal{S} \right\} \tag{3.21b}$$

Alternatively, if the regularized kinematics (2.2) is employed, the weak form (3.20) becomes: Find $\boldsymbol{u} \in \mathscr{U}$ such that

$$\int_{\Omega} \nabla^{\text{sym}} \delta\bar{\boldsymbol{u}} : \boldsymbol{\sigma} \, \mathrm{d}\Omega + \int_{\mathcal{B}} \delta\boldsymbol{e} \cdot \boldsymbol{t} \, \mathrm{d}\mathcal{B} = \int_{\Omega} \delta\boldsymbol{u} \cdot \boldsymbol{b}^* \, \mathrm{d}\Omega + \int_{\Gamma_t} \delta\boldsymbol{u} \cdot \boldsymbol{t}^* \, \mathrm{d}\Gamma \qquad \forall \delta\boldsymbol{u} \in \mathcal{V} \tag{3.22}$$

where the trial function $\boldsymbol{u} \in \mathscr{U}$ and its variation $\delta\boldsymbol{u} \in \mathcal{V}$ are chosen within the spaces

$$\mathscr{U} := \left\{ \boldsymbol{u} \middle| \boldsymbol{u} = \bar{\boldsymbol{u}} + \mathscr{H}_{\mathcal{B}} \, \hat{\boldsymbol{u}};\ \boldsymbol{u} = \boldsymbol{u}^* \text{ in } \Gamma_u;\ \hat{\boldsymbol{u}} = \boldsymbol{w} \text{ in } \mathcal{S} \right\} \tag{3.23a}$$

$$\mathcal{V} := \left\{ \delta\boldsymbol{u} \middle| \delta\boldsymbol{u} = \delta\bar{\boldsymbol{u}} + \mathscr{H}_{\mathcal{B}} \, \delta\hat{\boldsymbol{u}};\ \delta\boldsymbol{u} = \boldsymbol{0} \text{ in } \Gamma_u;\ \delta\hat{\boldsymbol{u}} = \delta\boldsymbol{w} \text{ in } \mathcal{S} \right\} \tag{3.23b}$$

In the weak form (3.20) or (3.22), the displacement boundary condition $(2.7)_2$ are enforced in strong form, and the variations $(\delta\bar{\boldsymbol{u}}, \delta\hat{\boldsymbol{u}})$ are of sufficient regularity.

To proceed, the above weak form (3.20) or (3.22) has to be supplemented with constitutive relations for both the bulk stress $\boldsymbol{\sigma}$ and tractions $\boldsymbol{t}$ transferred across the discontinuity (band). The linear elastic relation (3.7) is assumed for the bulk. As the tractions $\boldsymbol{t}$ are work conjugated to the displacement jumps $\boldsymbol{w}$, a cohesive model in terms of tractions vs. displacement jumps (or inelastic deformations) should be fed to the discontinuity (band). This task can be accomplished within the framework of irreversible thermodynamics.

3.3.1. Cohesive model for the discontinuity

The discontinuity (band) induces both stiffness degradation and irreversible deformations. To account for them, the displacement jump $\boldsymbol{w}$ and the resulting singular inelastic strain $\boldsymbol{\epsilon}^{\text{in}}$ are decomposed as

$$\boldsymbol{w} = \boldsymbol{w}^{\text{d}} + \boldsymbol{w}^{\text{p}}, \qquad \boldsymbol{\epsilon}^{\text{in}} = \boldsymbol{\epsilon}^{\text{d}} + \boldsymbol{\epsilon}^{\text{p}} \tag{3.24}$$

where $(\boldsymbol{w}^{\text{d}}, \boldsymbol{w}^{\text{p}})$ represent the recoverable/unrecoverable parts of the displacement jump $\boldsymbol{w}$; the resulting damage (recoverable) strain $\boldsymbol{\epsilon}^{\text{d}} = \left(\boldsymbol{w}^{\text{d}} \otimes \boldsymbol{n}\right)^{\text{sym}} \delta_{\mathcal{S}}$ and plastic (unrecoverable) strain $\boldsymbol{\epsilon}^{\text{p}} = \left(\boldsymbol{w}^{\text{p}} \otimes \boldsymbol{n}\right)^{\text{sym}} \delta_{\mathcal{S}}$ are both singular.

Similarly, the inelastic free energy density field ψ^{in} in Eq. (3.5) is also singular, i.e.,

$$\psi^{\text{in}} = \widetilde{\psi}^{\text{in}}\,\delta_{\mathcal{S}}, \qquad \widetilde{\psi}^{\text{in}} = \widetilde{\psi}^{\text{d}}(\boldsymbol{w}^{\text{d}}, \widetilde{\boldsymbol{E}}^{\text{d}}) + \tilde{\chi}(\tilde{\kappa}) \tag{3.25}$$

where the damage free energy function $\widetilde{\psi}^{\text{d}}(\cdot,\cdot)$ is expressed in terms of a second-order (variable) stiffness tensor $\widetilde{\boldsymbol{E}}^{\text{d}}$ and the recoverable displacement jumps $\boldsymbol{w}^{\text{d}}$ as

$$\widetilde{\psi}^{\text{d}}(\boldsymbol{w}^{\text{d}}, \widetilde{\boldsymbol{E}}^{\text{d}}) = \frac{1}{2}\,\boldsymbol{w}^{\text{d}} \cdot \widetilde{\boldsymbol{E}}^{\text{d}} \cdot \boldsymbol{w}^{\text{d}} \tag{3.26}$$

The inelastic potential function $\tilde{\chi}(\cdot)$ is characterized by a *displacement jump*-like internal variable $\tilde{\kappa}$.

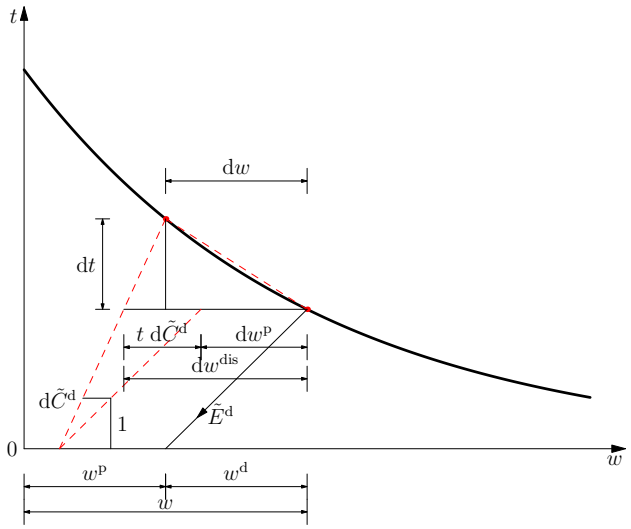

Figure 4: 1D definition of the dissipative jump rate and its damage/plastic components for an increment deformation

With above definitions, the second law of thermodynamics (3.9) becomes

$$\int_{\Omega} \mathscr{D}\,\mathrm{d}\Omega = \int_{\mathcal{S}} \left(\boldsymbol{t}\cdot\dot{\boldsymbol{w}} - \dot{\widetilde{\psi}}^{\text{in}}\right)\mathrm{d}\mathcal{S} \geq 0 \tag{3.27}$$

Accordingly, standard arguments yield the following cohesive relations

$$\boldsymbol{t} = \frac{\partial\widetilde{\psi}^{\text{d}}}{\partial\boldsymbol{w}^{\text{d}}} = \widetilde{\boldsymbol{E}}^{\text{d}}\cdot\boldsymbol{w}^{\text{d}} = \widetilde{\boldsymbol{E}}^{\text{d}}\cdot\left(\boldsymbol{w}-\boldsymbol{w}^{\text{p}}\right), \qquad \boldsymbol{w}^{\text{d}} = \boldsymbol{w}-\boldsymbol{w}^{\text{p}} = \widetilde{\boldsymbol{C}}^{\text{d}}\cdot\boldsymbol{t} \tag{3.28}$$

or the rate forms

$$\dot{\boldsymbol{t}} = \widetilde{\boldsymbol{E}}^{\text{d}}\cdot\left(\dot{\boldsymbol{w}}-\dot{\boldsymbol{w}}^{\text{dis}}\right), \qquad \dot{\boldsymbol{w}} = \widetilde{\boldsymbol{C}}^{\text{d}}\cdot\dot{\boldsymbol{t}} + \dot{\boldsymbol{w}}^{\text{dis}} \tag{3.29}$$

where $\widetilde{\boldsymbol{C}}^{\text{d}} := \left(\widetilde{\boldsymbol{E}}^{\text{d}}\right)^{-1}$ denotes the second-order (variable) compliance tensor of the discontinuity; $\dot{\boldsymbol{w}}^{\text{dis}}$ represents the *dissipative displacement jump rate* meaningful only in rate sense, defined as

$$\dot{\boldsymbol{w}}^{\text{dis}} = \dot{\widetilde{\boldsymbol{C}}}^{\text{d}}\cdot\boldsymbol{t} + \dot{\boldsymbol{w}}^{\text{p}} \tag{3.30}$$

with $\dot{\widetilde{\boldsymbol{C}}}^{\mathrm{d}} \cdot \boldsymbol{t}$ and $\dot{\boldsymbol{w}}^{\mathrm{p}}$ being its damage and plastic components; see Fig. 4.

In the above cohesive relations, the compliance $\widetilde{\boldsymbol{C}}^{\mathrm{d}}$ (or the stiffness $\widetilde{\boldsymbol{E}}^{\mathrm{d}}$), the unrecoverable displacement jump $\boldsymbol{w}^{\mathrm{p}}$ and the displacement-like variable $\tilde{\kappa}$ are all internal variables. Their evolution laws have to fulfill the second law of thermodynamics (3.27), or equivalently, the following energy dissipation inequality

$$\int_{\Omega} \mathscr{D} \, \mathrm{d}\Omega = \int_{\mathcal{S}} \widetilde{\mathscr{D}} \, \mathrm{d}\mathcal{S} \geq 0 \tag{3.31}$$

for the localized energy dissipation $\widetilde{\mathscr{D}}$

$$\widetilde{\mathscr{D}} = \frac{1}{2} \boldsymbol{t} \cdot \dot{\widetilde{\boldsymbol{C}}}^{\mathrm{d}} \cdot \boldsymbol{t} + \boldsymbol{t} \cdot \dot{\boldsymbol{w}}^{\mathrm{p}} + \left(q^0 - q\right) \cdot \dot{\tilde{\kappa}} \geq 0 \tag{3.32}$$

where the strength decay $q^0 - q := -\partial \tilde{\chi} / \partial \tilde{\kappa}$ is work conjugate to the internal variable $\tilde{\kappa}$, with q^0 being the initial value of the cohesive strength $q(\tilde{\kappa})$, i.e., $q^0 := q(\tilde{\kappa} = 0)$.

In analogy to the classical plasticity theory, associated evolution laws can be derived from the postulate of maximum energy dissipation [59]. That is, for a given admissible state $\{\boldsymbol{t}, q\}$ constrained by the failure criterion (3.13), the rates $\{\dot{\widetilde{\boldsymbol{C}}}^{\mathrm{d}}, \dot{\boldsymbol{w}}^{\mathrm{p}}, \dot{\tilde{\kappa}}\}$ are those maximizing the energy dissipation $\widetilde{\mathscr{D}}$. The resulting evolution laws are given by

$$\dot{\boldsymbol{w}}^{\mathrm{dis}} = \dot{\widetilde{\boldsymbol{C}}}^{\mathrm{d}} \cdot \boldsymbol{t} + \dot{\boldsymbol{w}}^{\mathrm{p}} = \tilde{\lambda} \boldsymbol{\gamma}, \qquad \dot{\tilde{\kappa}} = \tilde{\lambda} h \tag{3.33}$$

where the localized Lagrangian multiplier $\tilde{\lambda}$ satisfies the following Kuhn-Tucker loading/unloading rules

$$\tilde{\lambda} \geq 0, \qquad \widehat{f} \leq 0, \qquad \tilde{\lambda} \widehat{f} = 0 \tag{3.34}$$

for the dissipative flow vector $\boldsymbol{\gamma} = \widehat{\boldsymbol{\gamma}}$ and softening function $h = \widehat{h}$ given in Eq. (3.14).

To discriminate between damage and plastic contributions to the dissipative displacement jump rate $\dot{\boldsymbol{w}}^{\mathrm{dis}}$, a material parameter $\xi \in [0, 1]$ is introduced so that

$$\dot{\boldsymbol{w}}^{\mathrm{p}} = \left(1 - \xi\right) \dot{\boldsymbol{w}}^{\mathrm{dis}} = \left(1 - \xi\right) \tilde{\lambda} \boldsymbol{\gamma} \tag{3.35a}$$

$$\dot{\widetilde{\boldsymbol{C}}}^{\mathrm{d}} \cdot \boldsymbol{t} = \xi \, \dot{\boldsymbol{w}}^{\mathrm{dis}} = \xi \, \tilde{\lambda} \boldsymbol{\gamma} \tag{3.35b}$$

The postulate of maximum energy dissipation determines only the components of the compliance $\widetilde{\boldsymbol{C}}^{\mathrm{d}}$ appearing in the product $\boldsymbol{t} \cdot \dot{\widetilde{\boldsymbol{C}}}^{\mathrm{d}} \cdot \boldsymbol{t}$, leaving the remaining ones undefined. A particular evolution law satisfying Eq. (3.35b) is given by

$$\dot{\widetilde{\boldsymbol{C}}}^{\mathrm{d}} = \xi \, \tilde{\lambda} \frac{\boldsymbol{\gamma} \otimes \boldsymbol{\gamma}}{\boldsymbol{\gamma} \cdot \boldsymbol{t}} \tag{3.36}$$

as long as the denominator $\boldsymbol{\gamma} \cdot \boldsymbol{t} \neq 0$. The cases $\xi = 0$ and $\xi = 1$ correspond to cohesive models of pure plastic and pure damage types, respectively. For the intermediate value $\xi \in (0, 1)$, the discontinuity compliance $\widetilde{\boldsymbol{C}}^{\mathrm{d}}$ and the plastic displacement jump $\boldsymbol{w}^{\mathrm{p}}$ are both internal variables and a combined plastic-damage cohesive model follows.

When the discontinuity is inactive, i.e., $\widehat{f}(\boldsymbol{t}, q) < 0$, it follows from Eq. (3.34) that $\tilde{\lambda} = 0$; when the discontinuity evolves, i.e., $\tilde{\lambda} > 0$, it follows that $\widehat{f}(\boldsymbol{t}, q) = 0$, and the consistency condition reads

$$\dot{\widehat{f}} = \boldsymbol{\gamma} \cdot \dot{\boldsymbol{t}} - \tilde{\lambda} h \cdot \widetilde{H} \cdot h = \boldsymbol{\gamma} \cdot \widetilde{\boldsymbol{E}}^{\mathrm{d}} \cdot \left(\dot{\boldsymbol{w}} - \tilde{\lambda} \boldsymbol{\gamma}\right) - \tilde{\lambda} h \cdot \widetilde{H} \cdot h = 0 \tag{3.37}$$

so that the localized Lagrangian multiplier $\tilde{\lambda} > 0$ is solved as

$$\tilde{\lambda} = \frac{\boldsymbol{\gamma} \cdot \widetilde{\boldsymbol{E}}^{\mathrm{d}} \cdot \dot{\boldsymbol{w}}}{\boldsymbol{\gamma} \cdot \widetilde{\boldsymbol{E}}^{\mathrm{d}} \cdot \boldsymbol{\gamma} + h \cdot \widetilde{H} \cdot h} = \frac{\boldsymbol{\gamma} \cdot \dot{\boldsymbol{t}}}{h \cdot \widetilde{H} \cdot h} \tag{3.38}$$

for the softening modulus $\widetilde{H} := \partial q / \partial \tilde{\kappa} < 0$.

Combination of Eqs. (3.29) and (3.33) then yields the following rate constitutive relations

$$\dot{\boldsymbol{t}} = \widetilde{\boldsymbol{E}} \cdot \left(\dot{\boldsymbol{w}} - \tilde{\lambda} \boldsymbol{\gamma} \right) = \widetilde{\boldsymbol{E}}^{\mathrm{d}}_{\mathrm{tan}} \cdot \dot{\boldsymbol{w}} \tag{3.39a}$$

$$\dot{\boldsymbol{w}} = \widetilde{\boldsymbol{C}} \cdot \boldsymbol{t} + \tilde{\lambda} \boldsymbol{\gamma} = \widetilde{\boldsymbol{C}}^{\mathrm{d}}_{\mathrm{tan}} \cdot \dot{\boldsymbol{t}} \tag{3.39b}$$

where the tangent stiffness and compliance are expressed as

$$\widetilde{\boldsymbol{E}}^{\mathrm{d}}_{\mathrm{tan}} = \widetilde{\boldsymbol{E}}^{\mathrm{d}} - \frac{\widetilde{\boldsymbol{E}}^{\mathrm{d}} \cdot (\boldsymbol{\gamma} \otimes \boldsymbol{\gamma}) \cdot \widetilde{\boldsymbol{E}}^{\mathrm{d}}}{\boldsymbol{\gamma} \cdot \widetilde{\boldsymbol{E}}^{\mathrm{d}} \cdot \boldsymbol{\gamma} + h \cdot \widetilde{H} \cdot h} \tag{3.40a}$$

$$\widetilde{\boldsymbol{C}}^{\mathrm{d}}_{\mathrm{tan}} = \widetilde{\boldsymbol{C}}^{\mathrm{d}} + \frac{\boldsymbol{\gamma} \otimes \boldsymbol{\gamma}}{h \cdot \widetilde{H} \cdot h} \tag{3.40b}$$

both being symmetric due to the associated evolution laws adopted.

Remark 3.4 Calling for the evolution laws (3.33) $\sim$ (3.36), the energy dissipation (3.32) is evaluated as

$$\widetilde{\mathscr{D}} = \left(1 - \frac{1}{2}\xi\right) \tilde{\lambda} \boldsymbol{\gamma} \cdot \boldsymbol{t} + (q^0 - q) \cdot \dot{\tilde{\kappa}} = \left(q^0 - \frac{1}{2}\xi q\right) \cdot \dot{\tilde{\kappa}} \geq 0 \tag{3.41}$$

where the relation (3.19) has been considered for an active discontinuity. As can be seen, non-negative energy dissipation is automatically guaranteed for any softening law $q(\tilde{\kappa}) \leq q^0$. $\square$

3.3.2. Regularized cohesive model for the discontinuity band

Correspondingly to the decomposition (3.24), the inelastic deformation vector $\boldsymbol{e} := \boldsymbol{w}/b$ and the resulting inelastic strain $\boldsymbol{\epsilon}^{\mathrm{in}}$ admit similar additive forms

$$\boldsymbol{e} = \boldsymbol{e}^{\mathrm{d}} + \boldsymbol{e}^{\mathrm{p}}, \qquad \boldsymbol{\epsilon}^{\mathrm{in}} = \boldsymbol{\epsilon}^{\mathrm{d}} + \boldsymbol{\epsilon}^{\mathrm{p}} \tag{3.42}$$

where the damage and plastic strains $(\boldsymbol{\epsilon}^{\mathrm{d}}, \boldsymbol{\epsilon}^{\mathrm{p}})$, localized within the discontinuity band, are expressed as

$$\boldsymbol{\epsilon}^{\mathrm{d}} = \left(\boldsymbol{e}^{\mathrm{d}} \otimes \boldsymbol{n}\right)^{\mathrm{sym}} \Xi_{\mathcal{B}}, \qquad \boldsymbol{\epsilon}^{\mathrm{p}} = \left(\boldsymbol{e}^{\mathrm{p}} \otimes \boldsymbol{n}\right)^{\mathrm{sym}} \Xi_{\mathcal{B}} \tag{3.43}$$

for the recoverable and unrecoverable deformation vectors $\boldsymbol{e}^{\mathrm{d}} := \boldsymbol{w}^{\mathrm{d}}/b$ and $\boldsymbol{e}^{\mathrm{p}} := \boldsymbol{w}^{\mathrm{p}}/b$, respectively.

Similarly to the inelastic strain $(3.5)_2$, the inelastic free energy density field ψ^{in} is expressed as

$$\psi^{\mathrm{in}} = \overline{\psi}^{\mathrm{in}} \Xi_{\mathcal{B}}, \qquad \overline{\psi}^{\mathrm{in}} = \overline{\psi}^{\mathrm{d}}(\boldsymbol{e}^{\mathrm{d}}, \boldsymbol{E}^{\mathrm{d}}) + \overline{\chi}(\kappa) \tag{3.44}$$

where the damage free energy function $\overline{\psi}^{\mathrm{d}}(\cdot, \cdot)$ is expressed in terms of the stiffness $\boldsymbol{E}^{\mathrm{d}}$ of the discontinuity band

$$\overline{\psi}^{\mathrm{d}} = \frac{1}{2} \boldsymbol{e}^{\mathrm{d}} \cdot \boldsymbol{E}^{\mathrm{d}} \cdot \boldsymbol{e}^{\mathrm{d}} \tag{3.45}$$

The inelastic potential function $\overline{\chi}(\cdot)$ is characterized by the *strain*-like internal variable κ.

In this case, the second law of thermodynamics (3.9) becomes

$$\int_{\Omega} \mathscr{D}\, \mathrm{d}\Omega = \int_{\mathcal{B}} \left(\boldsymbol{t} \cdot \dot{\boldsymbol{e}} - \dot{\overline{\psi}}^{\mathrm{in}} \right) \mathrm{d}\mathcal{B} \geq 0 \tag{3.46}$$

Standard arguments yield the following regularized cohesive relations

$$\boldsymbol{t} = \frac{\partial \overline{\psi}^{\mathrm{d}}}{\partial \boldsymbol{e}^{\mathrm{d}}} = \boldsymbol{E}^{\mathrm{d}} \cdot \boldsymbol{e}^{\mathrm{d}} = \boldsymbol{E}^{\mathrm{d}} \cdot \left(\boldsymbol{e} - \boldsymbol{e}^{\mathrm{p}} \right), \qquad \boldsymbol{e}^{\mathrm{d}} = \boldsymbol{e} - \boldsymbol{e}^{\mathrm{p}} = \boldsymbol{C}^{\mathrm{d}} \cdot \boldsymbol{t} \tag{3.47}$$

or the rate forms

$$\dot{\boldsymbol{t}} = \boldsymbol{E}^{\mathrm{d}} \cdot \left(\dot{\boldsymbol{e}} - \dot{\boldsymbol{e}}^{\mathrm{dis}} \right), \qquad \dot{\boldsymbol{e}} = \boldsymbol{C}^{\mathrm{d}} \cdot \dot{\boldsymbol{t}} + \dot{\boldsymbol{e}}^{\mathrm{dis}} \tag{3.48}$$

where the second-order tensor $\boldsymbol{C}^{\mathrm{d}} = \left(\boldsymbol{E}^{\mathrm{d}} \right)^{-1}$ represents the compliance of the discontinuity band; the *dissipative deformation rate* $\dot{\boldsymbol{e}}^{\mathrm{dis}}$ is defined as

$$\dot{\boldsymbol{e}}^{\mathrm{dis}} = \dot{\boldsymbol{C}}^{\mathrm{d}} \cdot \boldsymbol{t} + \dot{\boldsymbol{e}}^{\mathrm{p}} \tag{3.49}$$

with $\dot{\boldsymbol{C}}^{\mathrm{d}} \cdot \boldsymbol{t}$ and $\dot{\boldsymbol{e}}^{\mathrm{p}}$ being its damage and plastic components, respectively; see Fig. 5.

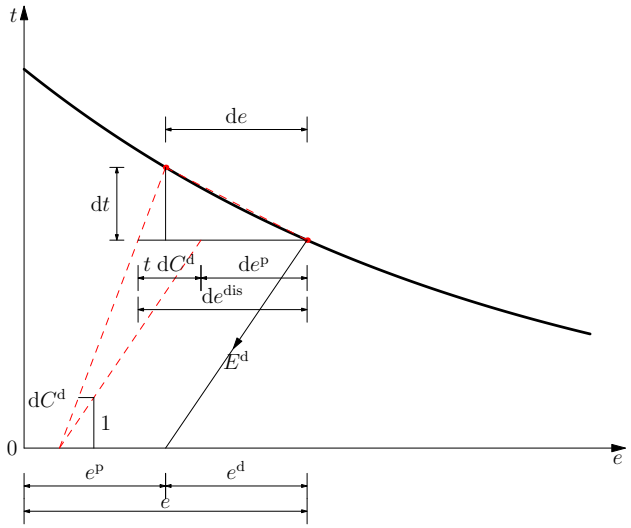

Figure 5: 1D definition of the dissipative deformation rate and its damage/plastic components for an increment deformation

Moreover, the second law of thermodynamics (3.46) gives the following energy dissipation inequality

$$\int_{\Omega} \mathscr{D}\, \mathrm{d}\Omega = \int_{\mathcal{B}} \overline{\mathscr{D}}\, \mathrm{d}\mathcal{B} \geq 0 \tag{3.50}$$

for the localized energy dissipation $\overline{\mathscr{D}}$

$$\overline{\mathscr{D}} = \frac{1}{2} \boldsymbol{t} \cdot \dot{\boldsymbol{C}}^{\mathrm{d}} \cdot \boldsymbol{t} + \boldsymbol{t} \cdot \dot{\boldsymbol{e}}^{\mathrm{p}} + \left(q^{0} - q \right) \cdot \dot{\kappa} \geq 0 \tag{3.51}$$

where $q^0 - q := -\partial\bar{\chi}/\partial\kappa$ is work conjugate to the strain-like internal variable κ, with q^0 being the initial failure strength $q(\kappa)$, i.e., $q^0 := q(\kappa = 0)$.

Similarly to the strong discontinuity model, the evolution laws for the internal variables $\{\boldsymbol{C}^{\mathrm{d}}, \boldsymbol{e}^{\mathrm{p}}, \kappa\}$ are derived from the maximization conditions of the energy dissipation $\bar{\mathscr{D}}$ constrained by the traction-based failure criterion (3.13), i.e.,

$$\dot{\boldsymbol{e}}^{\mathrm{dis}} = \dot{\lambda}\boldsymbol{\gamma}, \qquad \dot{\kappa} = \lambda h \tag{3.52}$$

where the dissipative flow vector $\boldsymbol{\gamma} = \widehat{\boldsymbol{\gamma}}$ and softening function $h = \widehat{h}$ are also given in Eq. (3.14); the regularized Lagrangian multiplier λ satisfies the Kuhn-Tucker loading/unloading rules

$$\lambda \geq 0, \qquad \widehat{f} \leq 0, \qquad \lambda\,\widehat{f} = 0 \tag{3.53}$$

Furthermore, a material parameter $\xi \in [0, 1]$ is introduced so that

$$\dot{\boldsymbol{e}}^{\mathrm{p}} = (1-\xi)\,\dot{\boldsymbol{e}}^{\mathrm{dis}} = (1-\xi)\,\lambda\boldsymbol{\gamma} \tag{3.54a}$$

$$\dot{\boldsymbol{C}}^{\mathrm{d}} \cdot \boldsymbol{t} = \xi\,\dot{\boldsymbol{e}}^{\mathrm{dis}} = \xi\,\lambda\boldsymbol{\gamma} \qquad \Longrightarrow \qquad \dot{\boldsymbol{C}}^{\mathrm{d}} = \xi\,\lambda\frac{\boldsymbol{\gamma}\otimes\boldsymbol{\gamma}}{\boldsymbol{\gamma}\cdot\boldsymbol{t}} \tag{3.54b}$$

as long as $\boldsymbol{\gamma}\cdot\boldsymbol{t} \neq 0$.

For an active discontinuity band, it follows from the consistency condition $\dot{\widehat{f}}(\boldsymbol{t}, q) = 0$ that

$$\dot{\widehat{f}} = \boldsymbol{\gamma}\cdot\dot{\boldsymbol{t}} - \lambda h\cdot H\cdot h = \boldsymbol{\gamma}\cdot\boldsymbol{E}^{\mathrm{d}}\cdot\left(\dot{\boldsymbol{e}} - \lambda\boldsymbol{\gamma}\right) - \lambda h\cdot H\cdot h = 0 \tag{3.55}$$

Accordingly, the regularized Lagrangian multiplier $\lambda > 0$ is solved as

$$\lambda = \frac{\boldsymbol{\gamma}\cdot\boldsymbol{E}^{\mathrm{d}}\cdot\dot{\boldsymbol{e}}}{\boldsymbol{\gamma}\cdot\boldsymbol{E}^{\mathrm{d}}\cdot\boldsymbol{\gamma} + h\cdot H\cdot h} = \frac{\boldsymbol{\gamma}\cdot\dot{\boldsymbol{t}}}{h\cdot H\cdot h} \tag{3.56}$$

for the strain-driven softening modulus $H := \partial q/\partial\kappa < 0$.

Therefore, the rate constitutive relations for the regularized discontinuity are expressed as

$$\dot{\boldsymbol{t}} = \boldsymbol{E}^{\mathrm{d}}\cdot\left(\dot{\boldsymbol{e}} - \lambda\boldsymbol{\gamma}\right) = \boldsymbol{E}^{\mathrm{d}}_{\mathrm{tan}}\cdot\dot{\boldsymbol{e}} \tag{3.57a}$$

$$\dot{\boldsymbol{e}} = \boldsymbol{C}^{\mathrm{d}}\cdot\dot{\boldsymbol{t}} + \lambda\boldsymbol{\gamma} = \boldsymbol{C}^{\mathrm{d}}_{\mathrm{tan}}\cdot\dot{\boldsymbol{t}} \tag{3.57b}$$

with the following tangent stiffness and compliance

$$\boldsymbol{E}^{\mathrm{d}}_{\mathrm{tan}} = \boldsymbol{E}^{\mathrm{d}} - \frac{\boldsymbol{E}^{\mathrm{d}}\cdot\left(\boldsymbol{\gamma}\otimes\boldsymbol{\gamma}\right)\cdot\boldsymbol{E}^{\mathrm{d}}}{\boldsymbol{\gamma}\cdot\boldsymbol{E}^{\mathrm{d}}\cdot\boldsymbol{\gamma} + h\cdot H\cdot h} \tag{3.58a}$$

$$\boldsymbol{C}^{\mathrm{d}}_{\mathrm{tan}} = \boldsymbol{C}^{\mathrm{d}} + \frac{\boldsymbol{\gamma}\otimes\boldsymbol{\gamma}}{h\cdot H\cdot h} \tag{3.58b}$$

As expected, the above tangent tensors are also symmetric due to the associated evolution laws adopted.

3.3.3. Fracture energy and the equivalence conditions

For a strong discontinuity with the singular inelastic free energy (3.25), it follows from Eq. (3.12) that

$$W = \int_{\mathcal{S}} \int_0^\infty \left(\dot{\tilde{\chi}} + \tilde{\mathscr{D}} \right) \mathrm{d}T \, \mathrm{d}\mathcal{S} = \int_{\mathcal{S}} \int_0^\infty \left(\frac{1}{2} \, \boldsymbol{t} \cdot \dot{\tilde{\boldsymbol{C}}}^{\mathrm{d}} \cdot \boldsymbol{t} + \boldsymbol{t} \cdot \dot{\boldsymbol{w}}^{\mathrm{p}} \right) \mathrm{d}T \, \mathrm{d}\mathcal{S} \tag{3.59}$$

Substitution of the evolution laws $(3.33)_2$ and (3.35) yields the fracture energy G_{f}, defined as energy dissipation per unit of discontinuity area $A_{\mathcal{S}}$, i.e.,

$$G_{\mathrm{f}} := \frac{W}{A_{\mathcal{S}}} = \left(1 - \frac{1}{2}\xi\right) \int_0^\infty \tilde{\lambda} \boldsymbol{\gamma} \, \mathrm{d}T = \left(1 - \frac{1}{2}\xi\right) \int_0^\infty q(\tilde{\kappa}) \, \mathrm{d}\tilde{\kappa} \tag{3.60}$$

where the relation (3.19) has been considered. Once the displacement-driven softening law $q(\tilde{\kappa})$ is given, the fracture energy G_{f} can be evaluated explicitly from Eq. (3.60). In other words, the parameters involved in the softening law $q(\tilde{\kappa})$ can be determined for the given fracture energy G_{f}, usually regarded as a material property.

Similarly, for the regularized discontinuity with the inelastic free energy (3.44), Eq. (3.12) gives

$$W = \int_{\mathcal{B}} \int_0^\infty \left(\dot{\bar{\chi}} + \bar{\mathscr{D}} \right) \mathrm{d}T \, \mathrm{d}\mathcal{B} = \int_{\mathcal{B}} \int_0^\infty \left(\frac{1}{2} \, \boldsymbol{t} \cdot \dot{\boldsymbol{C}}^{\mathrm{d}} \cdot \boldsymbol{t} + \boldsymbol{t} \cdot \dot{\boldsymbol{e}}^{\mathrm{p}} \right) \mathrm{d}T \, \mathrm{d}\mathcal{B} \tag{3.61}$$

Calling for the relation (3.19) and the evolution laws (3.54), the fracture energy G_{f} is evaluated as

$$G_{\mathrm{f}} := \frac{W}{A_{\mathcal{S}}} = \frac{W}{V_{\mathcal{B}}/b} = b\left(1 - \frac{1}{2}\xi\right) \int_0^\infty \lambda \boldsymbol{\gamma} \, \mathrm{d}T = b\left(1 - \frac{1}{2}\xi\right) \int_0^\infty q(\kappa) \, \mathrm{d}\kappa \tag{3.62}$$

for the volume $V_{\mathcal{B}} = bA_{\mathcal{S}}$ of the discontinuity band. It can be concluded that for the given fracture energy G_{f}, the softening function $q(\kappa)$ also depends on the band width b.

The fracture energy (3.62) allows introducing the so-called specific fracture energy g_{f}, i.e., the dissipation per unit volume of the discontinuity band $V_{\mathcal{B}}$, in a straightforward manner

$$g_{\mathrm{f}} := \frac{W}{V_{\mathcal{B}}} = \int_0^\infty \boldsymbol{\sigma} : \dot{\boldsymbol{\epsilon}} \, \mathrm{d}T = \frac{1}{b} G_{\mathrm{f}} \tag{3.63}$$

This is exactly the relation between the crack band theory [5] and the fictitious crack model [22].

For the case of a vanishing band width $b \to 0$, the relation $g_{\mathrm{f}} = G_{\mathrm{f}} \, \delta_{\mathcal{S}}$ holds. It then follows that

$$W = \int_{\mathcal{B}} g_{\mathrm{f}} \, \mathrm{d}\mathcal{B} = \int_{\mathcal{B}} G_{\mathrm{f}} \, \delta_{\mathcal{S}} \, \mathrm{d}\mathcal{B} = \int_{\mathcal{S}} G_{\mathrm{f}} \, \mathrm{d}\mathcal{S} \tag{3.64}$$

which recovers the classical definition of fracture energy.

For the same traction-based failure criterion $\widehat{f}(\boldsymbol{t}, q) \leq 0$ and equivalent softening laws $q(\kappa) = q(\tilde{\kappa})$, the results (3.60) and (3.62) imply that identical fracture energies G_{f} can be obtained for both models, providing that

$$\kappa = \frac{1}{b}\tilde{\kappa}, \qquad \dot{\kappa} = \frac{1}{b}\dot{\tilde{\kappa}} \qquad \Longleftrightarrow \qquad \lambda = \frac{1}{b}\tilde{\lambda}, \qquad \frac{1}{H} = \frac{1}{b}\frac{1}{\widetilde{H}} \tag{3.65}$$

Upon satisfying the above conditions, it follows from the damage evolution laws (3.36) and (3.54b) that

$$\boldsymbol{C}^{\mathrm{d}} = \frac{1}{b}\tilde{\boldsymbol{C}}^{\mathrm{d}}, \qquad \tilde{\boldsymbol{E}}^{\mathrm{d}} = \frac{1}{b}\boldsymbol{E}^{\mathrm{d}} \tag{3.66}$$

That is, the strong discontinuity transforms into an equivalent regularized counterpart with a finite band width $b \nrightarrow 0$.

Contrariwise, for the regularized discontinuity with a vanishing band width $b \to 0$, the conditions (3.65) become

$$\kappa = \tilde{\kappa}\delta_s, \qquad \dot{\kappa} = \dot{\tilde{\kappa}}\delta_s \qquad \Longleftrightarrow \qquad \lambda = \tilde{\lambda}\delta_s, \qquad \frac{1}{H} = \frac{1}{\widetilde{H}}\delta_s \tag{3.67}$$

so that the following relations hold

$$\boldsymbol{C}^{\mathrm{d}} = \widetilde{\boldsymbol{C}}^{\mathrm{d}}\delta_s, \qquad \widetilde{\boldsymbol{E}}^{\mathrm{d}} = \boldsymbol{E}^{\mathrm{d}}\delta_s \tag{3.68}$$

In this case, the regularized discontinuity localizes into an equivalent strong discontinuity.

As can be seen, all the kinematic variables are inversely proportional to the band width b for the regularized discontinuity or even singular for a strong one. ***The above results, together with kinematic equivalence stated in Remark 2.1, clearly show that the strong and regularized discontinuity approaches are consistently related.***

3.4. Embedded/smeared discontinuity approaches

Providing the cohesive model for the discontinuity (band) is known, e.g., as developed in Section 3.3, it is possible to establish alternative embedded/smeared discontinuity approaches.

In such approaches, the weak form of the governing equation $(2.6)_1$ and the traction boundary condition $(2.7)_1$ can be re-stated as: Find $\boldsymbol{u} \in \mathscr{U}$ such that

$$\int_{\Omega} \nabla^{\mathrm{sym}}\delta\boldsymbol{u} : \boldsymbol{\sigma}\, \mathrm{d}\Omega = \int_{\Omega} \delta\boldsymbol{u}\cdot\boldsymbol{b}^{*}\, \mathrm{d}\Omega + \int_{\Gamma_t} \delta\boldsymbol{u}\cdot\boldsymbol{t}^{*}\, \mathrm{d}\Gamma \qquad \forall\delta\boldsymbol{u} \in \mathcal{V} \tag{3.69}$$

with the stress $\boldsymbol{\sigma}_s$ at the discontinuity (band) determined from an inelastic material model satisfying the static constraint (3.11). Here, $\mathscr{U}$ is the trial space introduced in Eq. (3.21a) for a strong discontinuity or in Eq. (3.23a) for a regularized one; the standard test space $\mathcal{V}$ is defined as

$$\mathcal{V} := \left\{\delta\boldsymbol{u} \text{ of sufficient regularity} \middle| \delta\boldsymbol{u} = \boldsymbol{0} \text{ on } \Gamma_u\right\} \tag{3.70}$$

As can be seen, the traction continuity condition $(2.6)_2$ and the displacement jump $\boldsymbol{w}$ (or the inelastic deformation vector $\boldsymbol{e}$) are not explicitly considered in the weak form (3.69). But rather, they are accounted for indirectly at the local (material constitutive) level through the inelastic material models fulfilling the classical static constraint (3.11). Owing to the equivalence shown in Section 3.3.3, only the smeared discontinuity model employing the regularized kinematics (2.2) is addressed. Its correspondence to the embedded counterpart is briefly discussed in Remark 3.5.

To derive the smeared discontinuity model, let us recall the constitutive relations (3.8) and (3.57a). It follows from the static constraint $(3.11)_2$ that

$$\boldsymbol{E}^{\mathrm{d}}_{\mathrm{tan}}\cdot\dot{\boldsymbol{e}} = \mathbb{E}^{0} : \left[\dot{\boldsymbol{\epsilon}} - \left(\dot{\boldsymbol{e}}\otimes\boldsymbol{n}\right)^{\mathrm{sym}}\right]\cdot\boldsymbol{n} = \left(\mathbb{E}^{0} : \dot{\boldsymbol{\epsilon}}\right)\cdot\boldsymbol{n} - \left(\boldsymbol{n}\cdot\mathbb{E}^{0}\cdot\boldsymbol{n}\right)\cdot\dot{\boldsymbol{e}} \tag{3.71}$$

Accordingly, the inelastic deformation vector rate $\dot{\boldsymbol{e}}$ is determined in terms of the strain rate $\dot{\boldsymbol{\epsilon}}$ as

$$\dot{\boldsymbol{e}} = \left(\boldsymbol{E}^{\mathrm{d}}_{\mathrm{tan}} + \boldsymbol{n}\cdot\mathbb{E}^{0}\cdot\boldsymbol{n}\right)^{-1}\cdot\left(\mathbb{E}^{0} : \dot{\boldsymbol{\epsilon}}\right)\cdot\boldsymbol{n} \tag{3.72}$$

Therefore, the stress rate $\dot{\boldsymbol{\sigma}}$ is given from Eq. (3.8), i.e.,

$$\dot{\boldsymbol{\sigma}} = \mathbb{E}^0 : \left[\dot{\boldsymbol{\epsilon}} - \left(\dot{\boldsymbol{e}} \otimes \boldsymbol{n}\right)^{\text{sym}}\right] = \mathbb{E}_{\text{tan}} : \dot{\boldsymbol{\epsilon}} \tag{3.73}$$

where the tangent stiffness tensor $\mathbb{E}_{\text{tan}}$ is expressed as

$$\mathbb{E}_{\text{tan}} = \mathbb{E}^0 - \mathbb{E}^0 : \left[\left(\boldsymbol{E}^{\text{d}}_{\text{tan}} + \boldsymbol{n} \cdot \mathbb{E}^0 \cdot \boldsymbol{n}\right)^{-1} \overline{\otimes} \boldsymbol{N}\right]^{\text{sym}} : \mathbb{E}^0 \tag{3.74}$$

with a second-order geometric tensor $\boldsymbol{N} := \boldsymbol{n} \otimes \boldsymbol{n}$.

Alternatively, it follows from the relation (3.57b) and the static constraint $(3.11)_2$ that

$$\dot{\boldsymbol{\epsilon}}^{\text{in}} = \left(\dot{\boldsymbol{e}} \otimes \boldsymbol{n}\right)^{\text{sym}} = \left[\left(\boldsymbol{C}^{\text{d}}_{\text{tan}} \cdot \dot{\boldsymbol{\sigma}} \cdot \boldsymbol{n}\right) \otimes \boldsymbol{n}\right]^{\text{sym}} = \left(\boldsymbol{C}^{\text{d}}_{\text{tan}} \overline{\otimes} \boldsymbol{N}\right)^{\text{sym}} : \dot{\boldsymbol{\sigma}} \tag{3.75}$$

The strain rate $\dot{\boldsymbol{\epsilon}}$ is given from Eq. (3.3)

$$\dot{\boldsymbol{\epsilon}} = \dot{\boldsymbol{\epsilon}}^{\text{e}} + \dot{\boldsymbol{\epsilon}}^{\text{in}} = \mathbb{C}_{\text{tan}} : \dot{\boldsymbol{\sigma}} \tag{3.76}$$

for the tangent compliance $\mathbb{C}_{\text{tan}}$ expressed as

$$\mathbb{C}_{\text{tan}} = \mathbb{C}^0 + \left(\boldsymbol{C}^{\text{d}}_{\text{tan}} \overline{\otimes} \boldsymbol{N}\right)^{\text{sym}} \tag{3.77}$$

Note that the tangent compliance $\mathbb{C}_{\text{tan}}$ can also be directly derived from Eq. (3.74) through the Sherman-Morrison-Woodburg formula [18].

The above constitutive relations correspond exactly to those in the smeared crack model [54–56], as an extension of the original form proposed by Rashid [50]. As can be seen, owning to stress continuity (3.10) upon strain localization, the kinematic unknowns $\boldsymbol{w}$ (or $\boldsymbol{e} := \boldsymbol{w}/b$) can be eliminated at the local material-point level through the static constraint (3.11), resulting in a single constitutive model to describe the overall inelastic behavior of the solid.

Remark 3.5 If the singular kinematics (2.1) is adopted, constitutive relations similarly to Eqs. (3.73) and (3.76) can be obtained for the embedded discontinuity model, after accounting for the relations (3.68). For instance, the inelastic strain rate $\dot{\boldsymbol{\epsilon}}^{\text{in}}$ is expressed as

$$\dot{\boldsymbol{\epsilon}}^{\text{in}} = \left(\tilde{\boldsymbol{C}}^{\text{d}}_{\text{tan}} \overline{\otimes} \boldsymbol{N}\right)^{\text{sym}} \delta_s : \dot{\boldsymbol{\sigma}} \tag{3.78}$$

so that the tangent compliance in Eq. (3.76) becomes

$$\mathbb{C}_{\text{tan}} = \mathbb{C}^0 + \left(\tilde{\boldsymbol{C}}^{\text{d}}_{\text{tan}} \overline{\otimes} \boldsymbol{N}\right)^{\text{sym}} \delta_s \tag{3.79}$$

Other correspondences can be similarly established; the details are omitted here. □

Remark 3.6 Calling for the decomposition (3.24) or (3.42), the strain $\boldsymbol{\epsilon}$ at the discontinuity (band) is additively split into its elastic, damage and plastic parts

$$\boldsymbol{\epsilon} = \boldsymbol{\epsilon}^{\text{e}} + \boldsymbol{\epsilon}^{\text{in}} = \boldsymbol{\epsilon}^{\text{e}} + \boldsymbol{\epsilon}^{\text{d}} + \boldsymbol{\epsilon}^{\text{p}} \tag{3.80}$$

This is the kinematic decomposition suggested by Armero and Oller [2]; see Fig. 6. Accordingly, the above embedded/smeared discontinuity models fit the framework developed in that reference. As shown in next section, an equivalent traction-based elastoplastic damage model can be developed based on an alternative kinematic decomposition. □

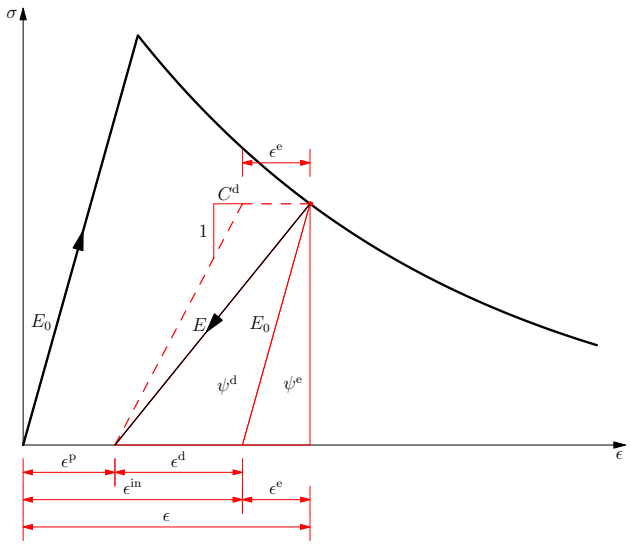

Figure 6: Different kinematic decompositions adopted in the elastoplastic damage framework

4. Strain localization of inelastic solids

In the methodology employed in Section 3, it is implicitly assumed *a priori* that strain localization occurs with a continuous stress field and the discontinuity (band) orientation is already known. However, on one hand, whether such strain localization can occur has not been checked yet; even though it can, the effects of stress continuity on the discontinuity orientation have not been identified, either. On the other hand, the traction-based failure criterion characterizing the discontinuity (band) is usually introduced in a heuristic or even *ad hoc* manner, and it is hard to determine the involved parameters from available experimental data.

In this section, an alternative methodology, i.e., strain localization in inelastic softening solids, is considered. As is well-known, for strain localization to occur in a softening solid and to develop eventually into a fully softened discontinuity at the final stage of the deformation process, material points inside the discontinuity (band) undergo inelastic loading while those outside it unload elastically [11, 40, 41]. This fact imposes a kinematic constraint on the discontinuity kinematics. Application of the resulting kinematic condition to an inelastic material model, e.g., a thermodynamically consistent unified elastoplastic damage model considered in this section, naturally yields all the ingredients characterizing the discontinuity (band), i.e., localized constitutive laws, traction-based failure criterion and discontinuity orientation, etc.

4.1. Maxwell's kinematic constraint upon strain localization

To discuss the stress field $\boldsymbol{\sigma}$ around the discontinuity (band), let us consider the generic inelastic constitutive relations (3.7) or the rate forms (3.8). Owing to the strain continuity (2.4) at both sides of the discontinuity (band), the stresses $\boldsymbol{\sigma}_{\mathcal{S}}^{+} := \boldsymbol{\sigma}(\boldsymbol{x} \in \Omega^{+} \cap \mathcal{S}^{+})$ "ahead of" the surface $\mathcal{S}^{+}$ and $\boldsymbol{\sigma}_{\mathcal{S}}^{-} := \boldsymbol{\sigma}(\boldsymbol{x} \in \Omega^{-} \cap \mathcal{S}^{-})$ "behind" the surface $\mathcal{S}^{-}$ are equal and denoted by $\boldsymbol{\sigma}_{\mathcal{S}}^{\pm}$. Being the material outside the discontinuity (band) elastic, they are determined as

$$\boldsymbol{\sigma}_{\mathcal{S}}^{+} = \boldsymbol{\sigma}_{\mathcal{S}}^{-} = \boldsymbol{\sigma}_{\mathcal{S}}^{\pm} = \mathbb{E}^{0} : \boldsymbol{\epsilon}_{\mathcal{S}}^{\pm} \tag{4.1}$$

Comparatively, the stress $\boldsymbol{\sigma}_{\mathcal{S}} := \boldsymbol{\sigma}(\boldsymbol{x} \in \mathcal{S})$ at the discontinuity (band) is expressed as

$$\boldsymbol{\sigma}_{\mathcal{S}} = \mathbb{E}^{0} : \boldsymbol{\epsilon}_{\mathcal{S}}^{\mathrm{e}} = \mathbb{E}^{0} : \left(\boldsymbol{\epsilon}_{\mathcal{S}} - \boldsymbol{\epsilon}_{\mathcal{S}}^{\mathrm{in}}\right) \tag{4.2}$$

for the corresponding elastic and inelastic strains $(\boldsymbol{\epsilon}_{\mathcal{S}}^{\mathrm{e}}, \boldsymbol{\epsilon}_{\mathcal{S}}^{\mathrm{in}})$. Accordingly, the stress jump $[\![\boldsymbol{\sigma}]\!] := \boldsymbol{\sigma}_{\mathcal{S}} - \boldsymbol{\sigma}_{\mathcal{S}}^{\pm}$ is given by

$$[\![\boldsymbol{\sigma}]\!] = \mathbb{E}^{0} : \left([\![\boldsymbol{\epsilon}]\!] - \boldsymbol{\epsilon}_{\mathcal{S}}^{\mathrm{in}}\right) = \mathbb{E}^{0} : \left[\left(\boldsymbol{e} \otimes \boldsymbol{n}\right)^{\mathrm{sym}} - \boldsymbol{\epsilon}_{\mathcal{S}}^{\mathrm{in}}\right] \tag{4.3}$$

where the strain jump $[\![\boldsymbol{\epsilon}]\!]$ is described by Maxwell's compatibility condition (2.5).

Once the discontinuity (band) forms, the traction continuity condition $(2.6)_2$ has to be fulfilled, i.e.,

$$[\![\boldsymbol{t}]\!] := \boldsymbol{\sigma}_{\mathcal{S}} \cdot \boldsymbol{n} - \boldsymbol{\sigma}_{\mathcal{S}}^{\pm} \cdot \boldsymbol{n} = [\![\boldsymbol{\sigma}]\!] \cdot \boldsymbol{n} = \boldsymbol{0} \tag{4.4}$$

Note that, owing to the relation (4.1) traction continuity between $\boldsymbol{\sigma}_{\mathcal{S}}^{+} \cdot \boldsymbol{n}$ and $\boldsymbol{\sigma}_{\mathcal{S}}^{-} \cdot \boldsymbol{n}$, necessary for the balance laws [39, 60], is automatically satisfied.

As the strains $\boldsymbol{\epsilon}_{\mathcal{S}}^{\pm}$ and the resulting stresses $\boldsymbol{\sigma}_{\mathcal{S}}^{\pm}$ outside the discontinuity (band) are regular, the traction continuity condition $(2.6)_2$ requires that both the traction $\boldsymbol{t} = \boldsymbol{\sigma}_{\mathcal{S}} \cdot \boldsymbol{n}$ and the stress $\boldsymbol{\sigma}_{\mathcal{S}}$ are bounded [42]. Therefore, though the strain jump $[\![\boldsymbol{\epsilon}]\!]$ and the inelastic strain $\boldsymbol{\epsilon}_{\mathcal{S}}^{\mathrm{in}}$ are both inversely proportional to the band width b (see Remark 4.4), the stress jump $[\![\boldsymbol{\sigma}]\!]$ has to be regular (bounded) and independent of b.

For the strong discontinuity with a vanishing band width $b \to 0$, stress boundedness requires *cancellation of the unbounded strain jump* [11, 40–42], i.e.,

$$\boxed{[\![\boldsymbol{\epsilon}]\!] = \boldsymbol{\epsilon}_{\mathcal{S}}^{\mathrm{in}} = \left(\boldsymbol{e} \otimes \boldsymbol{n}\right)^{\mathrm{sym}} = \frac{1}{b}\left(\boldsymbol{w} \otimes \boldsymbol{n}\right)^{\mathrm{sym}}} \tag{4.5}$$

This is equivalent to *satisfaction of the stress continuity condition* (3.10). As the stresses should not depend on the band width b, even if the deformation vector $\boldsymbol{e}$ and the strain $\boldsymbol{\epsilon}$ do, the above arguments also hold for the regularized discontinuity with a finite band width $b \nrightarrow 0$. Note that the stress continuity condition (3.10) and the equivalent kinematic constraint (4.5) can also be written in rate form.

The kinematic constraint (4.5) states that, ***if strain localization can occur with a continuous stress field, difference in the strains between interior and exterior points of the discontinuity (band), i.e., the strain jump characterized by Maxwell's compatibility condition, has to be completely inelastic***. This conclusion is consistent with

the methodology employed in the strong/regularized and embedded/smeared discontinuity approaches discussed in Section 3.

Remark 4.1 For a fully softened discontinuity (band) to develop at the final stage of the deformation process (i.e., the internal variable $\kappa \to \infty$), the bulk stresses have to unload completely and the transferred tractions should vanish, i.e.,

$$\lim_{\kappa\to\infty} \boldsymbol{\sigma} = \boldsymbol{0}, \qquad \lim_{\kappa\to\infty} \boldsymbol{t} = \boldsymbol{0} \tag{4.6}$$

In this case, the stress continuity condition (3.10) is also necessary for satisfaction of the above decohesion condition. Contrariwise, the traction continuity condition $(2.6)_2$ generally guarantees neither the stress continuity (3.10) nor the limit decohesion (4.6). Therefore, the stress continuity condition (3.10) is more stringent than the traction continuity condition $(2.6)_2$. □

4.2. A unified elastoplastic damage framework

To analyze strain localization in general inelastic softening solids, a thermodynamically consistent unified elastoplastic damage framework [31, 70] is presented in this section. Both stress- and traction-based elastoplastic damage models can be developed within this framework.

4.2.1. Stress–strain relations

To account for both stiffness degradation and irreversible deformations, the free energy density function ψ in Eq. (3.2) is postulated as

$$\psi = \psi^{\mathrm{ed}}(\boldsymbol{\epsilon} - \boldsymbol{\epsilon}^{\mathrm{p}}, \mathbb{E}) + \chi(\kappa) \tag{4.7}$$

where the stored strain energy density function $\psi^{\mathrm{ed}}(\cdot,\cdot)$ depends on the recoverable (elastic and damage) strain tensor $\boldsymbol{\epsilon} - \boldsymbol{\epsilon}^{\mathrm{p}}$ and the (variable) fourth-order material (unloading) stiffness tensor $\mathbb{E}$, with $\boldsymbol{\epsilon}^{\mathrm{p}}$ being the irreversible plastic strain tensor; $\chi(\cdot)$ is the inelastic potential function characterized by a single *strain-like* internal variable κ.

For a linear hyperelastic material, the stored strain energy density $\psi^{\mathrm{ed}}(\cdot,\cdot)$ can be expressed as a quadratic form

$$\psi^{\mathrm{ed}} = \frac{1}{2}\left(\boldsymbol{\epsilon} - \boldsymbol{\epsilon}^{\mathrm{p}}\right) : \mathbb{E} : \left(\boldsymbol{\epsilon} - \boldsymbol{\epsilon}^{\mathrm{p}}\right) \tag{4.8}$$

Making use of standard arguments yields the following constitutive relations

$$\boldsymbol{\sigma} = \frac{\partial \psi^{\mathrm{ed}}}{\partial\left(\boldsymbol{\epsilon} - \boldsymbol{\epsilon}^{\mathrm{p}}\right)} = \mathbb{E} : \left(\boldsymbol{\epsilon} - \boldsymbol{\epsilon}^{\mathrm{p}}\right) \tag{4.9a}$$

$$\boldsymbol{\epsilon} = \mathbb{C} : \boldsymbol{\sigma} + \boldsymbol{\epsilon}^{\mathrm{p}} \tag{4.9b}$$

for the (variable) fourth-order material (unloading) compliance tensor $\mathbb{C} = \mathbb{E}^{-1}$. As both the compliance $\mathbb{C}$ (or the stiffness $\mathbb{E}$) and the plastic strain $\boldsymbol{\epsilon}^{\mathrm{p}}$ are internal variables, their evolution laws have to be consistently postulated.

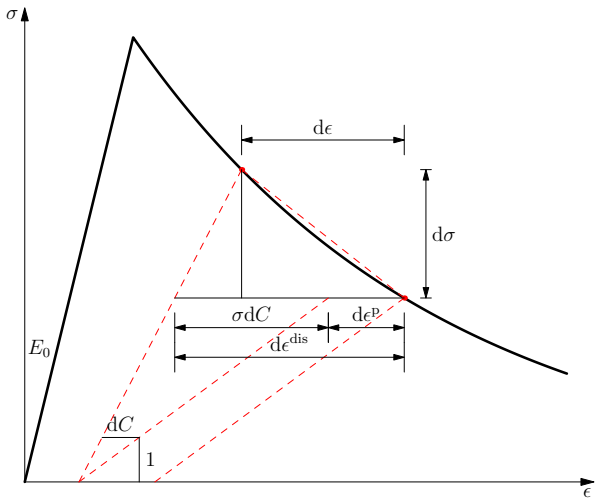

Figure 7: 1D definition of the dissipative strain rate and its damage/plastic components for an infinitesimal increment strain

By time differentiation, it follows that

$$\dot{\boldsymbol{\sigma}} = \mathbb{E} : \left(\dot{\boldsymbol{\epsilon}} - \dot{\boldsymbol{\epsilon}}^{\text{dis}}\right), \qquad \dot{\boldsymbol{\epsilon}} = \mathbb{C} : \dot{\boldsymbol{\sigma}} + \dot{\boldsymbol{\epsilon}}^{\text{dis}} \tag{4.10}$$

where the *dissipative strain tensor rate* $\dot{\boldsymbol{\epsilon}}^{\text{dis}}$ is defined as

$$\dot{\boldsymbol{\epsilon}}^{\text{dis}} := \dot{\mathbb{C}} : \boldsymbol{\sigma} + \dot{\boldsymbol{\epsilon}}^{\text{p}} \tag{4.11}$$

with $\dot{\mathbb{C}} : \boldsymbol{\sigma}$ and $\dot{\boldsymbol{\epsilon}}^{\text{p}}$ being its damage and plastic components, respectively; see Fig. 7. Note that the dissipative strain tensor rate $\dot{\boldsymbol{\epsilon}}^{\text{dis}}$ does not correspond to an actual "strain"; it is only defined in rate form when the involved energy dissipative mechanisms, i.e., damage evolution and plastic flows, are active.

As previously mentioned in Remark 3.6 and shown in Fig. 6, the strain tensor $\boldsymbol{\epsilon}$ and the rate $\dot{\boldsymbol{\epsilon}}$ can also be rewritten as the kinematic decomposition adopted in the classical smeared crack model [2, 54]

$$\boldsymbol{\epsilon} = \boldsymbol{\epsilon}^{\text{e}} + \boldsymbol{\epsilon}^{\text{in}} = \mathbb{C}^{\mathbf{0}} : \boldsymbol{\sigma} + \boldsymbol{\epsilon}^{\text{in}}, \qquad \dot{\boldsymbol{\epsilon}} = \dot{\boldsymbol{\epsilon}}^{\text{e}} + \dot{\boldsymbol{\epsilon}}^{\text{in}} = \mathbb{C}^{\mathbf{0}} : \dot{\boldsymbol{\sigma}} + \dot{\boldsymbol{\epsilon}}^{\text{in}} \tag{4.12}$$

so that

$$\boldsymbol{\sigma} = \mathbb{E}^{\mathbf{0}} : \boldsymbol{\epsilon}^{\text{e}} = \mathbb{E}^{\mathbf{0}} : \left(\boldsymbol{\epsilon} - \boldsymbol{\epsilon}^{\text{in}}\right), \qquad \dot{\boldsymbol{\sigma}} = \mathbb{E}^{\mathbf{0}} : \dot{\boldsymbol{\epsilon}}^{\text{e}} = \mathbb{E}^{\mathbf{0}} : \left(\dot{\boldsymbol{\epsilon}} - \dot{\boldsymbol{\epsilon}}^{\text{in}}\right) \tag{4.13}$$

with $\mathbb{E}^{\mathbf{0}}$ and $\mathbb{C}^{\mathbf{0}}$ being the elastic stiffness and compliance of the material, respectively. In the above constitutive relations, the elastic and inelastic strain tensors $(\boldsymbol{\epsilon}^{\text{e}}, \boldsymbol{\epsilon}^{\text{in}})$ are given by

$$\epsilon^{\text{e}} = \mathbb{C}^{\mathbf{0}} : \boldsymbol{\sigma}, \qquad \boldsymbol{\epsilon}^{\text{in}} = \boldsymbol{\epsilon}^{\text{d}} + \boldsymbol{\epsilon}^{\text{p}} = \mathbb{C}^{\text{d}} : \boldsymbol{\sigma} + \boldsymbol{\epsilon}^{\text{p}} \tag{4.14}$$

where the damage strain tensor $\epsilon^{\text{d}} := \mathbb{C}^{\text{d}} : \boldsymbol{\sigma}$ represents the *recoverable* inelastic strain; the fourth-order damage compliance $\mathbb{C}^{\text{d}}$ is defined as $\mathbb{C}^{\text{d}} := \mathbb{C} - \mathbb{C}^{\mathbf{0}}$, with identical evolution law $\dot{\mathbb{C}}^{\text{d}} = \dot{\mathbb{C}}$.

Remark 4.2 Similarly to the kinematic decomposition (4.12), the stored strain energy density (which is equal in magnitude to the complementary energy density for a linear hyperelastic material) ψ^{ed} defined in Eq. (4.8) can be decomposed as

$$\psi^{\mathrm{ed}} = \frac{1}{2}\,\boldsymbol{\sigma} : \mathbb{C} : \boldsymbol{\sigma} = \psi^{\mathrm{e}} + \psi^{\mathrm{d}} \tag{4.15}$$

where the elastic and damage strain energy densities (also equal in magnitude to their complementary counterparts) $(\psi^{\mathrm{e}}, \psi^{\mathrm{d}})$ are given by

$$\psi^{\mathrm{e}} = \frac{1}{2}\,\boldsymbol{\sigma} : \mathbb{C}^0 : \boldsymbol{\sigma} = \frac{1}{2}\,\boldsymbol{\sigma} : \boldsymbol{\epsilon}^{\mathrm{e}} = \frac{1}{2}\,\boldsymbol{\epsilon}^{\mathrm{e}} : \mathbb{E}^0 : \boldsymbol{\epsilon}^{\mathrm{e}} \tag{4.16a}$$

$$\psi^{\mathrm{d}} = \frac{1}{2}\,\boldsymbol{\sigma} : \mathbb{C}^{\mathrm{d}} : \boldsymbol{\sigma} = \frac{1}{2}\,\boldsymbol{\sigma} : \boldsymbol{\epsilon}^{\mathrm{d}} = \frac{1}{2}\,\boldsymbol{\epsilon}^{\mathrm{e}} : \mathbb{E}^0 : \boldsymbol{\epsilon}^{\mathrm{d}} \tag{4.16b}$$

Note again the recoverable nature of the damage strain $\boldsymbol{\epsilon}^{\mathrm{d}}$ and the corresponding energy density ψ^{d} upon unloading as shown in Fig. 6. ■

4.2.2. Evolution laws and rate constitutive relations

Besides the above constitutive relations, the following energy dissipation inequality has to be satisfied

$$\mathscr{D} = \frac{1}{2}\,\boldsymbol{\sigma} : \dot{\mathbb{C}} : \boldsymbol{\sigma} + \boldsymbol{\sigma} : \dot{\boldsymbol{\epsilon}}^{\mathrm{p}} - \dot{\chi} = \frac{1}{2}\,\boldsymbol{\sigma} : \dot{\mathbb{C}} : \boldsymbol{\sigma} + \boldsymbol{\sigma} : \dot{\boldsymbol{\epsilon}}^{\mathrm{p}} + \left(q^0 - q\right) \cdot \dot{\kappa} \geq 0 \tag{4.17}$$

where $q^0 - q := -\partial\chi/\partial\kappa$ denotes the internal variable conjugate to the strain-like one κ, with q^0 being the initial value of the residual material strength $q(\kappa)$, i.e., $q^0 := q(\kappa = 0)$.

In analogy to the classical plasticity theory, the evolution laws for the compliance tensor $\mathbb{C}$ (or the damage one $\mathbb{C}^{\mathrm{d}}$) and the strain-like internal variables $\left\{\boldsymbol{\epsilon}^{\mathrm{p}}, \kappa\right\}$ can be derived from the postulate of maximum energy dissipation [59]. That is, for a given admissible stress state $\left\{\boldsymbol{\sigma}, q\right\}$, the rates $\dot{\mathbb{C}} = \dot{\mathbb{C}}^{\mathrm{d}}$ and $\left\{\dot{\boldsymbol{\epsilon}}^{\mathrm{p}}, \dot{\kappa}\right\}$ are those values maximizing the energy dissipation (4.17). Without loss of generality, let us consider a rate-independent inelastic softening solid characterized by the following convex, smooth and differentiable failure criterion

$$\mathcal{F}(\boldsymbol{\sigma}, q) \leq 0 \tag{4.18}$$

where the loading function $\mathcal{F}(\boldsymbol{\sigma}, q)$ is a homogeneous function of degree $M \geq 1$, i.e.,

$$\mathcal{F}(\boldsymbol{\sigma}, q) = \frac{1}{M}\left(\partial_{\boldsymbol{\sigma}}\mathcal{F} : \boldsymbol{\sigma} + \partial_q\mathcal{F} \cdot q\right) = \frac{1}{M}\left(\boldsymbol{\Lambda} : \boldsymbol{\sigma} - h \cdot q\right) \tag{4.19}$$

for the derivatives $\boldsymbol{\Lambda} := \partial\mathcal{F}/\partial\boldsymbol{\sigma}$ and $h := -\partial\mathcal{F}/\partial q$. The homogeneous loading function (4.19), frequently encountered in practice, automatically guarantees the energy dissipation inequality (4.17) for any softening law $q(\kappa)$; see Remark 4.3. Furthermore, the dissipative flow tensor $\boldsymbol{\Lambda} := \partial\mathcal{F}/\partial\boldsymbol{\sigma}$, being coaxial to the stress tensor $\boldsymbol{\sigma}$ [23], can be expanded in the local base system $(\boldsymbol{n}, \boldsymbol{m}, \boldsymbol{p})$ as shown in Appendix A. In particular, the local tensorial components can be expressed in terms of the principal values Λ_i and the characteristic angles $\boldsymbol{\theta}$.

Accordingly, the postulate of maximum energy dissipation can be transformed into an optimization problem of the following constrained Lagrangian functional $\mathscr{L}$

$$\mathscr{L} = -\mathscr{D} + \lambda \mathcal{F}(\boldsymbol{\sigma}, q) = -\left[\frac{1}{2}\,\boldsymbol{\sigma} : \dot{\mathbb{C}} : \boldsymbol{\sigma} + \boldsymbol{\sigma} : \dot{\boldsymbol{\epsilon}}^{\mathrm{p}} + \left(q^0 - q\right) \cdot \dot{\kappa}\right] + \lambda \mathcal{F}(\boldsymbol{\sigma}, q) \tag{4.20}$$

where the Lagrangian multiplier λ satisfies the classical Kuhn-Tucker loading/unloading conditions

$$\lambda \geq 0, \qquad \mathcal{F}(\boldsymbol{\sigma}, q) \leq 0, \qquad \lambda \mathcal{F}(\boldsymbol{\sigma}, q) = 0 \tag{4.21}$$

The stationarity conditions of the functional (4.20) give the following associated evolution laws

$$\dot{\boldsymbol{\epsilon}}^{\mathrm{dis}} = \dot{\mathbb{C}} : \boldsymbol{\sigma} + \dot{\boldsymbol{\epsilon}}^{\mathrm{p}} = \lambda \boldsymbol{\Lambda}, \qquad \dot{\kappa} = \lambda h \tag{4.22}$$

where the tensor $\boldsymbol{\Lambda} := \partial \mathcal{F} / \partial \boldsymbol{\sigma}$, normal to the failure surface $\mathcal{F}(\boldsymbol{\sigma}, q) = 0$, is referred to as the *dissipative flow tensor*.

To differentiate the damage and plastic contributions to the dissipative strain tensor rate $\dot{\boldsymbol{\epsilon}}^{\mathrm{dis}}$, a material parameter $\xi \in [0, 1]$ is introduced so that [31, 46, 70]

$$\dot{\boldsymbol{\epsilon}}^{\mathrm{p}} = \left(1 - \xi\right) \dot{\boldsymbol{\epsilon}}^{\mathrm{dis}} = \left(1 - \xi\right) \lambda \boldsymbol{\Lambda} \tag{4.23a}$$

$$\dot{\mathbb{C}} : \boldsymbol{\sigma} = \xi\, \dot{\boldsymbol{\epsilon}}^{\mathrm{dis}} = \xi\, \lambda \boldsymbol{\Lambda} \tag{4.23b}$$

The cases $\xi = 0$ and $\xi = 1$ correspond to the classical plasticity model [15] and the elastic damage (degradation) model [8, 71], respectively. For the parameter $\xi \in (0, 1)$, both the material compliance $\mathbb{C}$ (or the damage one $\mathbb{C}^{\mathrm{d}}$) and the plastic strain $\boldsymbol{\epsilon}^{\mathrm{p}}$ are internal variables, resulting in a combined plastic-damage model.

The principle of maximum dissipation determines only the components of the material compliance $\mathbb{C}$ appearing in the product $\boldsymbol{\sigma} : \dot{\mathbb{C}} : \boldsymbol{\sigma}$, leaving the remaining ones undefined. For the homogeneous loading function (4.19), the evolution law for the compliance $\mathbb{C}$ satisfying Eq. (4.23b) is given by [31, 70]

$$\dot{\mathbb{C}} = \dot{\mathbb{C}}^{\mathrm{d}} = \xi\, \lambda \frac{\boldsymbol{\Lambda} \otimes \boldsymbol{\Lambda}}{\boldsymbol{\Lambda} : \boldsymbol{\sigma}} \tag{4.24}$$

as long as the condition $\boldsymbol{\Lambda} : \boldsymbol{\sigma} \neq 0$ is satisfied.

When the material is unloading, i.e., $\mathcal{F}(\boldsymbol{\sigma}, q) < 0$, it follows that $\lambda = 0$; for the loading case, $\lambda > 0$ is solved from the consistency condition $\dot{\mathcal{F}}(\boldsymbol{\sigma}, q) = 0$, i.e.,

$$\dot{\mathcal{F}}(\boldsymbol{\sigma}, q) = \boldsymbol{\Lambda} : \dot{\boldsymbol{\sigma}} - \lambda h \cdot H \cdot h = 0 \tag{4.25}$$

or, equivalently

$$\lambda = \frac{\boldsymbol{\Lambda} : \mathbb{E} : \dot{\boldsymbol{\epsilon}}}{\boldsymbol{\Lambda} : \mathbb{E} : \boldsymbol{\Lambda} + h \cdot H \cdot h} = \frac{\boldsymbol{\Lambda} : \dot{\boldsymbol{\sigma}}}{h \cdot H \cdot h} \tag{4.26}$$

Therefore, the rate constitutive relations are given by

$$\dot{\boldsymbol{\sigma}} = \mathbb{E}_{\mathrm{tan}} : \dot{\boldsymbol{\epsilon}}, \qquad \dot{\boldsymbol{\epsilon}} = \mathbb{C}_{\mathrm{tan}} : \dot{\boldsymbol{\sigma}} \tag{4.27}$$

where the material tangents $\mathbb{E}_{\text{tan}}$ and $\mathbb{C}_{\text{tan}}$ for the loading state (i.e., $\lambda > 0$) are expressed as

$$\mathbb{E}_{\text{tan}} = \mathbb{E} - \frac{\mathbb{E} : (\boldsymbol{\Lambda} \otimes \boldsymbol{\Lambda}) : \mathbb{E}}{\boldsymbol{\Lambda} : \mathbb{E} : \boldsymbol{\Lambda} + h \cdot H \cdot h} \tag{4.28a}$$

$$\mathbb{C}_{\text{tan}} = \mathbb{C} + \frac{\boldsymbol{\Lambda} \otimes \boldsymbol{\Lambda}}{h \cdot H \cdot h} \tag{4.28b}$$

both being symmetric due to the associated evolution laws considered.

Remark 4.3 For the homogeneous loading function (4.19), substitution of the evolution laws (4.22) and (4.23) yields the following energy dissipation

$$\mathscr{D} = \lambda \Big(1 - \frac{1}{2}\xi\Big) \boldsymbol{\Lambda} : \boldsymbol{\sigma} + \big(q^0 - q\big) \cdot \dot{\kappa} = \Big(q^0 - \frac{1}{2}\xi q\Big) \cdot \dot{\kappa} \geq 0 \tag{4.29}$$

where the following relation resulting from satisfaction of the failure criterion $\mathcal{F}(\boldsymbol{\sigma}, q) = 0$

$$\mathcal{F}(\boldsymbol{\sigma}, q) = 0 \qquad \Longrightarrow \qquad \boldsymbol{\Lambda} : \boldsymbol{\sigma} = h \cdot q \tag{4.30}$$

has been considered. Thus, the energy dissipation inequality (4.17) is automatically satisfied for any softening law $q(\kappa) \leq q^0$. ■

4.3. Fracture energy

Calling for Eqs. (3.2), (4.7), (4.15) and (4.17), the external energy density supplied to the solid during the failure process can be evaluated as

$$\int_0^\infty \boldsymbol{\sigma} : \dot{\boldsymbol{\epsilon}} \, \mathrm{d}T = \int_0^\infty \big(\dot{\psi}^{\text{ed}} + \dot{\chi} + \mathscr{D}\big) \mathrm{d}T = \int_0^\infty \left(\frac{1}{2}\, \boldsymbol{\sigma} : \dot{\mathbb{C}}^{\text{d}} : \boldsymbol{\sigma} + \boldsymbol{\sigma} : \dot{\boldsymbol{\epsilon}}^{\text{p}}\right) \mathrm{d}T \tag{4.31}$$

with T being the (pseudo-) time. Note that the identity $\int_0^\infty \dot{\psi}^{\text{ed}} \, \mathrm{d}T = 0$ holds for the state variable ψ^{ed}. Substitution of the evolution laws (4.23) yields

$$\int_0^\infty \boldsymbol{\sigma} : \dot{\boldsymbol{\epsilon}} \, \mathrm{d}T = \Big(1 - \frac{1}{2}\xi\Big) \int_0^\infty \lambda \boldsymbol{\Lambda} : \boldsymbol{\sigma} \, \mathrm{d}T = \Big(1 - \frac{1}{2}\xi\Big) \int_0^\infty \lambda h \cdot q(\kappa) \, \mathrm{d}T \tag{4.32}$$

where the relation (4.30) has been recalled.

Calling for the evolution law $(4.22)_2$, it is possible to define the so-called specific fracture energy (i.e., energy dissipation per unit volume) g_{f} from Eq. (4.32)

$$g_{\text{f}} = \int_0^\infty \boldsymbol{\sigma} : \dot{\boldsymbol{\epsilon}} \, \mathrm{d}T = \Big(1 - \frac{1}{2}\xi\Big) \int_0^\infty q(\kappa) \, \mathrm{d}\kappa = \frac{G_{\text{f}}}{b} \tag{4.33}$$

where G_{f} is the fracture energy (i.e., energy dissipation per unit surface area), assumed as a material property; b is a band width (see the discussion in next section) where the energy dissipation localizes. Therefore, the softening law $q(\kappa)$ has to be regularized with respect to the localized band width b in such a way that the energy dissipation during the whole failure process does not depend on it.

The above regularized procedure was advocated in the crack band theory [5]. It is equivalent to the cohesive (fictitious) crack model [3, 4, 17, 22]. In this latter context, Eq. (4.33) is rewritten as

$$G_{\mathrm{f}} = b g_{\mathrm{f}} = \Big(1 - \frac{1}{2}\xi\Big) \int_0^\infty q(\kappa) b \, \mathrm{d}\kappa = \Big(1 - \frac{1}{2}\xi\Big) \int_0^\infty q(\tilde{\kappa}) \, \mathrm{d}\tilde{\kappa} \tag{4.34}$$

It then allows introducing the softening law $q(\tilde{\kappa})$ expressed in terms of an alternative *displacement-like* internal variable $\tilde{\kappa}$

$$\tilde{\kappa} := b\kappa, \qquad \dot{\tilde{\kappa}} = \tilde{\lambda} h \qquad \Longrightarrow \qquad \widetilde{H} = \frac{1}{b} H, \qquad \lambda = \frac{1}{b} \tilde{\lambda} \tag{4.35}$$

where $H := \partial q / \partial \kappa$ and $\widetilde{H} := \partial q / \partial \tilde{\kappa}$ denote the strain- and displacement-driven softening moduli, respectively; $\tilde{\lambda} \geq 0$ is an alternative Lagrangian multiplier. Note that the above definitions coincide with the conditions (3.65) upon which the regularized discontinuity model is equivalent to a strong one.

Remark 4.4 It is concluded from Eqs. (4.35) that, both the strain-driven softening law $q(\kappa)$ and the displacement-driven one $q(\tilde{\kappa})$ are equivalent in the modeling of localized failure in solids and give identical results for the same fracture energy G_{f}. Furthermore, the kinematic internal variables characterizing the inelastic behavior of the material, e.g., the damage compliance $\mathbb{C}^{\mathrm{d}}$, the plastic strain $\boldsymbol{\epsilon}^{\mathrm{p}}$ and the inelastic strain $\boldsymbol{\epsilon}^{\mathrm{in}}$, etc., are all inversely proportional to the band width b. ■

4.4. Strain localization analysis of the elastoplastic damage solid

Let us now consider strain localization in an inelastic solid characterized by the above elastoplastic damage model. To this end, the kinematic constraint (4.5) has to be accounted for appropriately. More specifically, upon strain localization the dissipative flow tensor characterizing the evolution laws evolves into a particular structure expressed uniquely in terms of a dissipative flow vector and the discontinuity orientation. That is, the flow tensorial components in the directions orthogonal to the discontinuity orientation have to vanish. This property allows introducing a traction-based failure criterion and developing a localized plastic-damage model for the discontinuity (band).

4.4.1. Strain localization analysis

For the inelastic strain (4.14) of the elastoplastic damage model, the kinematic condition (4.5) upon strain localization is particularized into

$$\boldsymbol{\epsilon}^{\mathrm{in}} = \big(\boldsymbol{e} \otimes \boldsymbol{n}\big)^{\mathrm{sym}} = \boldsymbol{\epsilon}^{\mathrm{d}} + \boldsymbol{\epsilon}^{\mathrm{p}} = \mathbb{C}^{\mathrm{d}} : \boldsymbol{\sigma} + \boldsymbol{\epsilon}^{\mathrm{p}} \tag{4.36}$$

In the right hand side of the kinematic relation (4.36), the damage/plastic strains $(\boldsymbol{\epsilon}^{\mathrm{d}}, \boldsymbol{\epsilon}^{\mathrm{p}})$ correspond to the recoverable and unrecoverable components of the inelastic strain $\boldsymbol{\epsilon}^{\mathrm{in}}$, respectively. Therefore, the (apparent) displacement jump $\boldsymbol{w}$ and the inelastic deformation vector $\boldsymbol{e} := \boldsymbol{w}/b$ have to admit similar decompositions, i.e.,

$$\boldsymbol{w} = \boldsymbol{w}^{\mathrm{d}} + \boldsymbol{w}^{\mathrm{p}}, \qquad \boldsymbol{e} = \boldsymbol{e}^{\mathrm{d}} + \boldsymbol{e}^{\mathrm{p}} \tag{4.37}$$

such that

$$\big(\boldsymbol{e}^{\mathrm{p}} \otimes \boldsymbol{n}\big)^{\mathrm{sym}} = \boldsymbol{\epsilon}^{\mathrm{p}} \tag{4.38a}$$

$$\big(\boldsymbol{e}^{\mathrm{d}} \otimes \boldsymbol{n}\big)^{\mathrm{sym}} = \boldsymbol{\epsilon}^{\mathrm{d}} = \mathbb{C}^{\mathrm{d}} : \boldsymbol{\sigma} \tag{4.38b}$$

where the damage and plastic deformation vectors, $\boldsymbol{e}^{\mathrm{d}} := \boldsymbol{w}^{\mathrm{d}}/b$ and $\boldsymbol{e}^{\mathrm{p}} := \boldsymbol{w}^{\mathrm{d}}/b$, are defined as the recoverable and unrecoverable displacement jumps $(\boldsymbol{w}^{\mathrm{d}}, \boldsymbol{w}^{\mathrm{p}})$ normalized with respect to the band width b.

It follows from Eqs. (4.23a) and (4.38a) that

$$\big(\dot{\boldsymbol{e}}^{\mathrm{p}} \otimes \boldsymbol{n}\big)^{\mathrm{sym}} = \dot{\boldsymbol{\epsilon}}^{\mathrm{p}} = \big(1-\xi\big)\lambda\boldsymbol{\Lambda} \tag{4.39}$$

which implies the existence of a *dissipative flow vector* $\boldsymbol{\gamma}$ satisfying

$$\dot{\boldsymbol{e}}^{\mathrm{p}} = \big(1-\xi\big)\lambda\boldsymbol{\gamma}, \qquad \big(\boldsymbol{\gamma} \otimes \boldsymbol{n}\big)^{\mathrm{sym}} = \boldsymbol{\Lambda} \tag{4.40}$$

Note that, owing to the static constraint (3.11), the following identity holds

$$\boldsymbol{\Lambda} : \boldsymbol{\sigma} = \boldsymbol{\gamma} \cdot \big(\boldsymbol{\sigma} \cdot \boldsymbol{n}\big) = \boldsymbol{\gamma} \cdot \boldsymbol{t} \tag{4.41}$$

between the dissipative flow tensor $\boldsymbol{\Lambda}$ and vector $\boldsymbol{\gamma}$.

Pre-multiplying relation $(4.40)_2$ by the symmetric fourth-order identity tensor $\mathbb{I}$ and then by the orientation $\boldsymbol{n}$, it follows that [42]

$$\boldsymbol{\gamma} = 2\boldsymbol{n} \cdot \boldsymbol{\Lambda} - \boldsymbol{n}\Lambda_{nn} = \gamma_n \boldsymbol{n} + \gamma_m \boldsymbol{m} + \gamma_p \boldsymbol{p} \tag{4.42a}$$

where the components $(\gamma_n, \gamma_m, \gamma_p)$ of the dissipative flow vector $\boldsymbol{\gamma}$ in the local orthogonal system $(\boldsymbol{n}, \boldsymbol{m}, \boldsymbol{p})$ of the discontinuity (see Appendix A) are expressed as

$$\gamma_n := \boldsymbol{\gamma} \cdot \boldsymbol{n} = \Lambda_{nn}, \qquad \gamma_m := \boldsymbol{\gamma} \cdot \boldsymbol{m} = 2\Lambda_{nm}, \qquad \gamma_p := \boldsymbol{\gamma} \cdot \boldsymbol{p} = 2\Lambda_{np} \tag{4.42b}$$

Substitution of the above dissipative flow vector $\boldsymbol{\gamma}$ into the relation $(4.40)_2$ yields

$$\boxed{\boldsymbol{\Lambda} = \big(\boldsymbol{\gamma} \otimes \boldsymbol{n}\big)^{\mathrm{sym}}} = \Lambda_{nn}\big(\boldsymbol{n} \otimes \boldsymbol{n}\big) + 2\Lambda_{nm}\big(\boldsymbol{n} \otimes \boldsymbol{m}\big)^{\mathrm{sym}} + 2\Lambda_{np}\big(\boldsymbol{n} \otimes \boldsymbol{p}\big)^{\mathrm{sym}} \tag{4.43}$$

Its comparison with the dissipative flow tensor (A.5) gives the following constraints

$$\Lambda_{mm}(\boldsymbol{\theta}^{\mathrm{cr}}) = 0, \qquad \Lambda_{pp}(\boldsymbol{\theta}^{\mathrm{cr}}) = 0, \qquad \Lambda_{mp}(\boldsymbol{\theta}^{\mathrm{cr}}) = 0 \tag{4.44}$$

where $\boldsymbol{\theta}^{\mathrm{cr}}$ denote the characteristic discontinuity angles upon which the kinematic condition (4.5) and the resulting relation (4.43) are satisfied.

It can be seen from the constraints (4.44) that, upon strain localization, the failure criterion $\mathcal{F}(\boldsymbol{\sigma}, q) \leq 0$ no longer depends on the stress components σ_{mm}, σ_{pp} and σ_{mp}, but is only a function of the tractions $\boldsymbol{t} := \boldsymbol{\sigma} \cdot \boldsymbol{n} = \big\{\sigma_{nn}, \sigma_{nm}, \sigma_{np}\big\}^{\mathrm{T}}$ acting on the discontinuity with the orientation $\boldsymbol{n}(\boldsymbol{\theta}^{\mathrm{cr}})$. Therefore, as long as the characteristic angles $\boldsymbol{\theta}^{\mathrm{cr}}$ satisfying the kinematic constraints (4.44) exist, it is always possible to introduce an appropriate traction-based failure criterion to characterize the discontinuity (band). This topic is deferred to Section 4.5.

4.4.2. Localized constitutive model for the discontinuity (band)

Owing to the particular structure (4.43) of the dissipative flow tensor $\boldsymbol{\Lambda}$ upon strain localization, the evolution laws (4.22) $\sim$ (4.24) are naturally projected onto the discontinuity orientation $\boldsymbol{n}$. This property allows developing a localized plastic-damage model for the discontinuity (band).

For the dissipative flow tensor (4.43), the damage evolution law (4.24) can be rewritten as

$$\dot{\mathbb{C}} = \dot{\mathbb{C}}^{\mathrm{d}} = \big(\dot{\boldsymbol{C}}^{\mathrm{d}} \,\underline{\overline{\otimes}}\, \boldsymbol{N}\big)^{\mathrm{sym}} \qquad \Longrightarrow \qquad \mathbb{C}^{\mathrm{d}} = \big(\boldsymbol{C}^{\mathrm{d}} \,\underline{\overline{\otimes}}\, \boldsymbol{N}\big)^{\mathrm{sym}} \tag{4.45}$$

where $\boldsymbol{N} := \boldsymbol{n} \otimes \boldsymbol{n}$ is a second-order geometric tensor; $\boldsymbol{C}^{\mathrm{d}}$ denotes the second-order compliance tensor of the discontinuity (band), with the following evolution law

$$\dot{\boldsymbol{C}}^{\mathrm{d}} = \xi\, \lambda \frac{\boldsymbol{\gamma} \otimes \boldsymbol{\gamma}}{\boldsymbol{\gamma} \cdot \boldsymbol{t}} \tag{4.46}$$

In other words, upon strain localization, the damage behavior of the material is sufficiently characterized by a second-order internal variable $\boldsymbol{C}^{\mathrm{d}}$ rather than the original fourth-order one $\mathbb{C}^{\mathrm{d}}$; see Remark 4.5 for more details.

Accordingly, the damage strain tensor (4.38b) is given by

$$\boldsymbol{\epsilon}^{\mathrm{d}} = \big(\boldsymbol{e}^{\mathrm{d}} \otimes \boldsymbol{n}\big)^{\mathrm{sym}} = \Big[\big(\boldsymbol{C}^{\mathrm{d}} \cdot \boldsymbol{t}\big) \otimes \boldsymbol{n}\Big]^{\mathrm{sym}} \tag{4.47}$$

That is, the discontinuity (band) can be described by the following localized plastic-damage relations

$$\boldsymbol{e}^{\mathrm{d}} = \boldsymbol{e} - \boldsymbol{e}^{\mathrm{p}} = \boldsymbol{C}^{\mathrm{d}} \cdot \boldsymbol{t}, \qquad \boldsymbol{t} = \boldsymbol{E}^{\mathrm{d}} \cdot \boldsymbol{e}^{\mathrm{d}} = \boldsymbol{E}^{\mathrm{d}} \cdot \big(\boldsymbol{e} - \boldsymbol{e}^{\mathrm{p}}\big) \tag{4.48}$$

for the second-order stiffness tensor $\boldsymbol{E}^{\mathrm{d}} := \big(\boldsymbol{C}^{\mathrm{d}}\big)^{-1}$ and the localized plastic evolution law $(4.40)_1$.

By time differentiation, the rate constitutive relations are expressed as

$$\dot{\boldsymbol{t}} = \boldsymbol{E}^{\mathrm{d}} \cdot \big(\dot{\boldsymbol{e}} - \dot{\boldsymbol{e}}^{\mathrm{dis}}\big), \qquad \dot{\boldsymbol{e}} = \boldsymbol{C}^{\mathrm{d}} \cdot \dot{\boldsymbol{t}} + \dot{\boldsymbol{e}}^{\mathrm{dis}} \tag{4.49}$$

where the *dissipative deformation vector rate* $\dot{\boldsymbol{e}}^{\mathrm{dis}}$ is defined as

$$\dot{\boldsymbol{e}}^{\mathrm{dis}} := \dot{\boldsymbol{C}}^{\mathrm{d}} \cdot \boldsymbol{t} + \dot{\boldsymbol{e}}^{\mathrm{p}} = \lambda \boldsymbol{\gamma} \qquad \Longrightarrow \qquad \big(\dot{\boldsymbol{e}}^{\mathrm{dis}} \otimes \boldsymbol{n}\big)^{\mathrm{sym}} = \dot{\boldsymbol{\epsilon}}^{\mathrm{dis}} = \lambda \boldsymbol{\Lambda} \tag{4.50}$$

with $\dot{\boldsymbol{C}}^{\mathrm{d}} \cdot \boldsymbol{t}$ and $\dot{\boldsymbol{e}}^{\mathrm{p}}$ being its damage and plastic components, respectively; see Fig. 5.

Upon strain localization, for an active discontinuity the corresponding consistency condition $\dot{\mathcal{F}}(\boldsymbol{\sigma}, q) = 0$ in Eq. (4.25) becomes

$$\dot{\mathcal{F}} = \big(\boldsymbol{\gamma} \otimes \boldsymbol{n}\big)^{\mathrm{sym}} : \dot{\boldsymbol{\sigma}} - h \cdot H \cdot h = \boldsymbol{\gamma} \cdot \dot{\boldsymbol{t}} - h \cdot H \cdot h = 0 \tag{4.51}$$

from which the multiplier $\lambda > 0$ is solved as

$$\lambda = \frac{\boldsymbol{\gamma} \cdot \boldsymbol{E}^{\mathrm{d}} \cdot \dot{\boldsymbol{e}}}{\boldsymbol{\gamma} \cdot \boldsymbol{E}^{\mathrm{d}} \cdot \boldsymbol{\gamma} + h \cdot H \cdot h} = \frac{\boldsymbol{\gamma} \cdot \dot{\boldsymbol{t}}}{h \cdot H \cdot h} \tag{4.52}$$

Combination of Eqs. (4.49), (4.50) and (4.52) yields the following rate constitutive relations

$$\dot{\boldsymbol{t}} = \boldsymbol{E}^{\mathrm{d}} \cdot \left(\dot{\boldsymbol{e}} - \lambda \boldsymbol{\gamma}\right) = \boldsymbol{E}^{\mathrm{d}}_{\mathrm{tan}} \cdot \dot{\boldsymbol{e}}, \qquad \dot{\boldsymbol{e}} = \boldsymbol{C}^{\mathrm{d}} \cdot \dot{\boldsymbol{t}} + \lambda \boldsymbol{\gamma} = \boldsymbol{C}^{\mathrm{d}}_{\mathrm{tan}} \cdot \dot{\boldsymbol{t}} \tag{4.53}$$

where the tangent stiffness $\boldsymbol{E}^{\mathrm{d}}_{\mathrm{tan}}$ and compliance $\boldsymbol{C}^{\mathrm{d}}_{\mathrm{tan}}$ are expressed as

$$\boldsymbol{E}^{\mathrm{d}}_{\mathrm{tan}} = \boldsymbol{E}^{\mathrm{d}} - \frac{\boldsymbol{E}^{\mathrm{d}} \cdot \left(\boldsymbol{\gamma} \otimes \boldsymbol{\gamma}\right) \cdot \boldsymbol{E}^{\mathrm{d}}}{\boldsymbol{\gamma} \cdot \boldsymbol{E}^{\mathrm{d}} \cdot \boldsymbol{\gamma} + h \cdot H \cdot h} \tag{4.54a}$$

$$\boldsymbol{C}^{\mathrm{d}}_{\mathrm{tan}} = \boldsymbol{C}^{\mathrm{d}} + \frac{\boldsymbol{\gamma} \otimes \boldsymbol{\gamma}}{h \cdot H \cdot h} \tag{4.54b}$$

for the active discontinuity (band).

For the above localized plastic-damage model, the *strain-like* internal variable κ is employed in the softening law $q(\kappa)$. Accordingly, the resulting localized constitutive laws are expressed in terms of the traction $\boldsymbol{t}$ and the inelastic deformation vector $\boldsymbol{e}$. Recalling the relations (4.35), an equivalent traction $\boldsymbol{t}$ *versus* displacement jump $\boldsymbol{w}$ localized model can also be developed. The details are omitted here.

Remark 4.5 For the damage compliance tensor $\mathbb{C}^{\mathrm{d}}$ in Eq. $(4.45)_2$, the (complementary) damage free energy density function ψ^{d} introduced in Eq. (4.16b) localizes within the discontinuity (band), i.e.,

$$\psi^{\mathrm{d}} = \frac{1}{2}\boldsymbol{\sigma} : \mathbb{C}^{\mathrm{d}} : \boldsymbol{\sigma} = \frac{1}{2}\boldsymbol{t} \cdot \boldsymbol{C}^{\mathrm{d}} \cdot \boldsymbol{t} = \frac{1}{2}\boldsymbol{e}^{\mathrm{d}} \cdot \boldsymbol{E}^{\mathrm{d}} \cdot \boldsymbol{e}^{\mathrm{d}} \tag{4.55}$$

Similarly, the energy dissipation (4.17) becomes

$$\mathscr{D} = \frac{1}{2}\,\boldsymbol{t} \cdot \dot{\boldsymbol{C}}^{\mathrm{d}} \cdot \boldsymbol{t} + \boldsymbol{t} \cdot \dot{\boldsymbol{e}}^{\mathrm{p}} + \left(q^0 - q\right) \cdot \dot{\kappa} \geq 0 \tag{4.56}$$

Accordingly, the above localized plastic-damage model can also be derived as in Section 3.3. In particular, the material compliance $\mathbb{C}$ can be related to the discontinuity (band) compliance $\boldsymbol{C}^{\mathrm{d}}$ as follows

$$\mathbb{C} = \mathbb{C}^0 + \mathbb{C}^{\mathrm{d}} = \mathbb{C}^0 + \left(\boldsymbol{C}^{\mathrm{d}} \,\underline{\overline{\otimes}}\, \boldsymbol{N}\right)^{\mathrm{sym}} \tag{4.57a}$$

Inversely, the material stiffness tensor $\mathbb{E}$ is obtained from the Sherman-Morrison-Woodburg formula [18]

$$\mathbb{E} = \mathbb{C}^{-1} = \mathbb{E}^0 - \mathbb{E}^0 : \left[\left(\boldsymbol{E}^{\mathrm{d}} + \boldsymbol{n} \cdot \mathbb{E}^0 \cdot \boldsymbol{n}\right)^{-1} \underline{\overline{\otimes}}\, \boldsymbol{N}\right]^{\mathrm{sym}} : \mathbb{E}^0 \tag{4.57b}$$

Note that both the material compliance $\mathbb{C}$ and stiffness $\mathbb{E}$ are symmetric. □

Remark 4.6 It follows from the Sherman-Morrison-Woodburg formula [18] that the material tangents given in Eqs. (4.28) and (4.57) coincide with those in Eqs. (3.74) and (3.77). In summary, though they are developed based on different methodologies, ***the embedded/smeared discontinuity models are equivalent to the elastoplastic damage model, providing an identical traction-based failure criterion is employed in both methods.*** □

4.5. Failure criterion

As already shown in previous sections, upon strain localization, the discontinuity (band) can be sufficiently characterized by a traction-based localized model. With respect to the strategies dealing with the discontinuity orientation $\boldsymbol{n}$, two dual but not necessarily equivalent approaches can be followed.

4.5.1. Elastoplastic damage model with an explicit traction-based failure criterion

Let us first consider the elastoplastic damage model [70] with an explicit traction-based failure criterion. Providing the discontinuity orientation is known, say, $\boldsymbol{n} = \boldsymbol{n}(\widehat{\boldsymbol{\theta}}^{\rm cr})$ for the characteristic angles $\widehat{\boldsymbol{\theta}}^{\rm cr}$, the following failure criterion can be introduced as

$$\mathcal{F}(\boldsymbol{\sigma}, q) = \widehat{f}(\boldsymbol{\sigma} \cdot \boldsymbol{n}, q) = \widehat{f}(\boldsymbol{t}, q) \leq 0 \tag{4.58}$$

Consistent with the condition (4.19), $\widehat{f}(\boldsymbol{t}, q)$ is also a homogeneous function of degree $M \geq 1$, i.e.,

$$\widehat{f}(\boldsymbol{t}, q) = \frac{1}{M}\big(\partial_{\boldsymbol{t}} \widehat{f} \cdot \boldsymbol{t} + \partial_q \widehat{f} \cdot q\big) = \frac{1}{M}\big(\widehat{\boldsymbol{\gamma}} \cdot \boldsymbol{t} - \widehat{h} \cdot q\big) \leq 0 \tag{4.59}$$

for the dissipative flow vector $\widehat{\boldsymbol{\gamma}} := \partial \widehat{f} / \partial \boldsymbol{t}$ and the softening function $\widehat{h} := -\partial \widehat{f} / \partial q$.

Accordingly, the dissipative flow tensor $\boldsymbol{\Lambda} := \partial \mathcal{F} / \partial \boldsymbol{\sigma}$ is *evaluated* directly in terms of the known discontinuity orientation $\boldsymbol{n}(\widehat{\boldsymbol{\theta}}^{\rm cr})$ and the given dissipative flow vector $\widehat{\boldsymbol{\gamma}}$, i.e.,

$$\boldsymbol{\Lambda} = \frac{\partial \widehat{f}}{\partial \boldsymbol{\sigma}} = \frac{\partial \widehat{f}}{\partial \boldsymbol{t}} \cdot \frac{\partial \boldsymbol{t}}{\partial \boldsymbol{\sigma}} = \widehat{\boldsymbol{\gamma}} \cdot \boldsymbol{\mathcal{N}} = \big(\widehat{\boldsymbol{\gamma}} \otimes \boldsymbol{n}\big)^{\rm sym} \tag{4.60a}$$

or in the form (4.43)

$$\boxed{\boldsymbol{\Lambda} := \big(\boldsymbol{\gamma} \otimes \boldsymbol{n}\big)^{\rm sym}, \qquad \boldsymbol{\gamma} = \widehat{\boldsymbol{\gamma}} := \frac{\partial \widehat{f}}{\partial \boldsymbol{t}}} \tag{4.60b}$$

where the Cartesian components of the third-order tensor $\boldsymbol{\mathcal{N}} = \partial \boldsymbol{t} / \partial \boldsymbol{\sigma}$ is expressed as $\mathcal{N}_{ijk} = \frac{1}{2}\big(\delta_{ij} n_k + \delta_{ik} n_j\big)$ for the Kronecker-delta δ_{ij} and the components n_k of the normal vector $\boldsymbol{n}(\widehat{\boldsymbol{\theta}}^{\rm cr})$.

In the above traction-based elastoplastic damage, the kinematic constraint (4.60) holds for any arbitrary orientation $\boldsymbol{n}(\widehat{\boldsymbol{\theta}}^{\rm cr})$ so that the stress continuity condition (3.10) is always guaranteed, i.e.,

$$\boldsymbol{\Lambda} := \big(\widehat{\boldsymbol{\gamma}} \otimes \boldsymbol{n}\big)^{\rm sym} \qquad \Longrightarrow \qquad [\![\boldsymbol{\sigma}]\!] = \boldsymbol{0} \tag{4.61}$$

In other words, it is implicitly assumed *a priori* that strain localization with stress continuity can always occur.

Consequently, the discontinuity orientation $\boldsymbol{n}(\widehat{\boldsymbol{\theta}}^{\rm cr})$ cannot be determined uniquely based on the given traction-based failure criterion $\widehat{f}(\boldsymbol{t}, q) \leq 0$, unless extra auxiliary conditions are introduced. Similarly to the strong/regularized discontinuity approaches, the classical Mohr's maximization postulate [32] presented in Section 3.2 can be adopted.

Remark 4.7 Owning to the relation (4.41), the failure criterion $\widehat{f}(\boldsymbol{t}, q) \leq 0$ can be rewritten as

$$F(\boldsymbol{\sigma}, q) := \widehat{f}(\boldsymbol{t}, q) = \frac{1}{M}\big(\widehat{\boldsymbol{\gamma}} \cdot \boldsymbol{t} - \widehat{h} \cdot q\big) = \frac{1}{M}\big(\boldsymbol{\Lambda} : \boldsymbol{\sigma} - \widehat{h} \cdot q\big) \leq 0 \tag{4.62}$$

That is, once the discontinuity orientation $\boldsymbol{n}(\widehat{\boldsymbol{\theta}}^{\rm cr})$ is known, the given traction-based failure criterion $\widehat{f}(\boldsymbol{t}, q) \leq 0$ can be equivalently expressed as a stress-based counterpart $F(\boldsymbol{\sigma}, q) \leq 0$. $\square$

4.5.2. Projected discontinuity model with a stress-based failure criterion

Alternatively, the failure criterion $\mathcal{F}(\boldsymbol{\sigma}, q) \leq 0$ can also be expressed in terms of stress invariants and is then projected to the *yet-unknown* discontinuity orientation $\boldsymbol{n}(\boldsymbol{\theta}^{\mathrm{cr}})$ through the kinematic relation (4.43). Without loss of generality, the following failure function is considered

$$\mathcal{F}(\boldsymbol{\sigma}, q) := \widehat{F}(\mathcal{I}, q) \leq 0 \tag{4.63}$$

so that the dissipative flow tensor $\boldsymbol{\Lambda}$ is given by

$$\boldsymbol{\Lambda} = \widehat{\boldsymbol{\Lambda}} := \frac{\partial \widehat{F}}{\partial \boldsymbol{\sigma}} = \frac{\partial \widehat{F}}{\partial \sigma_1} \boldsymbol{v}_1 \otimes \boldsymbol{v}_1 + \frac{\partial \widehat{F}}{\partial I_1} \boldsymbol{I} + \frac{\partial \widehat{F}}{\partial J_2} \boldsymbol{s} + \cdots \tag{4.64}$$

where $\mathcal{I} := \{\sigma_1, I_1, J_2, \cdots\}$ collects the invariants of the stress tensor $\boldsymbol{\sigma}$; $\sigma_1 := \boldsymbol{v}_1 \cdot \boldsymbol{\sigma} \cdot \boldsymbol{v}_1$ denotes the major principal stress, with $\boldsymbol{v}_1$ being the corresponding principal vector; $I_1 := \mathrm{tr}(\boldsymbol{\sigma})$ is the first invariant of the stress $\boldsymbol{\sigma}$, and $J_2 := \frac{1}{2}\boldsymbol{s} : \boldsymbol{s}$ represents the second invariant of the deviatoric stress $\boldsymbol{s} := \boldsymbol{\sigma} - \frac{1}{3}\mathrm{tr}(\boldsymbol{\sigma})\boldsymbol{I}$, respectively.

Accordingly, the relation (4.43) becomes

$$\boxed{(\boldsymbol{\gamma} \otimes \boldsymbol{n})^{\mathrm{sym}} = \boldsymbol{\Lambda}, \qquad \boldsymbol{\Lambda} = \widehat{\boldsymbol{\Lambda}} := \frac{\partial \widehat{F}}{\partial \boldsymbol{\sigma}}} \tag{4.65}$$

If and only if the discontinuity orientation $\boldsymbol{n}(\boldsymbol{\theta}^{\mathrm{cr}})$ and the associated dissipative flow vector $\boldsymbol{\gamma}$ satisfying the kinematic constraint (4.65) exist for the given dissipative flow tensor $\widehat{\boldsymbol{\Lambda}}$, i.e.,

$$[\![\boldsymbol{\sigma}]\!] = \boldsymbol{0} \qquad \Longleftrightarrow \qquad \widehat{\boldsymbol{\Lambda}} = (\boldsymbol{\gamma} \otimes \boldsymbol{n})^{\mathrm{sym}} \tag{4.66}$$

can strain localization with stress continuity be guaranteed, and vice versa.

In the above stress-based projected discontinuity model, the orientation $\boldsymbol{n}(\boldsymbol{\theta}^{\mathrm{cr}})$ cannot be assumed *arbitrarily* as in the first approach. But rather, it has to be determined consistently from the kinematic constraints (4.44) together with the relations (A.6b) for the given stress-based dissipative flow tensor $\boldsymbol{\Lambda} = \widehat{\boldsymbol{\Lambda}}$. On one hand, as the resulting set of equations are nonlinear, the solution may not exist at all. On the other hand, providing the solution exists, it depends only on the given failure criterion and the stress state, but not on the elastic properties (i.e., Poisson's ratio).

Once the discontinuity orientation $\boldsymbol{n}(\boldsymbol{\theta}^{\mathrm{cr}})$ is so determined, the corresponding dissipative flow vector $\boldsymbol{\gamma}$ can be obtained from Eqs. (4.42a) and (4.42b). As the relation (4.41) holds for the given dissipative flow tensor $\boldsymbol{\Lambda} = \widehat{\boldsymbol{\Lambda}}$, the projected traction-based failure criterion $f(\boldsymbol{t}, q) \leq 0$ can be determined as

$$f(\boldsymbol{t}, q) := \widehat{F}(\boldsymbol{\sigma}, q) = \frac{1}{M}\big(\widehat{\boldsymbol{\Lambda}} : \boldsymbol{\sigma} - \widehat{h} \cdot q\big) = \frac{1}{M}\big(\boldsymbol{\gamma} \cdot \boldsymbol{t} - \widehat{h} \cdot q\big) \leq 0 \tag{4.67}$$

Note that the above traction-based failure function $f(\boldsymbol{t}, q) \leq 0$, projected from the given stress-based one $\widehat{F}(\boldsymbol{\sigma}, q) \leq 0$, does not necessarily coincide with the counterpart $\widehat{f}(\boldsymbol{t}, q) \leq 0$ assumed *a priori* in the first approach.

Therefore, ***providing the kinematic constraint resulting from the stress continuity condition is fulfilled, consistent traction-based constitutive relations for the discontinuity (band) naturally emerges from the strain localization analysis of stress-based models with regularized softening regime***.

5. Comparisons and discussion

Though different methodologies are employed, both the traction-based embedded/smeared discontinuity models (or the equivalent elastoplastic damage model) and the stress-based projected discontinuity model can be developed within the unified framework presented in in Section 4. It is worthwhile to investigate the *bi-directional* connections between these two families of models, in particular, the conditions upon which they are equivalent.

5.1. Evolution laws

In both families of models, the inelastic behavior, completely localized within the discontinuity (band), is characterized by a dissipative flow tensor $\boldsymbol{\Lambda}$, expressed as the unified form (4.43) in terms of the dissipative flow vector $\boldsymbol{\gamma}$ and the orientation $\boldsymbol{n}$; see Eqs. (4.60) and (4.65), respectively. However, the physical interpretations are different.

For the traction-based embedded/smeared discontinuity models, the inelastic flow vector is given as $\boldsymbol{\gamma} = \widehat{\boldsymbol{\gamma}} := \partial \widehat{f} / \partial \boldsymbol{t}$. In this case, the discontinuity orientation $\boldsymbol{n}(\widehat{\boldsymbol{\theta}}^{\mathrm{cr}})$ can be assumed arbitrarily. That is, the relation (4.60) imposes no kinematic constraint. But rather, it acts only as a definition, from which the dissipative flow tensor $\boldsymbol{\Lambda}$ is determined straightforwardly in such a way that the stress continuity (3.10) is always satisfied *a priori* upon strain localization.

Comparatively, in the stress-based projected discontinuity model both the dissipative flow vector $\boldsymbol{\gamma}$ and the orientation $\boldsymbol{n}(\boldsymbol{\theta}^{\mathrm{cr}})$ are unknown and even might not exist at all. In this case, the relation (4.65) imposes necessary and sufficient kinematic constraint on the occurrence of strain localization with a continuous stress field. Accordingly, the discontinuity orientation $\boldsymbol{n}(\widehat{\boldsymbol{\theta}}^{\mathrm{cr}})$ can only be determined from the kinematic constraints (4.44) for the given dissipative flow tensor $\boldsymbol{\Lambda} = \widehat{\boldsymbol{\Lambda}} := \partial \widehat{f} / \partial \boldsymbol{\sigma}$. If such discontinuity orientation exists, the dissipative flow tensor $\boldsymbol{\gamma}$ is given from the relations (4.42). Otherwise, strain localization cannot occur with stress continuity.

In summary, ***even if the dissipative flow vectors coincide in both families of models, the resulting evolution laws, characterized by the dissipative flow tensor*** (4.43)***, are not necessarily identical, since the discontinuity orientations might be different***. An interesting question then naturally arises: whether and when would the discontinuity orientations in both families of models coincide?

5.2. Orientation of the discontinuity (band)

As mentioned before, for the embedded/smeared discontinuity models the orientation $\boldsymbol{n}(\widehat{\boldsymbol{\theta}}^{\mathrm{cr}})$ cannot be determined uniquely from the given traction-based failure criterion $\widehat{f}(\boldsymbol{t}, q) \leq 0$. After recalling the relations (4.42b), the stationary condition (3.16) of the Mohr's maximization postulate can be rewritten as

$$\begin{aligned} \left.\frac{\partial \widehat{f}}{\partial \boldsymbol{\theta}}\right|_{\widehat{\boldsymbol{\theta}}^{\mathrm{cr}}} &= \left(\Lambda_{nn} \frac{\partial \sigma_{nn}}{\partial \boldsymbol{\theta}} + 2\Lambda_{nm} \frac{\partial \sigma_{nm}}{\partial \boldsymbol{\theta}} + 2\Lambda_{np} \frac{\partial \sigma_{np}}{\partial \boldsymbol{\theta}} \right)_{\widehat{\boldsymbol{\theta}}^{\mathrm{cr}}} \\ &= -\left(\Lambda_{mm} \frac{\partial \sigma_{mm}}{\partial \boldsymbol{\theta}} + 2\Lambda_{mp} \frac{\partial \sigma_{mp}}{\partial \boldsymbol{\theta}} + \Lambda_{pp} \frac{\partial \sigma_{pp}}{\partial \boldsymbol{\theta}} \right)_{\widehat{\boldsymbol{\theta}}^{\mathrm{cr}}} = \boldsymbol{0} \end{aligned} \tag{5.1}$$

Note that the identity $\boldsymbol{\Lambda} : (\partial \boldsymbol{\sigma} / \partial \boldsymbol{\theta}) = 0$, resulting from the coaxial property between the tensors $\boldsymbol{\Lambda} := \partial \widehat{f} / \partial \boldsymbol{\sigma}$ and $\boldsymbol{\sigma}$, has been considered. As the failure function $\widehat{f}(\boldsymbol{t}, q) \leq 0$ depends only on the tractions $\boldsymbol{t} := \{\sigma_{nn}, \sigma_{nm}, \sigma_{np}\}^{\mathrm{T}}$, the

condition (5.1) is fulfilled for arbitrary values of the remaining stress components $(\sigma_{mm}, \sigma_{mp}, \sigma_{pp})$. This fact yields

$$\Lambda_{mm}(\widehat{\boldsymbol{\theta}}^{\mathrm{cr}}) = 0, \qquad \Lambda_{pp}(\widehat{\boldsymbol{\theta}}^{\mathrm{cr}}) = 0, \qquad \Lambda_{mp}(\widehat{\boldsymbol{\theta}}^{\mathrm{cr}}) = 0 \tag{5.2}$$

These relations correspond exactly to the kinematic constraints (4.44). Note that the maximization condition (3.17) should be verified for the discontinuity angles $\widehat{\boldsymbol{\theta}}^{\mathrm{cr}}$ determined from Eqs. (5.2).

Inversely, in the projected discontinuity model with a given stress-based failure criterion, strain localization with a continuous stress field can occur, if and only if the critical angles $\boldsymbol{\theta}^{\mathrm{cr}}$ satisfying the kinematic constraints (4.44) exist. Upon this condition, a traction-based failure criterion $f(\boldsymbol{t}, q) \leq 0$ can always be obtained by projecting the given stress-based one $\widehat{F}(\boldsymbol{\sigma}, q) \leq 0$. Accordingly, for the discontinuity (band) to form along the orientation $\boldsymbol{n}(\boldsymbol{\theta}^{\mathrm{cr}})$, the projected traction-based failure criterion $f(\boldsymbol{t}, q) = 0$ is activated. Meanwhile, no discontinuity (band) forms at any other orientation $\boldsymbol{n}(\boldsymbol{\theta}) \neq \boldsymbol{n}(\boldsymbol{\theta}^{\mathrm{cr}})$. The above facts transform into

$$f\big[\boldsymbol{\sigma} \cdot \boldsymbol{n}(\boldsymbol{\theta}), q\big] \leq f\big[\boldsymbol{\sigma} \cdot \boldsymbol{n}(\boldsymbol{\theta}^{\mathrm{cr}}), q\big] = 0 \tag{5.3}$$

That is, the tractions $\boldsymbol{\sigma} \cdot \boldsymbol{n}(\boldsymbol{\theta}^{\mathrm{cr}})$ maximize the failure function $f(\boldsymbol{t}, q) = f[\boldsymbol{\sigma} \cdot \boldsymbol{n}(\boldsymbol{\theta}), q]$. Therefore, the discontinuity angles $\boldsymbol{\theta}^{\mathrm{cr}}$ satisfying Eqs. (4.44) coincide with those determined from Mohr's maximization postulate.

Remark 5.1 For the traction-based models, it is assumed *a priori* that strain localization with stress continuity can always occur. Therefore, if the solution to Eqs. (5.2) does not exist, the discontinuity angles $\widehat{\boldsymbol{\theta}}^{\mathrm{cr}}$ should be determined from another set of solution to Eqs. (5.1)

$$\left.\frac{\partial \sigma_{mm}}{\partial \boldsymbol{\theta}}\right|_{\widehat{\boldsymbol{\theta}}^{\mathrm{cr}}} = 0, \qquad \left.\frac{\partial \sigma_{mp}}{\partial \boldsymbol{\theta}}\right|_{\widehat{\boldsymbol{\theta}}^{\mathrm{cr}}} = 0, \qquad \left.\frac{\partial \sigma_{pp}}{\partial \boldsymbol{\theta}}\right|_{\widehat{\boldsymbol{\theta}}^{\mathrm{cr}}} = 0 \tag{5.4}$$

Contrariwise, for the stress-based projected discontinuity model, if the solution to the kinematic constraints (4.44) does not exist, the strain localization with stress continuity cannot occur. In this situation, the given stress-based failure criterion can be modified based on the solution to Eq. (5.4) in such a way that both families of models are completely equivalent; see the 2D cases presented in Sections 6 and 6.3. □

5.3. Equivalence conditions between traction- and stress-based localized models

With the above arguments, it can be concluded that:

- An embedded/smeared discontinuity model is equivalent to the projected discontinuity model with a given stress-based failure criterion $\widehat{F}(\boldsymbol{\sigma}, q) \leq 0$, providing the traction-based failure criterion in the former is adopted as $\widehat{f}(\boldsymbol{t}, q) = f(\boldsymbol{t}, q) \leq 0$ and Mohr's maximization postulate is used to determine the discontinuity orientation. Here, the traction-based failure criterion $f(\boldsymbol{t}, q) \leq 0$ is projected from the given stress-based counterpart $\widehat{F}(\boldsymbol{\sigma}, q) \leq 0$ to the orientation $\boldsymbol{n}(\boldsymbol{\theta}^{\mathrm{cr}})$ which satisfies the kinematic constraint (4.65).

- A projected discontinuity model is equivalent to the embedded/smeared discontinuity model with a traction-based failure criterion $\widehat{f}(\boldsymbol{t}, q) \leq 0$ and the discontinuity orientation $\boldsymbol{n}(\widehat{\boldsymbol{\theta}}^{\mathrm{cr}})$ determined from Mohr's maximization postulate, if the stress-based failure criterion in the former is adopted as $\widehat{F}(\boldsymbol{\sigma}, q) = \widehat{f}\big[\boldsymbol{\sigma} \cdot \boldsymbol{n}(\widehat{\boldsymbol{\theta}}^{\mathrm{cr}}), q\big] \leq 0$.

In this case, the discontinuity orientation $\boldsymbol{n}(\boldsymbol{\theta}^{\mathrm{cr}})$ and the associated dissipative flow vector $\boldsymbol{\gamma}$ satisfying the kinematic constraint (4.65) coincide with the given ones $\boldsymbol{n}(\widehat{\boldsymbol{\theta}}^{\mathrm{cr}})$ and $\widehat{\boldsymbol{\gamma}} := \partial \widehat{f}/\partial \boldsymbol{t}$.

Upon the above conditions, the inelastic evolution laws coincide for both families of models, i.e.,

$$\boldsymbol{\gamma} = \widehat{\boldsymbol{\gamma}}, \qquad \boldsymbol{n}(\boldsymbol{\theta}^{\mathrm{cr}}) = \boldsymbol{n}(\widehat{\boldsymbol{\theta}}^{\mathrm{cr}}) \qquad \Longleftrightarrow \qquad \boldsymbol{\Lambda} = \widehat{\boldsymbol{\Lambda}} \tag{5.5}$$

Providing identical softening laws $q(\kappa)$ or $q(\bar{\kappa})$ are used, the traction-based embedded/smeared discontinuity models (or the equivalent elastoplastic damage model) and the stress-based projected discontinuity model are equivalent to each other.

6. Closed-form 2D results and prototype examples

In this section the general results presented in previous sections are particularized to the 2D conditions of plane stress ($\sigma_3 = 0$) and plane strain ($\epsilon_3 = 0$). As shown in Figure 8, a 2D solid $\Omega \subset \mathbb{R}^2$ with a discontinuity $\mathcal{S}$ is considered. The unit normal vector $\boldsymbol{n}$ and the tangential vector $\boldsymbol{m}$ of the discontinuity $\mathcal{S}$ are on the plane of interest, with the other tangential vector $\boldsymbol{p}$ perpendicular to that plane. The in-plane principal stresses are denoted by σ_1 and σ_2 ($\sigma_1 \geq \sigma_2$), respectively, while the third one σ_3 is orthogonal to that plane. In such 2D cases, the discontinuity orientation can be characterized by the inclination angle (anti-clockwise) $\theta \in [-\pi/2, \pi/2]$ between the normal vector $\boldsymbol{n}$ and the principal vector $\boldsymbol{v}_1$ of the stress tensor; see Appendix A. The task is to derive explicitly the discontinuity angle θ^{cr} and the traction-based failure criterion $f(\boldsymbol{t}, q) \leq 0$ projected from the given stress-based counterpart $\widehat{F}(\boldsymbol{\sigma}, q) \leq 0$. Several classical failure criteria, i.e., Rankine, Mohr-Coulomb, von Mises and Drucker-Prager models, are considered as prototype examples.

6.1. Discontinuity angle

For a given stress-based failure criterion $\widehat{F}(\boldsymbol{\sigma}, q) \leq 0$, the discontinuity angle θ^{cr} can be determined explicitly through the projection relation (4.65) or, more specifically, through Eqs. (4.44). This requires cancellation of all the out-of-plane components of the dissipative flow tensor $\widehat{\boldsymbol{\Lambda}}$, i.e.,

$$\widehat{\Lambda}_{mm}(\theta^{\mathrm{cr}}) = 0, \qquad \widehat{\Lambda}_{pp}(\theta^{\mathrm{cr}}) = 0, \qquad \widehat{\Lambda}_{mp}(\theta^{\mathrm{cr}}) = 0 \tag{6.1}$$

Note that in 2D cases the last constraint $\widehat{\Lambda}_{mp}(\theta^{\mathrm{cr}}) = 0$ is automatically satisfied.

It follows from Eqs. (A.10) and the constraint $\widehat{\Lambda}_{mm}(\theta^{\mathrm{cr}}) = 0$ that

$$\sin^2\theta^{\mathrm{cr}} = -\frac{\widehat{\Lambda}_2}{\widehat{\Lambda}_1 - \widehat{\Lambda}_2}, \qquad \cos^2\theta^{\mathrm{cr}} = \frac{\widehat{\Lambda}_1}{\widehat{\Lambda}_1 - \widehat{\Lambda}_2} \tag{6.2a}$$

or, equivalently,

$$\cos(2\theta^{\mathrm{cr}}) = \frac{\widehat{\Lambda}_1 + \widehat{\Lambda}_2}{\widehat{\Lambda}_1 - \widehat{\Lambda}_2}, \qquad \sin(2\theta^{\mathrm{cr}}) = 2\mathrm{sign}(\sigma_{nm})\frac{\sqrt{-\widehat{\Lambda}_1\widehat{\Lambda}_2}}{\widehat{\Lambda}_1 - \widehat{\Lambda}_2} \tag{6.2b}$$

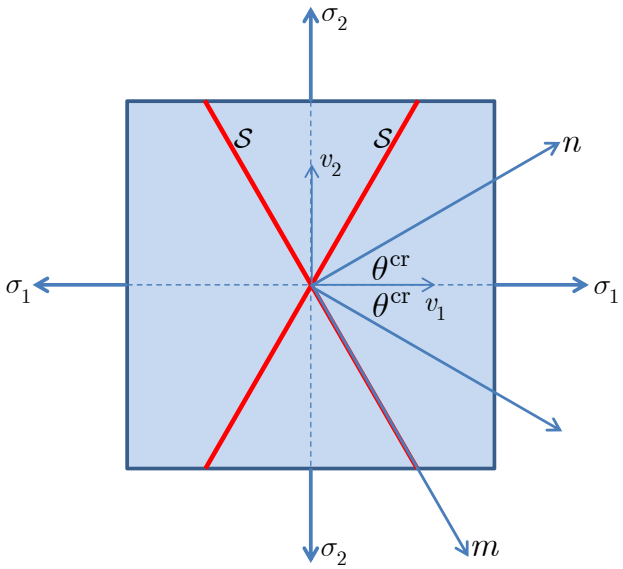

Figure 8: Definition of the discontinuity angle in 2D cases

with sign$(\cdot)$ being the sign function. Note that the above results apply upon the conditions $\hat{\Lambda}_1 \geq 0$ and $\hat{\Lambda}_2 \leq 0$. The exceptional case is referred to Section 6.3.

Obviously, the discontinuity angle θ^{cr} depends on the ratio $\hat{\Lambda}_2/\hat{\Lambda}_1$ or more precisely, the stress state upon strain localization. Regarding the remaining condition, $\hat{\Lambda}_{pp} = 0$, the conditions of plane stress and plane strain have to be considered independently.

6.1.1. Plane stress

In the case of plane stress, the out-of-plane stress component $\sigma_{pp} = \sigma_3 = 0$ vanishes. That is, the corresponding dissipative flow component $\hat{\Lambda}_{pp} = \hat{\Lambda}_3 = 0$ needs not be considered, and no extra constraint imposes on the stress state upon strain localization. Therefore, once the initial failure surface, i.e., the elastic limit $\hat{F}(\boldsymbol{\sigma}, q^0) = 0$, is reached, strain localization occurs at the same instant, with the orientation determined from Eqs. (6.2).

Note that for the material model with associated evolution laws the discontinuity angle θ^{cr} determined from Eqs. (6.2) coincides with that obtained from the classical discontinuous bifurcation analysis [58].

6.1.2. Plane strain

In the case of plane strain (i.e. $\epsilon_3 = 0$), on one hand, the out-of-plane stress σ_3 in the elastic regime is given by

$$\sigma_3 = \nu(\sigma_1 + \sigma_2) \tag{6.3}$$

with ν being the material Poisson's ratio. On the other hand, the condition $\hat{\Lambda}_{pp} = 0$ determines the stress state upon strain localization, i.e.,

$$\hat{\Lambda}_{pp} = \hat{\Lambda}_3 = 0 \qquad \Longrightarrow \qquad \sigma_3 = \eta_1(\sigma_1 + \sigma_2) + \eta_2 q \tag{6.4}$$

where η_1 and η_2 are related to the parameters involved in the specified stress-based failure criterion $\hat{F}(\boldsymbol{\sigma}, q) \leq 0$; see the examples presented later. As the in-plane principal values $\hat{\Lambda}_1$ and $\hat{\Lambda}_2$ depend on the out-of-plane stress $\sigma_3 \neq 0$, the discontinuity angle θ^{cr}, still determined from Eq. (6.2), is affected by this extra plane strain localization condition.

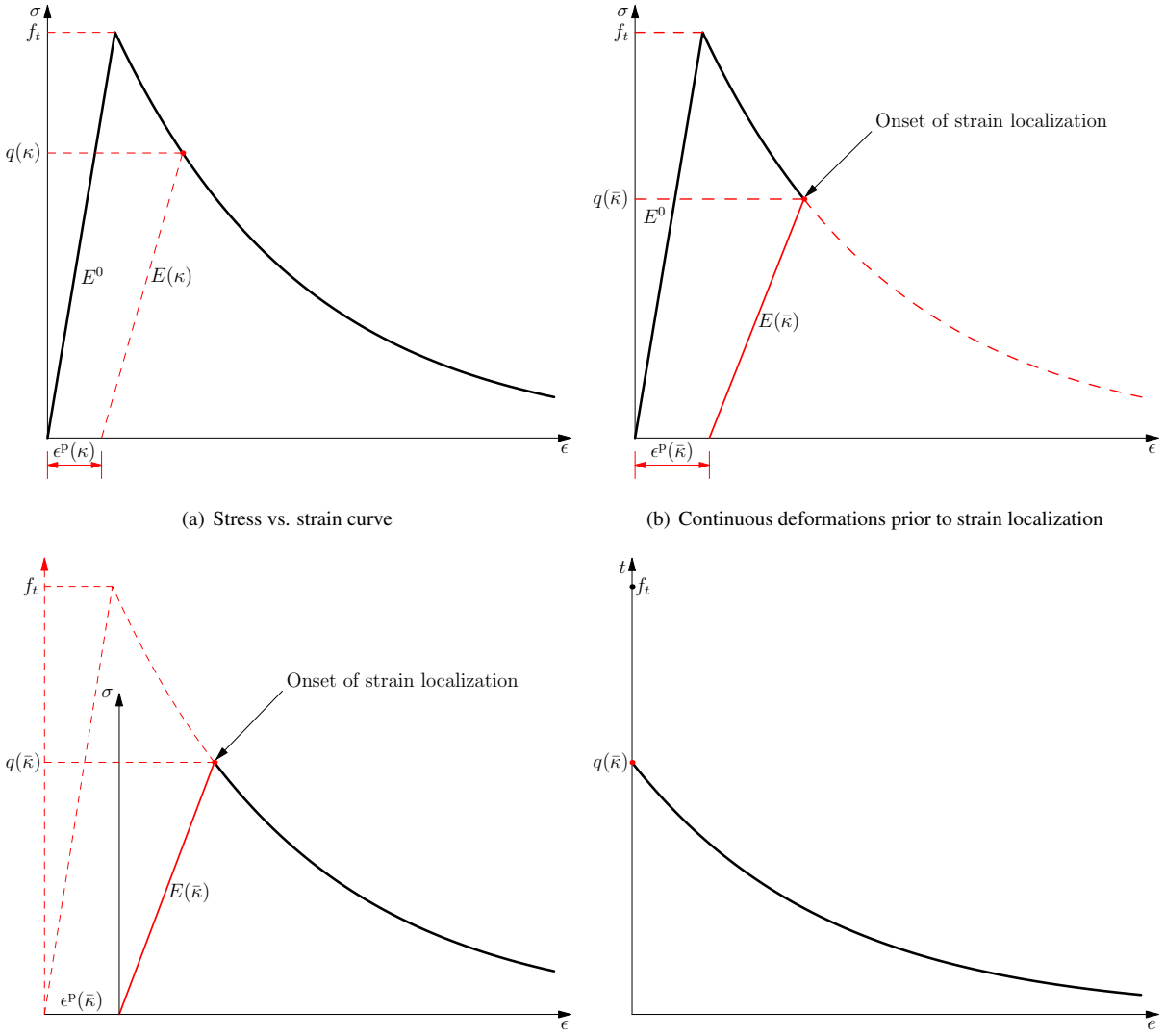

(a) Stress vs. strain curve

(b) Continuous deformations prior to strain localization

(c) Discontinuous deformations post strain localization

(d) Traction vs. *localized* inelastic deformation vector

Figure 9: Delayed strain localization in the condition of plane strain. Here, $\bar{\kappa}$ denotes the corresponding value of the strain-like internal variable κ at the onset of strain localization.

The out-of-plane stress (6.4), necessary for plane strain localization, is in general different from the elastic value (6.3). Furthermore, the initial limit surface $\hat{F}(\boldsymbol{\sigma}, q^0) = 0$ will be reached earlier with the elastic out-of-plane stress (6.3) than with the localized one (6.4). Accordingly, except for very particular cases, strain localization cannot occur at the onset of softening. Rather, some (continuous) inelastic deformations and substantial rotation of the principal strain directions have to occur first at the beginning of the softening regime, until the plane strain localization condition (6.4)

is fulfilled. From that moment on, the (continuous) inelastic deformations in the bulk material are frozen (unloading), and the discontinuous inelastic deformations within the discontinuity (band) occur due to strain localization. That is, similarly to the continuous-discontinuous failure [24], the bulk material is considered as linear elastic after strain localization occurs, however, with degraded (unloading) stiffness and plastic deformations corresponding to those at the time when strain localization is initiated; see Fig. 9 for the illustration.

This delayed strain localization in the plane strain condition was numerically observed in [11] for von Mises (J_2) model. As shown later, it also occurs for general failure criteria like the classical Drucker-Prager criterion.

6.2. *Traction-based failure criterion*

With the discontinuity angle $\theta^{\rm cr}$ determined from Eq. (6.2), the dissipative flow vector $\boldsymbol{\gamma}$ given in Eqs. (4.42a) and (4.42b) simplifies to

$$\boldsymbol{\gamma} = \gamma_n \boldsymbol{n} + \gamma_m \boldsymbol{m} \tag{6.5}$$

where the normal and tangent components (γ_n, γ_m) are given by

$$\gamma_n = \widehat{\Lambda}_{nn}(\theta^{\rm cr}) = \big(\widehat{\Lambda}_1 - \widehat{\Lambda}_2\big)\cos(2\theta^{\rm cr}) = \widehat{\Lambda}_1 + \widehat{\Lambda}_2 \tag{6.6a}$$

$$\gamma_m = 2\widehat{\Lambda}_{nm}(\theta^{\rm cr}) = \big(\widehat{\Lambda}_1 - \widehat{\Lambda}_2\big)\sin(2\theta^{\rm cr}) = 2{\rm sign}(\sigma_{nm})\sqrt{-\widehat{\Lambda}_1\widehat{\Lambda}_2} \tag{6.6b}$$

In accordance with Eq. (4.67), the traction-based failure criterion $f(\boldsymbol{t}, q) \le 0$ is projected from the stress-based counterpart $\widehat{F}(\boldsymbol{\sigma}, q) \le 0$ as

$$f(\boldsymbol{t}, q) = \frac{1}{M}\Big[\big(\widehat{\Lambda}_1 + \widehat{\Lambda}_2\big)t_n + 2\sqrt{-\widehat{\Lambda}_1\widehat{\Lambda}_2}\,|t_m| - \widehat{h}\cdot q\Big] \le 0 \tag{6.7}$$

Similarly, the projected traction-based failure criterion (6.7) holds for the cases $\widehat{\Lambda}_1 \ge 0$ and $\widehat{\Lambda}_2 \le 0$.

Remark 6.1 For the traction-based failure criterion (6.7), its first-order derivative with respect to θ reads

$$\begin{aligned}\frac{\partial f}{\partial \theta} &= -\big(\sigma_1 - \sigma_2\big)\Big[\gamma_n \sin\big(2\theta\big) - \gamma_m \cos\big(2\theta\big)\Big] \\ &= -\frac{1}{2}\big(\sigma_1 - \sigma_2\big)\Big[\big(\widehat{\Lambda}_1 + \widehat{\Lambda}_2\big) - \big(\widehat{\Lambda}_1 - \widehat{\Lambda}_2\big)\cos(2\theta)\Big]\sin(2\theta)\end{aligned} \tag{6.8a}$$

together with the following second-order one

$$\frac{\partial^2 f}{\partial \theta^2} = -\big(\sigma_1 - \sigma_2\big)\Big[\big(\widehat{\Lambda}_1 + \widehat{\Lambda}_2\big)\cos(2\theta) - \big(\widehat{\Lambda}_1 - \widehat{\Lambda}_2\big)\cos(4\theta)\Big] \tag{6.8b}$$

where the relations (A.10) have been considered. For the discontinuity angle $\theta^{\rm cr}$ given from Eq. (6.2), it follows that

$$\left.\frac{\partial f}{\partial \theta}\right|_{\theta^{\rm cr}} = 0, \qquad \left.\frac{\partial^2 f}{\partial \theta^2}\right|_{\theta^{\rm cr}} < 0 \tag{6.9}$$

Therefore, providing strain localization with stress continuity can occur, the tractions (t_n, t_m) do maximize the projected traction-based failure criterion $f(\boldsymbol{t}, q) \le 0$, as proved in Section 5. ■

6.3. Exceptional 2D cases

For the cases $\widehat{\Lambda}_2 > 0$ or $\widehat{\Lambda}_1 < 0$, the discontinuity angle determined from Eq. (6.2) does not hold. It implies that strain localization with stress continuity cannot occur for the given stress-based failure criterion $\widehat{F}(\boldsymbol{\sigma}, q) \leq 0$. In this situation, the given stress-based failure criterion can be modified as suggested in Remark 5.1, so that the projected traction-based one (6.7) still applies. In 2D cases, the corresponding maximization conditions (6.8) and (6.9) give the following discontinuity angle

$$\sin(2\theta^{\mathrm{cr}}) = 0 \qquad \Longrightarrow \qquad \theta^{\mathrm{cr}} = \begin{cases} 0 & \widehat{\Lambda}_1 > \widehat{\Lambda}_2 > 0 \\ \pi/2 & \widehat{\Lambda}_2 < \widehat{\Lambda}_1 < 0 \end{cases} \tag{6.10}$$

which corresponds to the limit values $\widehat{\Lambda}_2 = 0$ and $\widehat{\Lambda}_1 = 0$, respectively.

Accordingly, the given stress-based failure function $\widehat{F}(\boldsymbol{\sigma}, q)$ is modified as

$$\widehat{F}(\boldsymbol{\sigma}, q) = \begin{cases} \dfrac{1}{M}\left[\left(\widehat{\Lambda}_1\Big|_{\widehat{\Lambda}_2=0}\right)\sigma_1 - \widehat{h}\cdot q\right] & \widehat{\Lambda}_1 > \widehat{\Lambda}_2 > 0 \\ \dfrac{1}{M}\left[\left(\widehat{\Lambda}_2\Big|_{\widehat{\Lambda}_1=0}\right)\sigma_2 - \widehat{h}\cdot q\right] & \widehat{\Lambda}_2 < \widehat{\Lambda}_1 < 0 \end{cases} \tag{6.11}$$

As will be clear, this modification introduces tension- and compression-extensions into the original stress-based failure criterion $\widehat{F}(\boldsymbol{\sigma}, q) \leq 0$. Similarly, the projected traction-based failure function $f(\boldsymbol{t}, q)$ is expressed as

$$f(\boldsymbol{t}, q) = \begin{cases} \dfrac{1}{M}\left[\left(\widehat{\Lambda}_1\big|_{\widehat{\Lambda}_2=0}\right)t_n - h\cdot q\right] & \widehat{\Lambda}_1 > \widehat{\Lambda}_2 > 0 \\ \dfrac{1}{M}\left[\left(\widehat{\Lambda}_2\big|_{\widehat{\Lambda}_1=0}\right)t_n - h\cdot q\right] & \widehat{\Lambda}_2 < \widehat{\Lambda}_2 < 0 \end{cases} \tag{6.12}$$

where the tangential traction is removed from the failure criterion (6.7). With the above modifications, the stress- and traction-based models are completely equivalent to each other.

6.4. Example: Rankine criterion

The Rankine criterion, widely adopted for the modeling of tensile failure in quasi-brittle materials, is expressed in terms of the major principal stress $\sigma_1 = \boldsymbol{v}_1 \cdot \boldsymbol{\sigma} \cdot \boldsymbol{v}_1 > 0$ as

$$\widehat{F}(\boldsymbol{\sigma}, q) = \langle\sigma_1\rangle - q = \mathscr{H}(\sigma_1)\,\sigma_1 - q \leq 0 \tag{6.13}$$

where the Macaulay brackets $\langle\cdot\rangle$ and Heaviside function $\mathscr{H}(\cdot)$ are defined as: $\langle x\rangle = x$, $\mathscr{H}(x) = 1$ if $x > 0$, and $\langle x\rangle = 0$, $\mathscr{H}(x) = 0$ otherwise, respectively.

As the out-of-plane principal value $\widehat{\Lambda}_3 = 0$ vanishes in both plane stress and plane strain conditions, it follows from Eq. (6.2) that

$$\sin^2\theta^{\mathrm{cr}} = 0 \qquad \Longrightarrow \qquad \theta^{\mathrm{cr}} = 0 \tag{6.14}$$

As expected, only a mode I discontinuity (in the context of fracture mechanics) can be initiated from the Rankine criterion. With the critical angle (6.14), the traction-based failure criterion (6.7) becomes

$$f(\boldsymbol{t},q) = \mathscr{H}(\sigma_1)t_n - q = \langle t_n \rangle - q \leq 0 \tag{6.15}$$

where the relation $\sigma_1 = \boldsymbol{n}\cdot\boldsymbol{\sigma}\cdot\boldsymbol{n} = t_n$ has been considered for mode-I failure.

6.5. Example: Mohr-Coulomb criterion

Let us then consider the Mohr-Coulomb criterion, with the failure function defined as

$$\widehat{F}(\boldsymbol{\sigma},q) = \begin{cases} \frac{1}{2}\Big[(\sigma_1+\sigma_3)\sin\varphi + (\sigma_1-\sigma_3)\Big] - q\cos\varphi & \text{Region 1} : \sigma_1 \geq \sigma_2 \geq \sigma_3 \\ \frac{1}{2}\Big[(\sigma_1+\sigma_2)\sin\varphi + (\sigma_1-\sigma_2)\Big] - q\cos\varphi & \text{Region 2} : \sigma_1 \geq \sigma_3 \geq \sigma_2 \\ \frac{1}{2}\Big[(\sigma_3+\sigma_2)\sin\varphi + (\sigma_3-\sigma_2)\Big] - q\cos\varphi & \text{Region 3} : \sigma_3 \geq \sigma_1 \geq \sigma_2 \end{cases} \tag{6.16}$$

where the internal friction angle $\varphi \in [0, \pi/2]$ is determined from

$$\sin\varphi = \frac{\rho-1}{\rho+1} \qquad \Longleftrightarrow \qquad \rho = \frac{1+\sin\varphi}{1-\sin\varphi} \tag{6.17}$$

for the ratio $\rho := f_c/f_t \geq 1$ between the uniaxial compressive strength f_c and the tensile one f_t.

In the case of plane stress ($\sigma_3 = 0$), the principal values $\widehat{\Lambda}_i$ of the inelastic flow tensor $\widehat{\boldsymbol{\Lambda}}$ are given by

$$\begin{cases} \widehat{\Lambda}_1 = \frac{1}{2}\big(1+\sin\varphi\big), \quad \widehat{\Lambda}_2 = 0 & \text{Region 1} : \sigma_1 \geq \sigma_2 \geq \sigma_3 \\ \widehat{\Lambda}_1 = \frac{1}{2}\big(1+\sin\varphi\big), \quad \widehat{\Lambda}_2 = \frac{1}{2}\big(-1+\sin\varphi\big) & \text{Region 2} : \sigma_1 \geq \sigma_3 \geq \sigma_2 \\ \widehat{\Lambda}_1 = 0, \quad \widehat{\Lambda}_2 = \frac{1}{2}\big(-1+\sin\varphi\big) & \text{Region 3} : \sigma_3 \geq \sigma_1 \geq \sigma_2 \end{cases} \tag{6.18}$$

Accordingly, it follows from Eq. (6.2) that $\theta^{\text{cr}} = 0$ in Region 1 and $\theta^{\text{cr}} = \pi/2$ in Region 3, respectively; in Region 2 (i.e., $\sigma_1 \geq \sigma_3 \geq \sigma_2$), the discontinuity angle θ^{cr} is determined as

$$\sin^2\theta^{\text{cr}} = \frac{1}{2}\big(1-\sin\varphi\big) \qquad \Longrightarrow \qquad \theta^{\text{cr}} = \pm\Big(\frac{\pi}{4} - \frac{\varphi}{2}\Big) \tag{6.19}$$

The above results coincide with those obtained from Mohr's maximization postulate.

In the case of plane strain, the principal values $\widehat{\Lambda}_i$ of the inelastic flow vector $\widehat{\boldsymbol{\Lambda}}$ are expressed as

$$\begin{cases} \widehat{\Lambda}_1 = \frac{1}{2}\big(1+\sin\varphi\big), \quad \widehat{\Lambda}_2 = 0, \quad \widehat{\Lambda}_3 = \frac{1}{2}\big(-1+\sin\varphi\big) & \text{Region 1} : \sigma_1 \geq \sigma_2 \geq \sigma_3 \\ \widehat{\Lambda}_1 = \frac{1}{2}\big(1+\sin\varphi\big), \quad \widehat{\Lambda}_2 = \frac{1}{2}\big(-1+\sin\varphi\big), \quad \widehat{\Lambda}_3 = 0 & \text{Region 2} : \sigma_1 \geq \sigma_3 \geq \sigma_2 \\ \widehat{\Lambda}_1 = 0, \quad \widehat{\Lambda}_2 = \frac{1}{2}\big(-1+\sin\varphi\big), \quad \widehat{\Lambda}_3 = \frac{1}{2}\big(1+\sin\varphi\big) & \text{Region 3} : \sigma_3 \geq \sigma_1 \geq \sigma_2 \end{cases} \tag{6.20}$$

In Regions 1 and 3, the extra constraint $\widehat{\Lambda}_3 = 0$ cannot be satisfied in general; only in Region 2 (i.e., $\sigma_1 \geq \sigma_3 \geq \sigma_2$) can strain localization occur, with the same discontinuity angle (6.19).

For the discontinuity angle (6.19), in Region 2 ($\sigma_1 \geq \sigma_3 \geq \sigma_2$) the traction-based failure criterion (6.6) reads

$$f(\boldsymbol{t}, q) = \cos\varphi\Big(t_n \tan\varphi + \big|t_m\big| - q\Big) \leq 0 \tag{6.21a}$$

or, equivalently,

$$\tan\varphi \cdot t_n + \big|t_m\big| - q \leq 0 \tag{6.21b}$$

in both cases of plane stress and plane strain. This is exactly the classical Mohr-Coulomb criterion.

Remark 6.2 Tresca's criterion is recovered for the friction angle $\varphi = 0$ in the Mohr-Coulomb criterion (6.16). In Region 2 ($\sigma_1 \geq \sigma_3 \geq \sigma_2$), the discontinuity angle is then $\theta^{\text{cr}} = \pi/4$, and the corresponding traction-based failure criterion is expressed as

$$f(\boldsymbol{t}, q) = \big|t_m\big| - q \leq 0 \tag{6.22}$$

for both cases of plane stress and plane strain. ■

6.6. Example: von Mises (J_2) criterion

The von Mises (J_2) criterion is now considered

$$\widehat{F}(\boldsymbol{\sigma}, q) = \sqrt{3J_2} - q = \sqrt{\frac{3}{2}}\,\big\|\boldsymbol{s}\big\| - q \leq 0 \tag{6.23}$$

in terms of the second invariant $J_2 := \frac{1}{2}\boldsymbol{s} : \boldsymbol{s}$ or the norm $\big\|\boldsymbol{s}\big\| := \boldsymbol{s} : \boldsymbol{s}$ of the deviatoric stress tensor $\boldsymbol{s}$.

The discontinuity angle θ^{cr} is given from Eq. (6.2) as

$$\sin^2\theta^{\text{cr}} = -\frac{s_2}{s_1 - s_2}, \qquad \cos^2\theta^{\text{cr}} = \frac{s_1}{s_1 - s_2} \tag{6.24}$$

for the principal values s_i $(i = 1, 2, 3)$ of the deviatoric stress tensor $\boldsymbol{s}$.

6.6.1. Plane stress

In the case of plane stress ($\sigma_3 = 0$), the in-plane principal values of the deviatoric stress $\boldsymbol{s}$ are evaluated as $s_1 = (2\sigma_1 - \sigma_2)/3$ and $s_2 = (2\sigma_2 - \sigma_1)/3$, respectively. Accordingly, the discontinuity angle θ^{cr} is determined as

$$\sin^2\theta^{\text{cr}} = \frac{\sigma_1 - 2\sigma_2}{3\big(\sigma_1 - \sigma_2\big)}, \qquad \cos^2\theta^{\text{cr}} = \frac{2\sigma_1 - \sigma_2}{3\big(\sigma_1 - \sigma_2\big)} \tag{6.25}$$

if the conditions $\sigma_1 \geq \frac{1}{2}\sigma_2$ and $\sigma_1 \geq 2\sigma_2$ are satisfied. The resulting discontinuity angles θ^{cr} for different stress ratios σ_1/σ_2, summarized in Table 1, are depicted in Fig. 10.

With the discontinuity angle (6.25), the corresponding normal and tangential tractions (t_n, t_m) are evaluated from Eqs. (A.9) as

$$t_n = \sigma_{nn} = \frac{2}{3}\big(\sigma_1 + \sigma_2\big), \qquad t_m^2 = \sigma_{nm}^2 = -s_1 s_2 \tag{6.26}$$

Table 1: Discontinuity angles θ^{cr} for the von Mises criterion in the condition of plane stress

	Stress ratio σ_1/σ_2							
	-1: -2	-1: -5	0: -1	1: -5	1: -1	1: 0	1: 0.25	1: 0.5
θ^{cr}	90.00°	60.00°	54.74°	51.42°	45.00°	35.26°	28.12°	0.00°

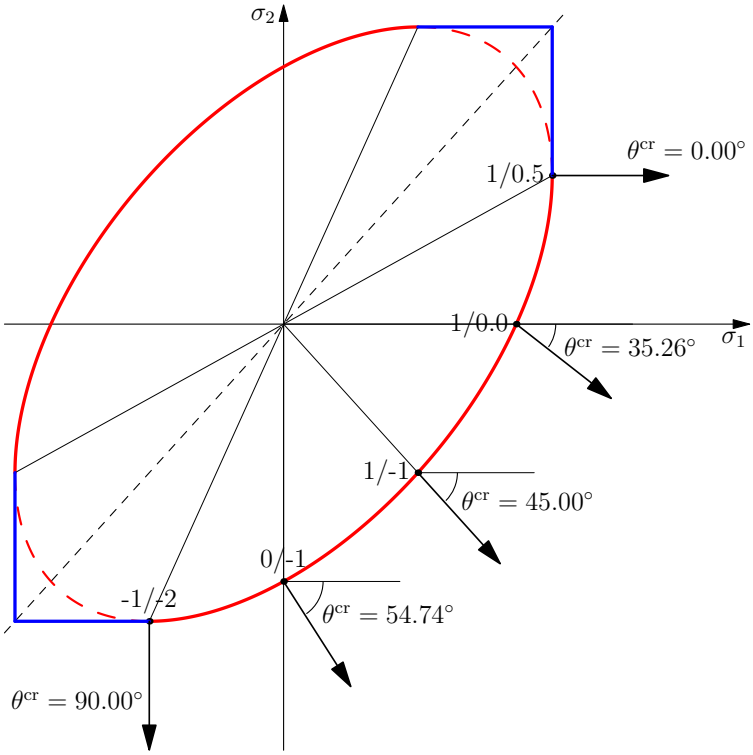

(a) Principal stress space

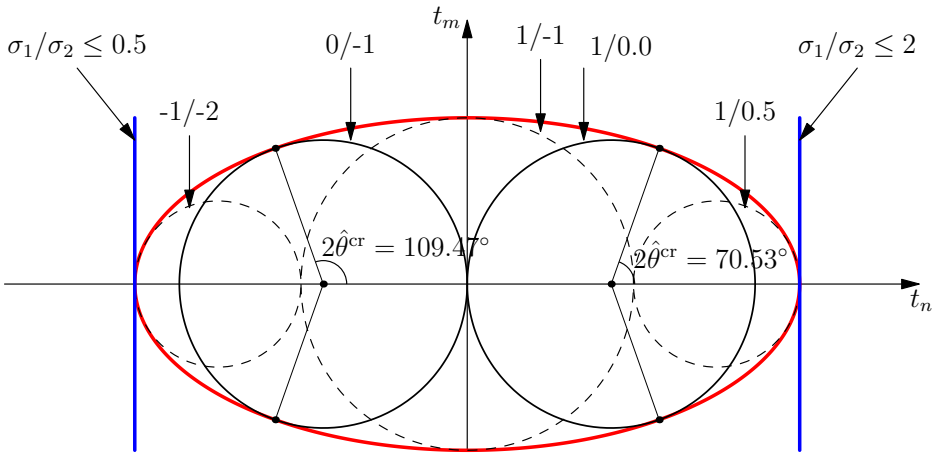

(b) Traction space

Figure 10: Discontinuity angles of the von Miese criterion in the condition of plane stress

so that

$$J_2 = \frac{1}{3}\left(\sigma_1^2 + \sigma_2^2 - \sigma_1\sigma_2\right) = \frac{1}{4}t_n^2 + t_m^2 \tag{6.27}$$

Substitution of the result (6.27) into Eq. (6.23) yields the following traction-based failure function

$$f(\boldsymbol{t}, q) = \sqrt{3\left(\frac{1}{4}t_n^2 + t_m^2\right)} - q \le 0 \tag{6.28}$$

The above failure criterion can also be derived from the definition (6.7). For the equi-biaxial tension/compression stress state, i.e., $\sigma_2 = -\sigma_1$ and $t_n = 0$, the expected pure shear failure criterion is recovered.

Remark 6.3 For the cases $\sigma_1 \le \frac{1}{2}\sigma_2$ or $\sigma_1 \le 2\sigma_2$, the discontinuity angle θ^{cr} in Eq. (6.10) applies. Accordingly, the modified stress- and traction-based failure criteria are given from Eqs. (6.11) and (6.12), respectively, i.e.,

$$\widehat{F}(\boldsymbol{\sigma}, q) = \begin{cases} \dfrac{\sqrt{3}}{2}\sigma_1 - q & 0 < \sigma_2 < \sigma_1 < 2\sigma_2 \\ -\dfrac{\sqrt{3}}{2}\sigma_2 - q & 2\sigma_1 < \sigma_2 < \sigma_1 < 0 \end{cases} \tag{6.29a}$$

$$f(\boldsymbol{t}, q) = \frac{\sqrt{3}}{2}\left|t_n\right| - q \le 0 \tag{6.29b}$$

The above modified failure criteria with tension- and compression-extensions are also illustrated in Fig. 10. ■

6.6.2. Plane strain

In the case of plane strain, the condition (6.4) requires that

$$\widehat{\Lambda}_3 = 0 \qquad \Longrightarrow \qquad s_3 = 0, \qquad \sigma_3 = \frac{1}{2}\left(\sigma_1 + \sigma_2\right) \tag{6.30}$$

That is, $\eta_1 = 1/2$ and $\eta_2 = 0$ for the out-of-plane principal stress (6.4).

Upon the above stress state, the in-plane principal values of the deviatoric stress tensor $\boldsymbol{s}$ are expressed as

$$s_1 = -s_2 = \frac{\sigma_1 - \sigma_2}{2} \ge 0 \tag{6.31}$$

The discontinuity angle θ^{cr} is determined from Eq. (6.24) as

$$\sin^2\theta^{\text{cr}} = -\frac{s_2}{s_1 - s_2} = \frac{1}{2} \qquad \Longrightarrow \qquad \theta^{\text{cr}} = 45^\circ \tag{6.32}$$

As can be seen, in the condition of plane strain the discontinuity angle is fixed as $\theta^{\text{cr}} = 45^\circ$ independently of the stress ratio σ_1/σ_2.

For the discontinuity angle (6.32), the traction-based failure function (6.7) is expressed as

$$f(\boldsymbol{t}, q) = \sqrt{3}\,\left|t_m\right| - q \le 0 \tag{6.33}$$

As expected, for the von Mises criterion a pure mode II discontinuity forms upon strain localization, whatever the stress state is.

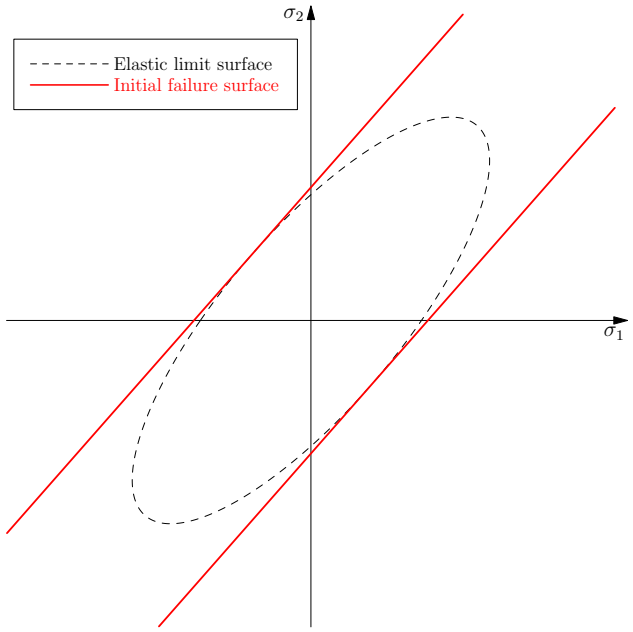

Figure 11: Elastic limit surface and initial failure surface of the von Miese criterion in the condition of plane strain

Remark 6.4 With the elastic out-of-plane stress (6.3) in the case of plane strain, the limit surface $\widehat{F}(\boldsymbol{\sigma}, q^0) = 0$ is expressed as

$$\sqrt{(1-\nu+\nu^2)(\sigma_1^2+\sigma_2^2)-(1+2\nu-2\nu^2)\sigma_1\sigma_2} = q^0 \tag{6.34}$$

With the out-of-plane stress (6.30) upon plane strain localization, the failure criterion $\widehat{F}(\boldsymbol{\sigma}, q) \leq 0$ becomes two parallel straight lines, i.e.,

$$\widehat{F}(\boldsymbol{\sigma}, q) = \frac{\sqrt{3}}{2}\,|\sigma_1 - \sigma_2| - q \leq 0 \tag{6.35}$$

As depicted in Fig. 11, only for the particular cases $\nu = 0.5$ or $\sigma_2 = -\sigma_1$ can strain localization occur at the onset of strain softening. For all other cases, the elastic limit surface (6.34) will be reached first and then strain softening occurs accompanied with (continuous) inelastic deformations. Only when the re-orientation of the principal strain directions is completed so that the plane strain localization condition (6.30) is fulfilled, strain localization may be set in motion while guaranteeing stress continuity. ■

6.7. Example: Drucker-Prager criterion

Finally, let us consider the following Drucker-Prager criterion

$$\widehat{F}(\boldsymbol{\sigma}, q) = \frac{1}{1+\alpha}\left(\alpha I_1 + \sqrt{3J_2}\right) - q \leq 0 \tag{6.36}$$

where the parameter $\alpha = (\rho-1)/(\rho+1) \in [0, 1)$ is related to the ratio $\rho := f_c/f_t \geq 1$ between the uniaxial compressive strength f_c and the tensile one f_t. For an activated discontinuity, it follows from the fact $\widehat{F}(\boldsymbol{\sigma}, q) = 0$

that

$$\sqrt{\frac{2}{3}}\,\|\boldsymbol{s}\| = \frac{2}{3}\Big[(1+\alpha)q - \alpha I_1\Big] \geq 0 \tag{6.37}$$

This relation is useful for later derivation of the traction-based failure criterion $f(\boldsymbol{t}, q) \leq 0$.

The discontinuity angle θ^{cr} is computed from Eq. (6.2) as

$$\sin^2\theta^{\mathrm{cr}} = -\frac{\sqrt{2/3}\,\alpha\|\boldsymbol{s}\| + s_2}{s_1 - s_2}, \qquad \cos^2\theta^{\mathrm{cr}} = \frac{\sqrt{2/3}\,\alpha\|\boldsymbol{s}\| + s_1}{s_1 - s_2} \tag{6.38}$$

where s_1 and s_2 denote the in-plane principal values of the deviatoric stress tensor $\boldsymbol{s}$.

6.7.1. Plane stress

In the case of plane stress ($\sigma_3 = 0$), it follows from Eq. (6.38) that

$$\sin^2\theta^{\mathrm{cr}} = -\frac{(2\sigma_2 - \sigma_1) + 2\alpha\sqrt{\sigma_1^2 + \sigma_2^2 - \sigma_1\sigma_2}}{3(\sigma_1 - \sigma_2)} \tag{6.39a}$$

$$\cos^2\theta^{\mathrm{cr}} = \frac{(2\sigma_1 - \sigma_2) + 2\alpha\sqrt{\sigma_1^2 + \sigma_2^2 - \sigma_1\sigma_2}}{3(\sigma_1 - \sigma_2)} \tag{6.39b}$$

if the conditions $\sigma_1 \geq \widetilde{\alpha}_1\sigma_2$ and $\sigma_1 \geq \sigma_2/\widetilde{\alpha}_2$ are satisfied, with $\widetilde{\alpha}_1$ and $\widetilde{\alpha}_2$ expressed as $\widetilde{\alpha}_{1,2} := \frac{1}{2}\Big[1 \pm \alpha\sqrt{3/(1-\alpha^2)}\Big]$. The above discontinuity angle θ^{cr}, dependent on the stress ratio σ_1/σ_2 and model parameter α, is summarized in Table 2. Similarly, the exceptional cases can be obtained from the arguments in Section 6.3; the details are omitted.

Table 2: Discontinuity angles θ^{cr} for the Drucker-Prager criterion in the condition of plane stress

f_c/f_t	Stress ratio σ_1/σ_2										
	-1: -1.24	-1: -2	-1: -5	0: -1	1: -5	1: -1	1: -0.5	1: -0.25	1: -0.15	1: 0	1 : 0.19
2.00	90.00°	51.65°	44.74°	41.81°	39.52°	33.68°	29.90°	26.30°	24.15°	19.47°	0.00°
3.00	43.48°	40.55°	37.35°	35.26°	33.32°	27.37°	22.82°	17.90°	14.51°	0.00°	0.00°
4.00	—	33.66°	32.69°	31.09°	29.33°	23.07°	17.62°	10.53°	0.00°	0.00°	0.00°

With the above discontinuity angle, the following traction-based failure criterion can be determined (see Appendix B for the derivation)

$$t_m^2 - \frac{4\alpha^2 - 1}{4(1-\alpha^2)}t_n^2 + \frac{\alpha}{1-\alpha}qt_n - \frac{1+\alpha}{3(1-\alpha)}q^2 \leq 0 \tag{6.40}$$

As depicted in Fig. 12, depending on the model parameter $\alpha \in [0, 1)$ (or, equivalently, $\rho \geq 1$), the following three cases can be identified for the stress-based failure criterion (6.36) and its projected traction-based counterpart (6.40):

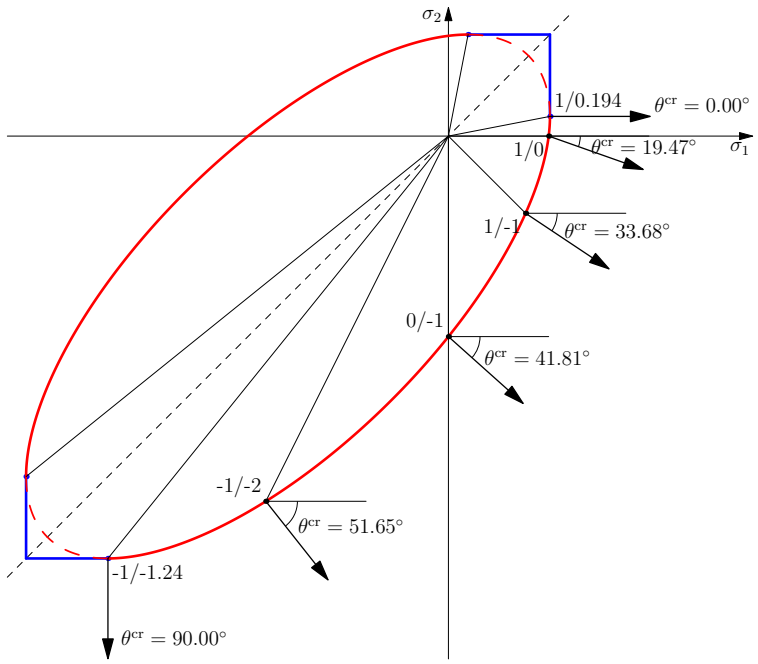

(a) Elliptic type ($\rho = 2.0$)

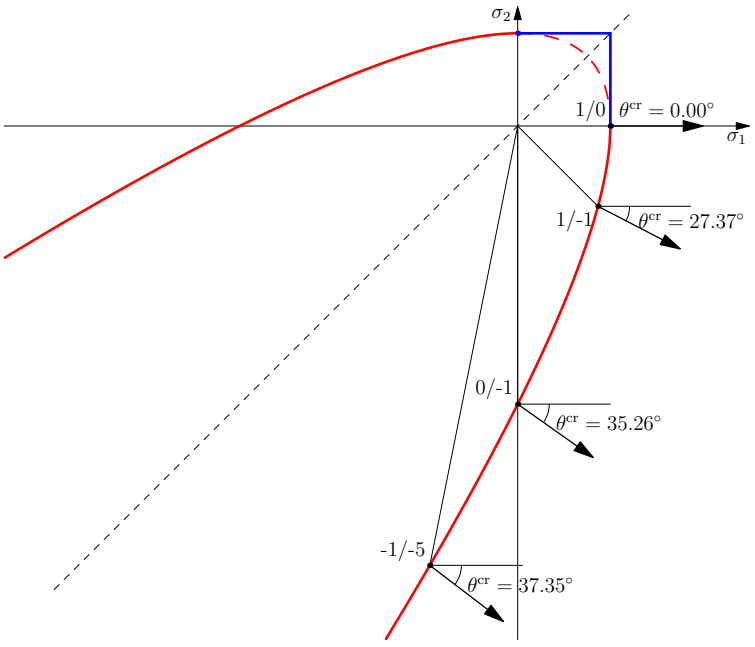

(b) Parabolic type ($\rho = 3.0$)

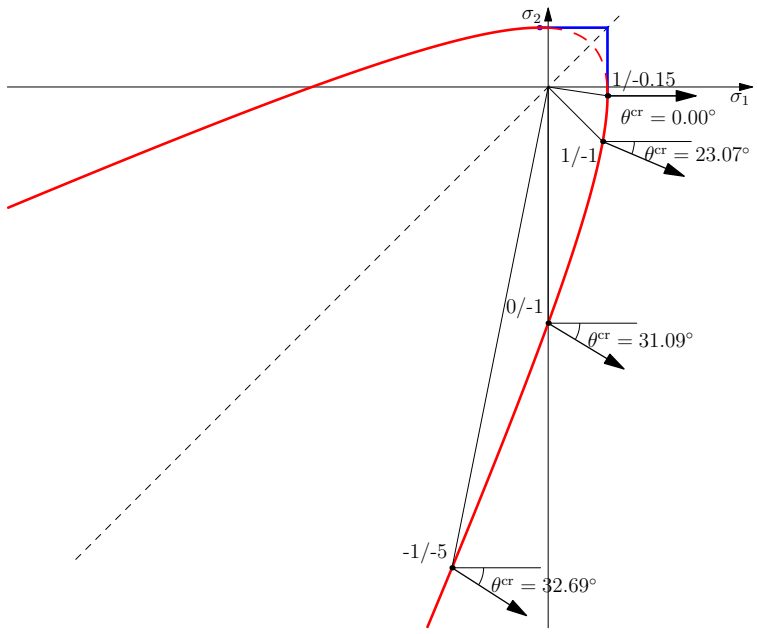

(c) Hyperbolic type ($\rho = 4.0$)

Figure 12: The Drucker-Prager criteria of different types in the condition of plane stress

- $0 \leq \alpha < 1/2$ or $1 \leq \rho < 3$: The stress-based failure criterion (6.36) is an ellipse on the $\sigma_1 - \sigma_2$ plane and the traction-based counterpart (6.40) also defines an ellipse on the $t_n - t_m$ plane

$$t_m^2 + \frac{1-4\alpha^2}{4(1-\alpha^2)}\left[t_n + \frac{2\alpha(1+\alpha)}{1-4\alpha^2}q\right]^2 - \frac{(1+\alpha)^2}{3(1-4\alpha^2)}q^2 \leq 0 \tag{6.41}$$

  The classical von Mises criterion belongs to this type (i.e., $\alpha = 0$).

- $\alpha = 1/2$ or $\rho = 3$: The stress-based failure criterion (6.36) defines a parabola on the $\sigma_1 - \sigma_2$ plane, while the traction-based counterpart (6.40) becomes

$$t_m^2 + q t_n - q^2 \leq 0 \tag{6.42}$$

  which is a parabola on the $t_n - t_m$ plane.

- $1/2 < \alpha < 1$ or $\rho > 3$: The stress-based failure criterion (6.36) defines a hyperbola on the $\sigma_1 - \sigma_2$ plane. Similarly, the failure criterion (6.40) is a hyperbola on the $t_n - t_m$ plane, with the left branch of interest for the current purpose given by

$$\tan\varphi \cdot t_n + \sqrt{t_m^2 + \omega^2 q^2} - c \leq 0 \tag{6.43}$$

  where the parameters $\tan\varphi, \omega$ and c are expressed as

$$\tan\varphi = \sqrt{\frac{4\alpha^2-1}{4(1-\alpha^2)}}, \qquad \omega = \frac{1+\alpha}{\sqrt{3(4\alpha^2-1)}}, \qquad c = \frac{\alpha(1+\alpha)}{\sqrt{(4\alpha^2-1)(1-\alpha^2)}}q \tag{6.44}$$

This hyperbolic failure criterion asymptotically approaching to a Mohr-Coulomb one has been widely adopted in the modeling of mixed-mode failure in solids [7, 14, 34, 66].

Remark 6.5 For the parameter $\alpha \in [1/2, 1)$, the Drucker-Prager failure criterion (6.36) defines an open surface in the principle $\sigma_1 - \sigma_2$ space. Accordingly, there exists a limit value for the discontinuity angle θ^{cr}. Regarding the parabolic failure criterion (i.e., $\alpha = 1/2$), it follows that

$$\lim_{\sigma_2 \to \sigma_1 < 0} \sin^2 \theta^{\text{cr}} = \lim_{\sigma_2 \to \sigma_1 < 0} -\frac{(2\sigma_2 - \sigma_1) + \sqrt{\sigma_1^2 + \sigma_2^2 - \sigma_1 \sigma_2}}{3(\sigma_1 - \sigma_2)} = \frac{1}{2} \tag{6.45}$$

Namely, the limit discontinuity angle is $\lim_{\sigma_2 \to \sigma_1 < 0} \theta^{\text{cr}} = 45°$. For the hyperbolic one with $\alpha \in (1/2, 1)$, the admissible stress ratio σ_1/σ_2 in the compression-compression quadrant (i.e., $\sigma_1 < 0$ and $\sigma_2 < 0$) is constrained by the value of parameter α, and so is the discontinuity angle θ^{cr}, i.e.,

$$\sin \theta^{\text{cr}} \le \sqrt{\frac{(1 + 2\alpha^2)\sigma_1/\sigma_2 - 2(1 - \alpha^2)}{3(\sigma_1/\sigma_2 - 1)}} \qquad \text{with} \qquad \frac{\sigma_1}{\sigma_2} \le \frac{1 + 2\alpha^2 - \sqrt{3(4\alpha^2 - 1)}}{2(1 - \alpha^2)} \tag{6.46}$$

For instance, it follows that $0° \le \theta^{\text{cr}} \le 33.74°$ for the parameter $\rho = 4.0$ or equivalently, $\alpha = 0.6$. □

6.7.2. Plane strain

In the case of plane strain, the extra condition (6.4) gives the following out-of-plane stress $\sigma_3 \neq 0$, i.e.,

$$\alpha + \sqrt{\frac{3}{2}} \frac{1}{\|\boldsymbol{s}\|} s_3 = 0 \qquad \Longrightarrow \qquad \sigma_3 = \frac{2\alpha^2 + 1}{2(1 - \alpha^2)}(\sigma_1 + \sigma_2) - \frac{\alpha}{1 - \alpha} q \tag{6.47}$$

where the relation (6.37) has been considered. As the trace of the deviatoric stress tensor $\boldsymbol{s}$ vanishes, it follows that

$$s_1 + s_2 = -s_3 = \sqrt{\frac{2}{3}}\, \alpha \|\boldsymbol{s}\| \ge 0 \qquad \text{or} \qquad s_1^2 + \frac{6 - 4\alpha^2}{3 - 4\alpha^2}\, s_1 s_2 + s_2^2 = 0 \tag{6.48}$$

Accordingly, the discontinuity angle (6.39) becomes

$$\sin^2 \theta^{\text{cr}} = -\frac{s_1 + 2s_2}{s_1 - s_2} = -\frac{\alpha_s + 2}{\alpha_s - 1}, \qquad \cos^2 \theta^{\text{cr}} = \frac{2s_1 + s_2}{s_1 - s_2} = \frac{2\alpha_s + 1}{\alpha_s - 1} \tag{6.49}$$

where $\alpha_s := s_1/s_2$ is determined from the relation (6.48)

$$\alpha_s := \frac{s_1}{s_2} = \frac{2\alpha^2 - 3 - 2\alpha\sqrt{3(1 - \alpha^2)}}{3 - 4\alpha^2} \in [-1, -2] \tag{6.50}$$

Note that the above result holds if the following condition

$$2s_1 + s_2 \ge 0, \qquad s_1 + 2s_2 \le 0 \qquad \Longleftrightarrow \qquad 0 \le \alpha \le \frac{1}{2} \tag{6.51}$$

is satisfied. Compared to the result (6.39) for the case of plane stress, the discontinuity angle θ^{cr} determined from Eqs. (6.49) and (6.50) depends only on the model parameter $\alpha \in [0, 1/2]$, whatever the stress state is; see Table 3. Note that the result for the von Mises criterion corresponds to the parameter $\alpha = 0$.

Table 3: Discontinuity angles θ^{cr} for the Drucker-Prager criterion in the condition of plane strain

f_c/f_t	1.0	1.50	2.00	2.50	3.00
θ^{cr}	45.00°	34.65°	26.12°	17.38°	0.00°

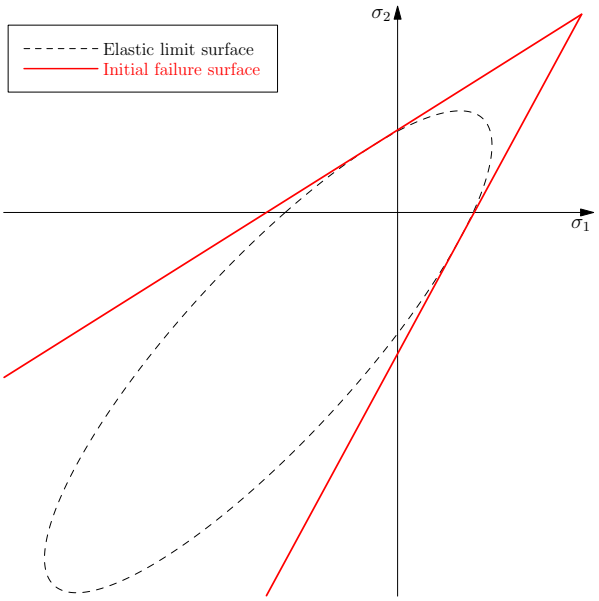

(a) Elastic limit surface of elliptic type

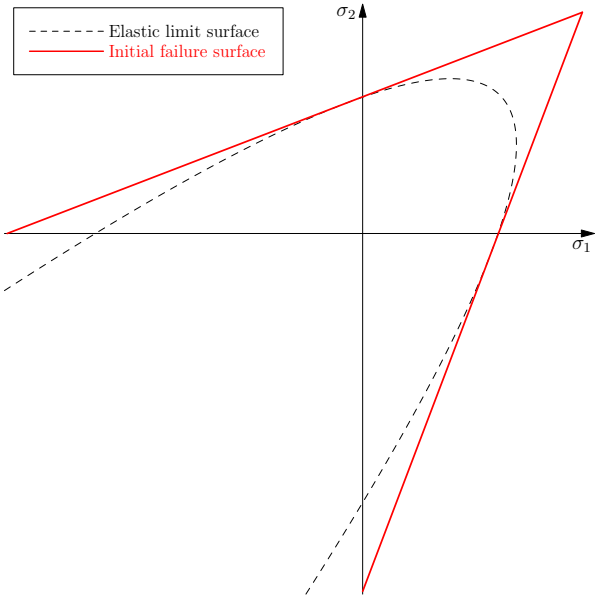

(b) Elastic limit surface of parabolic type

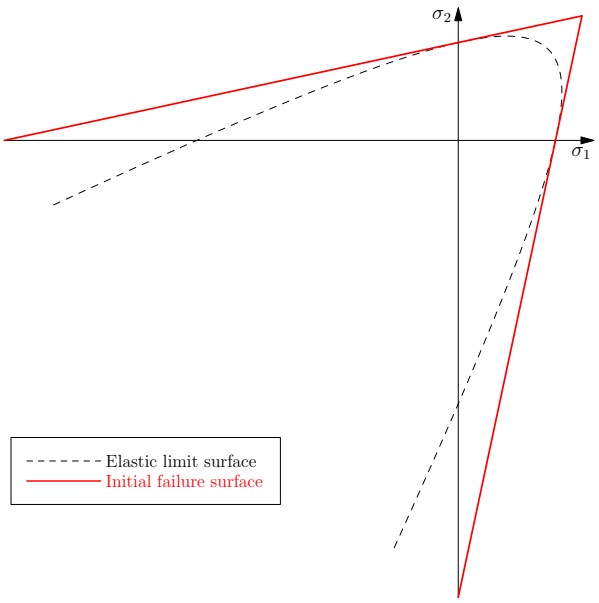

(c) Elastic limit surface of hyperbolic type

Figure 13: Elastic limit surface and initial failure surface of the Drucker-Prager criterion in the condition of plane strain

With the above discontinuity angle, the traction-based failure criterion (6.7) can be derived as (see Appendix B)

$$t_m^2 - \frac{3\alpha^2}{1-4\alpha^2}\Big(t_n - \frac{1+\alpha}{3}q\Big)^2 \le 0 \tag{6.52}$$

with the left branch of interest expressed as

$$t_n \cdot \tan\varphi + \big|t_m\big| - c \le 0 \tag{6.53}$$

where the friction angle φ and the cohesion c are given by

$$\tan\varphi = \alpha\sqrt{\frac{3}{1-4\alpha^2}}, \qquad c = \frac{1+\alpha}{\sqrt{3\big(1-4\alpha^2\big)}}q \tag{6.54}$$

That is, in the case of plane strain, the material characterized by the Drucker-Prager model localizes into a Mohr-Coulomb discontinuity; see Remark 6.6 for more discussion.

Remark 6.6 The relations (6.54) can be rewritten as

$$\alpha = \frac{\tan\varphi}{\sqrt{3+4\tan^2\varphi}}, \qquad \big(1+\alpha\big)q = \frac{3c}{\sqrt{3+4\tan^2\varphi}} \tag{6.55}$$

The above relations are exactly the matching conditions under which the Drucker-Prager and Mohr-Coulomb models give identical limit load for *perfectly-plastic* materials in the case of plane strain. Upon satisfaction of these plane strain matching conditions, both models produce identical energy dissipation [15]. ■

Remark 6.7 In the case of plane strain, on one hand, calling for the out-of-plane stress (6.3) the elastic limit surface $\widehat{F}(\boldsymbol{\sigma}, q^0) = 0$ of the Drucker-Prager criterion (6.36) is given by

$$\frac{1}{1+\alpha}\Big[\alpha\big(1+\nu\big)\big(\sigma_1+\sigma_2\big) + \sqrt{\big(1-\nu+\nu^2\big)\big(\sigma_1^2+\sigma_2^2\big) - \big(1+2\nu-2\nu^2\big)\sigma_1\sigma_2}\Big] = q^0 \tag{6.56}$$

The above elastic limit surface can be either an ellipse for $\alpha < (1/2-\nu)/(1+\nu)$, a parabola for $\alpha = (1/2-\nu)/(1+\nu)$, or a hyperbola for $\alpha > (1/2-\nu)/(1+\nu)$ on the $\sigma_1 - \sigma_2$ plane, respectively. On the other hand, for the plane strain localization condition (6.47), the Drucker-Prager criterion (6.36) becomes

$$\big|\sigma_1 - \sigma_2\big| = \sqrt{\frac{3}{1-\alpha^2}}\Big[\frac{2}{3}\big(1+\alpha\big)q - \alpha\big(\sigma_1+\sigma_2\big)\Big] \ge 0 \tag{6.57}$$

It follows from Eqs. (6.3) and (6.50) that only for the particular stress state

$$\frac{\sigma_2}{\sigma_1} = \frac{1+\nu+\alpha_s\big(2-\nu\big)}{2-\nu+\alpha_s\big(1+\nu\big)} \tag{6.58}$$

can strain localization occur at the onset of softening; see Fig. 13. For all other cases, continuous inelastic deformations and re-orientation of the principal strain directions have to take place until the condition (6.47) or (6.50) is reached, after which strain localization with stress continuity occurs. ■

7. Application to a generic failure criterion

In this section a generic stress-based failure criterion is considered in the conditions of plane stress and plane strain. Depending on the involved material parameters, the failure surface defines either an ellipse, a parabola, a hyperbola or the product of two straight lines. The classical von Mises, Drucker-Prager and Mohr-Coulomb criteria are recovered as particular examples. In all cases, the discontinuity angles and the associated traction-based failure criteria are derived explicitly.

7.1. Stress-based failure criterion

Without loss of generality, let us consider the following failure criterion $\widehat{F}(\boldsymbol{\sigma}, q) \leq 0$

$$\widehat{F}(\boldsymbol{\sigma}, q) = J_2 - \frac{1}{6}A_0 I_1^2 + \frac{1}{3}B_0 q I_1 - C_0 q^2 \leq 0 \tag{7.1}$$

where the non-negative parameters B_0 and C_0 are related to the parameter $A_0 < 2$ through

$$B_0 = \frac{2 - A_0}{2}(\rho - 1) \geq 0, \qquad C_0 = \frac{2 - A_0}{6}\rho \geq 0 \tag{7.2}$$

with $\rho := f_c/f_t \geq 1$ being the ratio between the uniaxial compressive and tensile strengths f_c and f_t. The residual strength $q(\kappa)$ is normalized so that its initial value is $q^0 = f_t$.

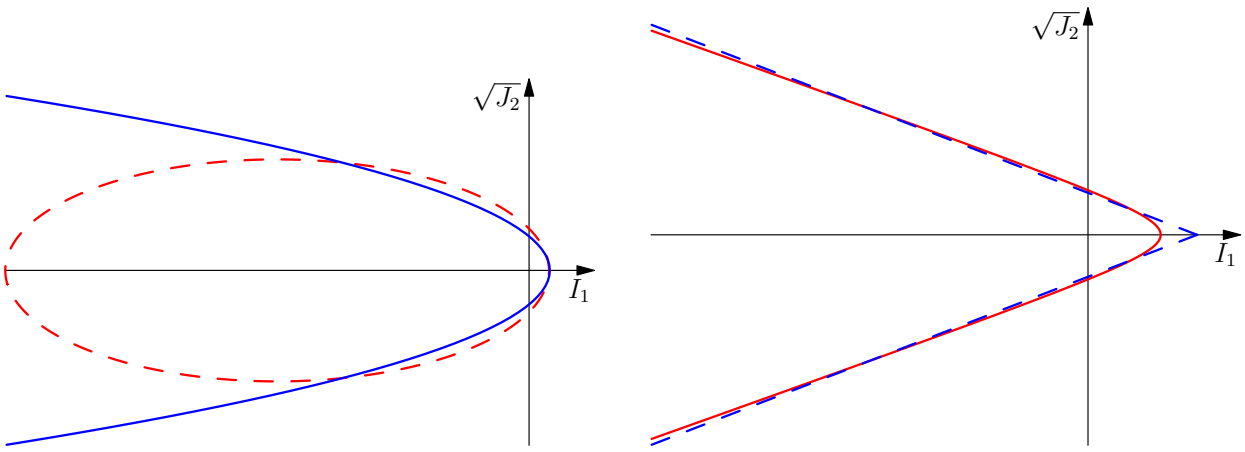

(a) Elliptic and parabolic failure surfaces

(b) Hyperbolic surface and the product of two straight lines

Figure 14: Different functional types of the generic failure criterion in the $I_1 - \sqrt{J_2}$ meridian plane

For the case $A_0 > B_0^2/(6C_0)$, Eq. (7.1) is a hyperbola on the meridian $I_1 - \sqrt{J_2}$ plane with the foci on the axis $\sqrt{J_2}$. This is inappropriate for current purposes. Accordingly, only the case $A_0 \leq B_0^2/(6C_0) < 2$ is discussed. Depending on the values of parameter A_0, the following four cases can be identified as shown in Fig. 14:

- $A_0 < 0$: Eq. (7.1) is an ellipse on the meridian $I_1 - \sqrt{J_2}$ plane. This type of failure criterion was adopted in Comi and Perego [16] to model the behavior of concrete in compression-compression.

- $A_0 = 0$: Eq. (7.1) becomes the so-called parabolic Druker-Prager criterion [26, 37, 65]

$$\widehat{F}(\boldsymbol{\sigma}, q) = J_2 + \frac{1}{3} B_0 q I_1 - C_0 q^2 \tag{7.3}$$

with the material parameters $B_0 = \rho - 1$ and $C_0 = \rho/3$.

- $0 < A_0 < B_0^2/(6C_0)$: Eq. (7.1) defines a hyperbola on the meridian $I_1 - \sqrt{J_2}$ plane with the foci at the axis I_1. In this case, only the left branch (i.e., $I_1 \leq B_0 q/A_0$) is considered. Similar hyperbolic functions were adopted in both plasticity [37, 53] and damage models [16] for concrete.

- $A_0 = B_0^2/(6C_0)$: It follows from the relations (7.2) that

$$A_0 = 2\alpha^2, \qquad B_0 = 2\alpha\big(1+\alpha\big), \qquad C_0 = \frac{1}{3}\big(1+\alpha\big)^2 \tag{7.4}$$

for a material constant $\alpha := (\rho - 1)/(\rho + 1) \in [0, 1)$. In this case, the failure criterion (7.1) simplifies to the product of two straight lines, with the left branch of interested given by

$$\frac{1}{1+\alpha}\Big(\alpha I_1 + \sqrt{3J_2}\Big) - q \leq 0 \tag{7.5}$$

As can be seen, the classical Von Mises (J_2) and Drucker-Prager criteria are recovered for the cases $\alpha = 0$ and $\alpha \in (0, 1)$, respectively.

Remark 7.1 It can be easily verified that the failure criterion $\widehat{F}(\boldsymbol{\sigma}, q) \leq 0$ introduced in Eq. (7.1) is a homogeneous function of degree $M = 2$. The corresponding dissipative flow tensor $\widehat{\boldsymbol{\Lambda}} := \partial \widehat{F}/\partial \boldsymbol{\sigma}$ and its principal values $\widehat{\Lambda}_i := \partial \widehat{F}/\partial \sigma_i$ $(i = 1, 2, 3)$ are expressed as

$$\widehat{\boldsymbol{\Lambda}} = \boldsymbol{s} + \frac{1}{3}\big(B_0 q - A_0 I_1\big)\boldsymbol{I}, \qquad \widehat{\Lambda}_i = s_i + \frac{1}{3}\big(B_0 q - A_0 I_1\big) \tag{7.6}$$

together with the following softening function $\widehat{h} := -\partial \widehat{F}/\partial q$

$$\widehat{h} = -\frac{1}{3} B_0 I_1 + 2C_0 q \tag{7.7}$$

where σ_i and s_i denote the principal values of the stress tensor $\boldsymbol{\sigma}$ and its deviatoric part $\boldsymbol{s}$, respectively. Moreover, it follows from Eq. (7.6) that

$$\widehat{\Lambda}_1 - \widehat{\Lambda}_2 = s_1 - s_2 = \sigma_1 - \sigma_2 \tag{7.8}$$

Accordingly, the tangential traction t_m and dissipative flow component γ_m are evaluated as

$$t_m = \text{sign}(t_m)\sqrt{-\widehat{\Lambda}_1 \widehat{\Lambda}_2}, \qquad \gamma_m = 2\text{sign}(t_m)\big|t_m\big| = 2t_m \tag{7.9}$$

for the discontinuity angle θ^{cr} determined from Eq. (6.2). The above results are rather useful in determination of the projected traction-based failure criterion $f(\boldsymbol{t}, q) \leq 0$. □

7.2. Plane stress

In the plane stress condition ($\sigma_3 = 0$), the failure criterion (7.1) becomes

$$\widehat{F}(\boldsymbol{\sigma}, q) = \frac{2 - A_0}{6}\big(\sigma_1^2 + \sigma_2^2\big) - \frac{1 + A_0}{3}\sigma_1\sigma_2 + \frac{B_0}{3}\big(\sigma_1 + \sigma_2\big)q - C_0 q^2 \le 0 \tag{7.10}$$

in the $\sigma_1 - \sigma_2$ principal stress space. For the model parameter $A_0 < 2$ the failure surface $\widehat{F}(\boldsymbol{\sigma}, q) = 0$ is less open than a right angle [16], which is the case interested here. Furthermore, only for the parameters satisfying $A_0 \le 1/2 + B_0^2/(6C_0)$ can the failure surface $\widehat{F}(\boldsymbol{\sigma}, q) = 0$ intersect the hydrostatic axis $\sigma_1 = \sigma_2$. It then follows from the relations (7.2) that the admissible parameter A_0 is within the range

$$A_0 \le \frac{2(\rho^2 - \rho + 1)}{(\rho + 1)^2} < 2 \tag{7.11}$$

Accordingly, the following function types can be defined for the failure criterion (7.10)

$$\begin{cases} A_0 < \frac{1}{2} & \text{Elliptical function; see Figure 15(a)} \\ A_0 = \frac{1}{2} & \text{Parabolic function; see Figure 16(a)} \\ \frac{1}{2} < A_0 < 2(\rho^2 - \rho + 1)/(\rho + 1)^2 & \text{Hyperbolic function; see Figure 17(a)} \\ A_0 = 2(\rho^2 - \rho + 1)/(\rho + 1)^2 & \text{Product of two straight lines; see Figure 18(a)} \end{cases} \tag{7.12}$$

Remark 7.2 In the plane stress condition the model parameters satisfying $B_0^2 = 3(2A_0 - 1)C_0$ are determined as

$$A_0 = \frac{2(\rho^2 - \rho + 1)}{(\rho + 1)^2}, \qquad B_0 = \frac{3\rho(\rho - 1)}{(\rho + 1)^2}, \qquad C_0 = \frac{\rho^2}{(\rho + 1)^2} \tag{7.13}$$

Accordingly, the failure criterion (7.10) becomes

$$\widehat{F}(\boldsymbol{\sigma}, q) = \frac{\rho\sigma_1 - \sigma_2 - \rho q}{\rho + 1} \cdot \frac{\sigma_1 - \rho\sigma_2 + \rho q}{\rho + 1} \le 0 \tag{7.14}$$

The left branch interested coincides with the classical Mohr-Coulomb criterion (6.16), i.e.,

$$\frac{\rho\sigma_1 - \sigma_2 - \rho q}{\rho + 1} = \frac{1}{2}\Big[\big(\sigma_1 + \sigma_2\big)\sin\varphi + \big(\sigma_1 - \sigma_2\big) - q\big(1 + \sin\varphi\big)\Big] \le 0 \tag{7.15}$$

where the internal friction angle $\varphi \in [0, \pi/2]$ of the material is given by

$$\sin\varphi = \frac{\rho - 1}{\rho + 1} \qquad \Longleftrightarrow \qquad \rho = \frac{1 + \sin\varphi}{1 - \sin\varphi} \tag{7.16}$$

Note that the Mohr-Coulomb criterion (7.15) applies for $\sigma_1 \ge 0$ and $\sigma_2 \le 0$ in the plane stress state ($\sigma_3 = 0$). □

7.3. Discontinuity angle and traction-based failure criterion

For a discontinuity (band) to form, the failure criterion (7.10) is activated. That is, the residual strength $q \in [0, f_t]$ can be expressed in terms of the principal stress σ_1

$$\widehat{F}(\boldsymbol{\sigma}, q) = 0 \qquad \Longrightarrow \qquad q = \alpha_r \sigma_1 \tag{7.17}$$

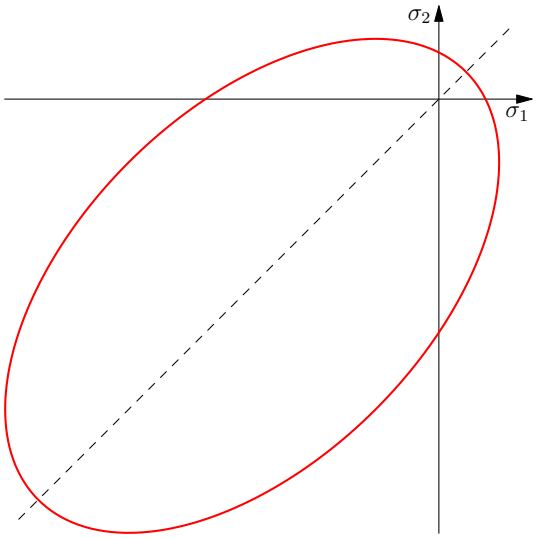

(a) Stress-based failure surface

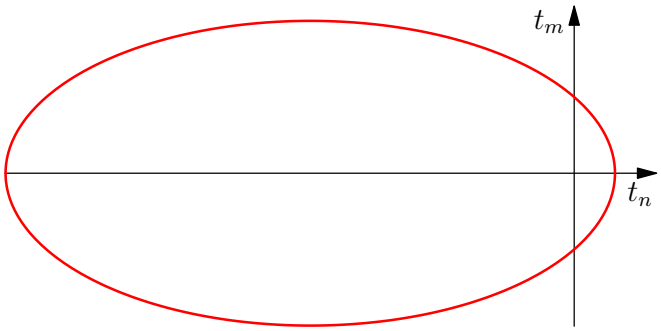

(b) Traction-based failure surface

Figure 15: Elliptic stress- and traction-based failure surfaces in plane stress ($\rho = 5.0, A_0 = 0.0$)

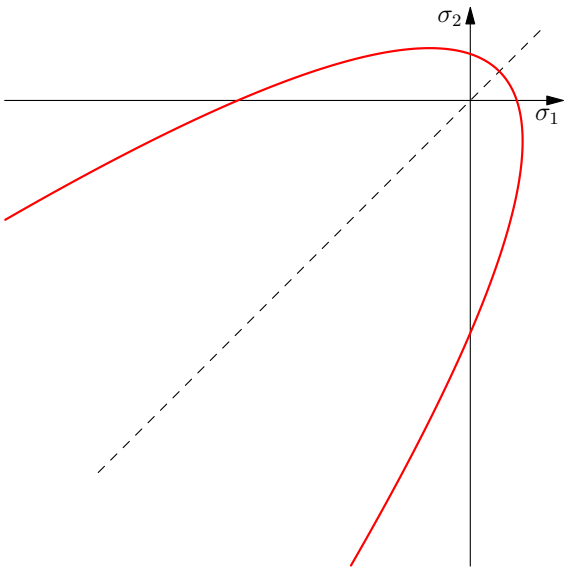

(a) Stress-based failure surface

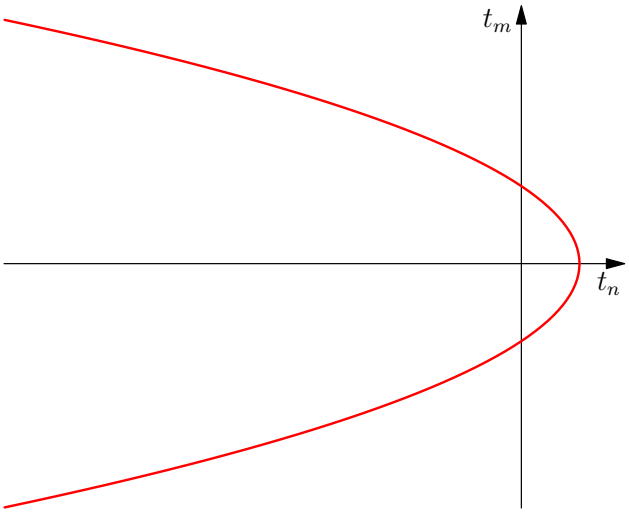

(b) Traction-based failure surface

Figure 16: Parabolic stress- and traction-based failure surfaces in plane stress ($\rho = 5.0, A_0 = 0.5$)

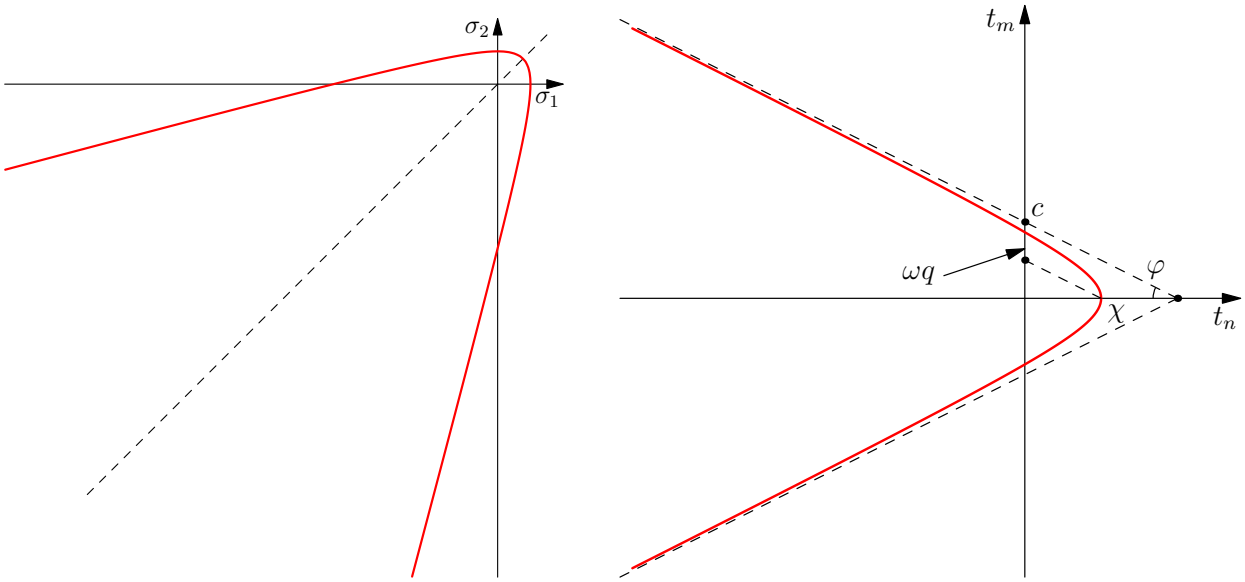

(a) Stress-based failure surface

(b) Traction-based failure surface

Figure 17: Hyperbolic stress- and traction-based failure surfaces in plane stress ($\rho = 5.0$, $A_0 = 1.0$)

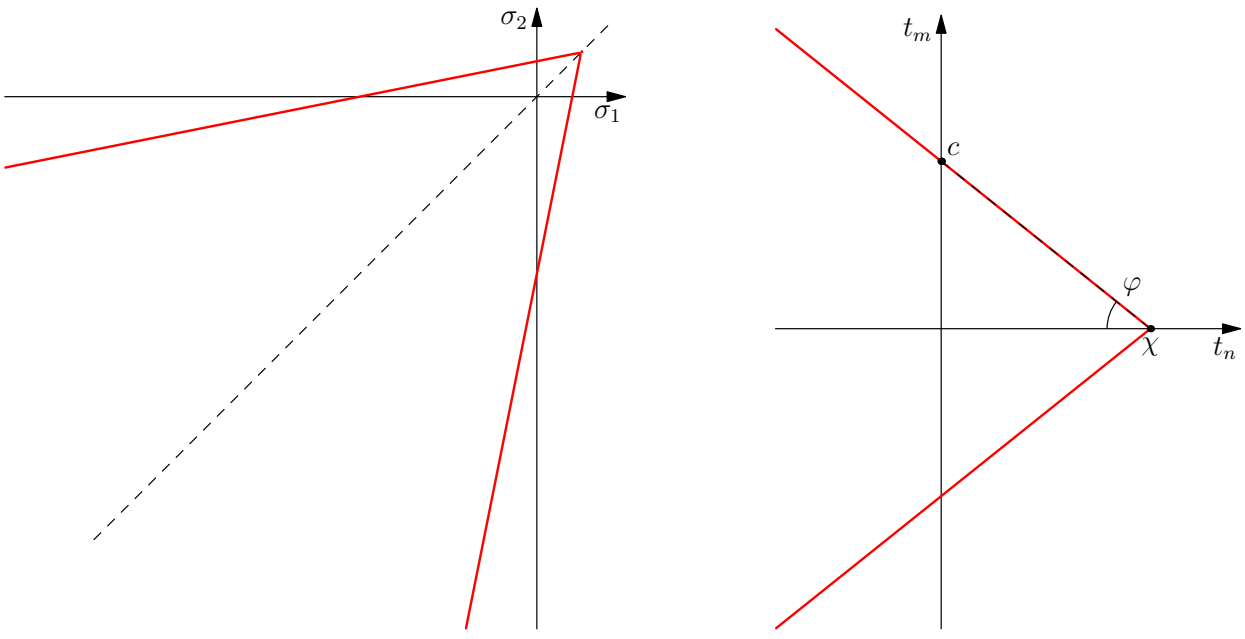

(a) Stress-based failure surface

(b) Traction-based failure surface

Figure 18: Bilinear stress- and traction-based failure surfaces in plane stress ($\rho = 5.0$, $A_0 = 7/6$)

where the coefficient $\alpha_r(r) \in [0,1]$ depends on the stress ratio $r := \sigma_2/\sigma_1$

$$\alpha_r = \frac{B_0(1+r) \pm \text{sign}(\sigma_1)\sqrt{B_0^2(1+r)^2 + 6A_rC_0}}{6C_0} \tag{7.18a}$$

$$A_r = (2-A_0) - 2(1+A_0)r + (2-A_0)r^2 \tag{7.18b}$$

The discontinuity angle θ^{cr} is then given from Eq. (6.2) by

$$\cos(2\theta^{\text{cr}}) = \frac{2B_0q + (1-2A_0)(\sigma_1+\sigma_2)}{3(\sigma_1-\sigma_2)} = \frac{2B_0\alpha_r + (1-2A_0)(1+r)}{3(1-r)} \tag{7.19}$$

Clearly, it depends on the stress ratio $r := \sigma_2/\sigma_1$ which remains fixed for a proportional load path.

For the discontinuity angle (7.19), it follows from Eqs. (A.9), (6.6) and $(7.6)_2$ that

$$\gamma_n = \frac{B_0q - (2A_0-1)t_n}{2-A_0}, \qquad \widehat{h} = -\frac{B_0}{2-A_0}t_n + \left[\frac{B_0^2}{3(2-A_0)} + 2C_0\right]q \tag{7.20}$$

Recalling the results (7.9), the projected traction-based failure criterion $f(\boldsymbol{t},q) \leq 0$, also homogeneous of degree $M = 2$, is determined from Eq. (6.7) as

$$f(\boldsymbol{t},q) = t_m^2 - \frac{1}{2-A_0}\left[\left(A_0 - \frac{1}{2}\right)t_n^2 - B_0qt_n + \frac{1}{6}B_0^2q^2\right] - C_0q^2 \leq 0 \tag{7.21}$$

For the admissible parameter $A_0 \leq 2(\rho^2-\rho+1)/(\rho+1)^2$, the following cases can be identified:

- $A_0 < \frac{1}{2}$: As shown in Figure 15(b), the failure criterion (7.21) defines an ellipse on the $t_n - t_m$ plane

  $$f(\boldsymbol{t},q) = t_m^2 + \frac{\frac{1}{2}-A_0}{2-A_0}\left(t_n + \frac{B_0}{1-2A_0}q\right)^2 - \left[\frac{B_0^2}{3(1-2A_0)} + C_0\right]q^2 \leq 0 \tag{7.22}$$

  with its foci on the axis t_n and centered at $t_n = -B_0q/(1-2A_0)$. An interesting particular case corresponds to $\rho = 1.0$, i.e., $B_0 = 0$ and $C_0 = (2-A_0)/6$. In this case, the failure criterion (7.22) becomes

  $$f(\boldsymbol{t},q) = t_m^2 + \frac{\frac{1}{2}-A_0}{2-A_0}t_n^2 - \frac{2-A_0}{6}q^2 \leq 0 \tag{7.23a}$$

  or, equivalently,

  $$\sqrt{t_n^2 + \beta^{-2}\,t_m^2} - \frac{2-A_0}{\sqrt{3(1-2A_0)}}q \leq 0 \tag{7.23b}$$

  for the parameter $\beta := \sqrt{(\frac{1}{2}-A_0)/(2-A_0)} \in [0,1]$. The failure criterion (7.23b) is exactly the one suggested by Camacho and Ortiz [6], Pandolfi et al. [49], Jirásek and Zimmermann [24] for modeling mixed-mode failure.

- $A_0 = \frac{1}{2}$: As shown in Figure 16(b), the failure criterion (7.21) is a parabola on the $t_n - t_m$ plane

  $$f(\boldsymbol{t},q) = t_m^2 + \beta_1qt_n - \beta_2q^2 \leq 0 \tag{7.24}$$

  where the parameters β_1 and β_2 are expressed as

  $$\beta_1 = \frac{2}{3}B_0 = \frac{1}{2}(\rho-1), \qquad \beta_2 = \frac{1}{9}B_0^2 + C_0 = \frac{1}{16}(\rho+1)^2 \tag{7.25}$$

  The parabolic traction-based failure criterion has been adopted in the embedded discontinuity models [33, 36].

- $\frac{1}{2} < A_0 < 2(\rho^2-\rho+1)/(\rho+1)^2$, or equivalently, $B_0^2 > 3(2A_0-1)C_0$: As shown in Figure 17(b), the failure criterion (7.21) defines a hyperbola on the $t_n - t_m$ plane, with the left branch of interest expressed as

$$\tan\varphi \cdot t_n + \sqrt{t_m^2 + \omega^2 q^2} - c \le 0 \tag{7.26}$$

where $\tan\varphi$ and c denote the friction coefficient and cohesion of the asymptotic Mohr-Coulomb criterion

$$\tan\varphi = \sqrt{\frac{A_0 - 1/2}{2 - A_0}}, \qquad c = \frac{B_0 q}{\sqrt{2(2-A_0)(2A_0-1)}} \tag{7.27a}$$

together with the following parameter ω

$$\omega = \sqrt{\frac{B_0^2}{3(2A_0-1)} - C_0} \tag{7.27b}$$

Similar hyperbolic failure function has been adopted in the literature to describe the normal and shear coupling of cohesive cracks [7, 14, 34, 62, 66]; see Section 7.5 for further discussion.

- $A_0 = 2(\rho^2-\rho+1)/(\rho+1)^2$, or equivalently, $B_0^2 = 3(2A_0-1)C_0$: As shown in Figure 18(b), the failure function (7.21) becomes the product of two straight lines on the $t_n - t_m$ plane, with the left branch of interest corresponding to $\omega = 0$ in the hyperbolic criterion (7.26)

$$\tan\varphi \cdot t_n + |t_m| - c \le 0 \tag{7.28}$$

where the internal friction coefficient $\tan\varphi$ and the cohesion c are given by

$$\tan\varphi = \frac{1}{2}\,\frac{\rho-1}{\sqrt{\rho}}, \qquad c = \frac{1}{2}\sqrt{\rho}\, q \tag{7.29}$$

This is exactly the classical Mohr-Coulomb criterion.

As can be seen, the function types of the projected traction-based failure criterion $f(\boldsymbol{t}, q) \le 0$ coincide with those of the stress-based failure criterion $\widehat{F}(\boldsymbol{\sigma}, q) \le 0$ classified in Eq. (7.12).

Remark 7.3 The traction-based failure criterion (6.40) projected from the classical Drucker-Prager model can be obtained by substituting the model parameters (7.4) into Eq. (7.21). Note that the condition $A_0 = 2(\rho^2-\rho+1)/(\rho+1)^2$, corresponding to $B_0^2 = 3(2A_0-1)C_0$, cannot be reached for Drucker-Prager criterion in the case of plane stress. The above results coincide with those obtained in Section 6.7.1. □

7.4. Plane strain

In the case of plane strain, the constraint $\widehat{\Lambda}_3 = 0$ gives the out-of-plane stress (6.4) upon strain localization, with the coefficients η_1 and η_2 given by

$$\eta_1 = \frac{A_0+1}{2-A_0}, \qquad \eta_2 = -\frac{B_0}{2-A_0} \tag{7.30}$$

The stress-based failure criterion (7.1) can then be rewritten as

$$\widehat{F}(\boldsymbol{\sigma}, q) = \frac{\frac{1}{2} - A_0}{2 - A_0}\left(\sigma_1^2 + \sigma_2^2\right) - \frac{A_0 + 1}{2 - A_0}\sigma_1\sigma_2 + \frac{B_0}{2 - A_0}q\left(\sigma_1 + \sigma_2\right) - \left(\frac{B_0^2/6}{2 - A_0} + C_0\right)q^2 \leq 0 \tag{7.31}$$

Similarly, the following three cases can be identified:

$$\begin{cases} A_0 < 0 & \text{Elliptical function} \\ A_0 = 0 & \text{Parabolic function} \\ 0 < A_0 < 1/2 & \text{Hyperbolic function} \end{cases} \tag{7.32}$$

Note that the range of admissible parameter $A_0 < 1/2$ is much more restrictive than that for general 3D and plane stress.

Upon strain localization, the residual strength q is also determined as the same form as Eq. (7.17), with the following coefficient function $\alpha_r(r) \in [0, 1]$

$$\alpha_r = \frac{B_0\left(1 + r\right) \pm \text{sign}(\sigma_1)\sqrt{2\left(2 - A_0\right)\left[\left(r^2 + r + 1\right)B_0^2/3 + A_r C_0\right]}}{2B_0^2/3 + 2\left(2 - A_0\right)C_0} \tag{7.33a}$$

$$A_r = \left(1 - 2A_0\right) - 2\left(A_0 + 1\right)r + \left(1 - 2A_0\right)r^2 \tag{7.33b}$$

It then follows from Eq. (6.2) that

$$\cos(2\theta^{\text{cr}}) = \frac{2B_0 q - 3A_0\left(\sigma_1 + \sigma_2\right)}{\left(2 - A_0\right)\left(\sigma_1 - \sigma_2\right)} = \frac{2B_0 q - 3A_0\left(1 + r\right)}{\left(2 - A_0\right)\left(1 - r\right)} \tag{7.34}$$

In general the above discontinuity angle θ^{cr} also depends on the stress ratio $r := \sigma_2/\sigma_1$ except for the von Miese and Drucker-Prager criteria; see Remark 7.5.

For the out-of-plane stress (7.30) and the discontinuity angle (7.34), it follows from Eqs. (A.9), (6.6) and $(7.6)_2$ that

$$\gamma_n = \frac{B_0 q - 3A_0 t_n}{1 - 2A_0}, \qquad \widehat{h} = -\frac{B_0}{3\left(1 - 2A_0\right)}\left(3t_n - 2B_0 q\right) + 2C_0 q \tag{7.35}$$

Recalling the results (7.9), the traction-based failure criterion $f(\boldsymbol{t}, q) \leq 0$ is given from Eq. (6.7) as

$$f(\boldsymbol{t}, q) = t_m^2 - \frac{1}{1 - 2A_0}\left(\frac{3}{2}A_0 t_n^2 - B_0 q t_n + \frac{1}{3}B_0^2 q^2\right) - C_0 q^2 \leq 0 \tag{7.36}$$

With respect to the specific value of the parameter $A_0 < \frac{1}{2}$, the following cases can be identified:

- $A < 0$: The failure criterion (7.36) can be rewritten as

$$f(\boldsymbol{t}, q) = t_m^2 + \frac{3A_0}{2\left(2A_0 - 1\right)}\left(t_n + \frac{B_0}{-3A_0}q\right)^2 - \left(\frac{B_0^2}{-6A_0} + C_0\right)q^2 \leq 0 \tag{7.37}$$

  which defines an ellipse on the $t_n - t_m$ plane, centered at $t_n = B_0 q/(3A_0)$.

- $A = 0$: In this case Eq. (7.36) becomes a parabola on the $t_n - t_m$ plane

$$f(\boldsymbol{t}, q) = t_m^2 + \beta_1 q t_n - \beta_2 q^2 \leq 0 \tag{7.38}$$

where the material parameters β_1 and β_2 are expressed in terms of the strength ratio $\rho \geq 1$, i.e.

$$\beta_1 = B_0 = \rho - 1, \qquad \beta_2 = \frac{1}{3} B_0^2 + C_0 = \frac{1}{3}\left(\rho^2 - \rho + 1\right) \tag{7.39}$$

Note that the case $\rho = 1$ corresponds exactly to the classical Von Mises criterion.

- $0 < A < 1/2$: The failure criterion (7.36) defines a hyperbola on the $t_n - t_m$ plane, with the left branch expressed as

$$\tan\varphi \cdot t_n + \sqrt{t_m^2 + \omega^2 q^2} - c \leq 0 \tag{7.40}$$

where the internal friction angle φ and cohesion c as well as an additional parameter ω are given by

$$\tan\varphi = \sqrt{\frac{3A_0}{2(1-2A_0)}}, \qquad c = \frac{B_0}{\sqrt{6A_0(1-2A_0)}} q, \qquad \omega = \sqrt{\frac{B_0^2}{6A_0} - C_0} \tag{7.41}$$

The above hyperbolic failure criterion is of identical form as Eq. (7.26) in the condition of plane stress, with different definitions of involved parameters. In this case substitution of the relations (7.4) yields the results for Drucker-Prager criterion.

Remark 7.4 In the condition of plane strain, Eq. (7.1) together with the elastic out-of-plane principal stress $\sigma_3 = \nu(\sigma_1 + \sigma_2)$ defines the so-called elastic limit surface, with ν being Poisson's ratio. On the $\sigma_1 - \sigma_2$ principal plane, it is: *i*): an ellipse for $A_0 < \frac{1}{2}(1-2\nu)^2/(1+\nu)^2$, *ii*): a parabola for $A_0 = \frac{1}{2}(1-2\nu)^2/(1+\nu)^2$, or *iii*): a hyperbola for $A_0 > \frac{1}{2}(1-2\nu)^2/(1+\nu)^2$, respectively. Therefore, the following cases can be identified for the function types of the elastic limit and failure surfaces:

- $A_0 < 0$: Both surfaces are ellipses.
- $A_0 = 0$: The elastic limit surface is an ellipse while the failure surface is a parabola.
- $0 < A_0 < \frac{1}{2}(1-2\nu)^2/(1+\nu)^2$: The elastic limit surface is an ellipse while the failure surface is a hyperbola.
- $A_0 = \frac{1}{2}(1-2\nu)^2/(1+\nu)^2$: The elastic limit surface is a parabola while the failure surface is a hyperbola.
- $\frac{1}{2}(1-2\nu)^2/(1+\nu)^2 < A_0 < 1/2$: Both surfaces are hyperbolas.

For all the cases, the elastic limit surface will be reached earlier than the initial failure surface (7.31). Accordingly, some continuous inelastic deformations and substantial rotation of the principal strain directions have to occur before the plane strain localization condition (6.4) is fulfilled. □

Remark 7.5 In the condition of plane strain, it follows from the constraint $\widehat{\Lambda}_3 = 0$ and the identity $s_1 + s_2 + s_3 = 0$ that

$$s_1 + s_2 = -s_3 = \frac{B_0 q - A_0 I_1}{3} \tag{7.42}$$

Accordingly, the discontinuity angle (7.34) can be rewritten as

$$\sin^2 \theta^{\mathrm{cr}} = -\frac{s_2 + \big(B_0 q - A_0 I_1\big)/3}{s_1 - s_2} = -\frac{s_1 + 2s_2}{s_1 - s_2} \tag{7.43}$$

Satisfaction of the failure criterion (7.1) yields

$$\big(3 - 2A_0\big)s_1^2 + 2\big(3 - A_0\big)s_1 s_2 + \big(3 - 2A_0\big)s_2^2 - \big(B_0^2 - 6A_0 C_0\big)q^2 = 0 \tag{7.44}$$

Thus, the ratio s_2/s_1 (or, equivalently, the stress ratio $r := \sigma_2/\sigma_1$) and the resulting discontinuity angle θ^{cr}, in general depend on the stress state during the failure process. One exception is the Drucker-Prager criterion considered in Section 6.7.2, which corresponds to the case $B_0^2 = 6A_0 C_0$. □

7.5. Further discussion on the hyperbolic failure criterion

In the literature [7, 14, 34, 62, 66], different forms of hyperbolic traction-based failure criteria have been proposed for the modeling of localized failure in quasi-brittle materials, owing to the excellent data fitting capabilities and other advantageous features (e.g., no slope discontinuity at the tip, asymptotically approaching to Mohr-Coulomb criterion for increasing compression, and a constant friction angle, etc.). However, the involved parameters are essentially mesoscopical entities hard to be determined from standard experimental tests. This shortcoming restrains heavily its application. In previous sections we have established the theoretical connections and equivalence conditions between localized models with traction- and stress-based failure criteria. Such a correspondence facilitates identifying those mesoscopic parameters involved in the traction-based failure criterion from the easily obtained macroscopic ones.

Without loss of generality, the following traction-based failure criterion [7, 66] is considered

$$\widehat{f}(\boldsymbol{t}, q) = t_m^2 - \big(c - t_n \cdot \tan\varphi\big)^2 + \big(c - \chi \cdot \tan\varphi\big)^2 \leq 0 \tag{7.45}$$

with the left branch of interest expressed as [34]

$$\tan\varphi \cdot t_n + \sqrt{t_m^2 + \big(c - \chi \cdot \tan\varphi\big)^2} - c \leq 0 \tag{7.46}$$

where χ denotes the failure strength, not necessarily identical to the macroscopic material tensile strength f_t; $\tan\varphi$ and c represent the friction and cohesion of the asymptotic Mohr-Coulomb criterion. All these parameters cannot be determine easily and in general are assumed arbitrarily [7, 14, 66].

As shown in Section 7.3, for the model parameter $\frac{1}{2} < A_0 < 2(\rho^2 - \rho + 1)/(\rho + 1)^2$, in the condition of plane stress an inelastic softening solid characterized by the stress-based failure criterion (7.1) localizes into a discontinuity (band)

described by the traction-based failure criterion (7.26) of identical form to Eq. (7.46). Obviously, the equivalence between them implies that

$$\omega q = c - \chi \cdot \tan\varphi \qquad \Longleftrightarrow \qquad \chi = \frac{c - \omega q}{\tan\varphi} \tag{7.47}$$

where the friction coefficient $\tan\varphi$, the cohesion c and the parameter ω are given in Eq. (7.27).

Reversely, recalling the tractions (A.9) and making some straightforward manipulations, the stationarity condition (6.9) for the failure criterion (7.45) yields the following discontinuity angle $\widehat{\theta}^{\mathrm{cr}}$

$$\cos(2\widehat{\theta}^{\mathrm{cr}}) = \frac{\tan\varphi}{1+\tan^2\varphi} \cdot \frac{2c - (\sigma_1+\sigma_2)\tan\varphi}{\sigma_1 - \sigma_2} \tag{7.48}$$

In accordance with Eqs. (A.9), the normal and tangential tractions (t_n, t_m) acting on the orientation $\boldsymbol{n}(\widehat{\theta}^{\mathrm{cr}})$ can be expressed in terms of the principal stresses σ_1 and σ_2. Substitution of the obtained results into Eq. (7.45) yields

$$F(\boldsymbol{\sigma}, q) = \frac{(\sigma_1-\sigma_2)^2}{4} - \frac{1}{1+\tan^2\varphi}\left(c - \frac{\sigma_1+\sigma_2}{2}\tan\varphi\right)^2 + \left(c - \chi\cdot\tan\varphi\right)^2 \leq 0 \tag{7.49}$$

With the relations (7.27) and (7.47), the discontinuity angle (7.19) are recovered and the reconstructed stress-based failure criterion (7.49) coincides with the given counterpart (7.10).

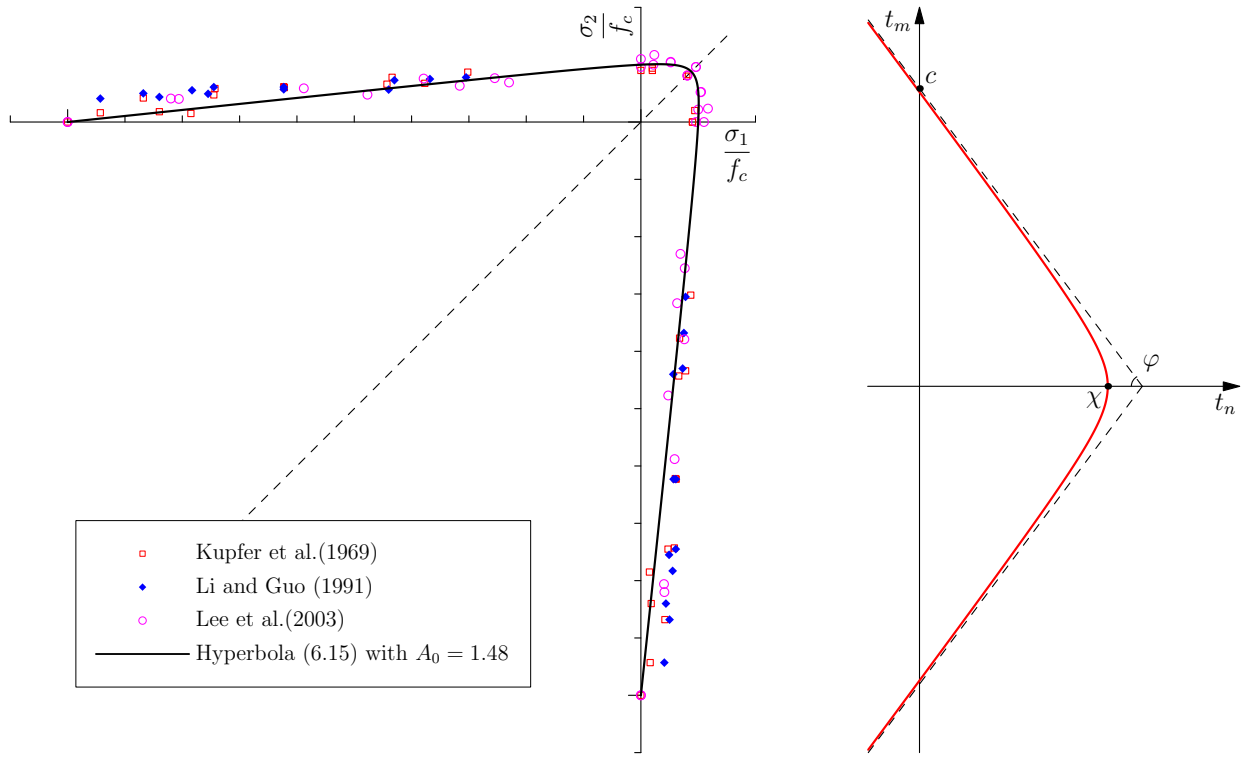

(a) Biaxial strength envelope

(b) Hyperbolic traction-based failure surface

Figure 19: Stress- and traction-based failure surface typical for concrete in plane stress

Therefore, a localized model with the stress-based failure criterion (7.10) is indeed equivalent to that with the given traction-based failure criterion (7.45), providing the involved parameters are consistently connected as in Eqs. (7.27) and (7.47).

As an example, let us consider a strength ratio $\rho := f_c/f_t = 10$, typical for concrete. In order for a discontinuity (band) characterized by the hyperbolic traction-based failure criterion (7.26) to form in the plane stress condition, the model parameter A_0 has to be in the range $A_0 \in (0.5, 1.504)$. As shown in Figure 19(a), the biaxial strength envelope corresponding to the following parameters

$$A_0 = 1.48 \qquad \Longrightarrow \qquad B_0 = 2.34, \qquad C_0 = 0.93 \tag{7.50}$$

fits the test data of normal concrete in tension-tension and tension-compression rather well. It immediately follows from the relations (7.27) and (7.47) that

$$\tan\varphi = 1.37, \qquad c = 1.64q, \qquad \chi = q \tag{7.51}$$

The corresponding traction-based failure criterion is shown in Figure 19(b). Furnished with an appropriate softening law $q(\kappa)$, it can be used in the modeling of localized failure in concrete. This topic will be reported elsewhere.

8. Conclusions

This paper addresses strain localization and failure mechanics for elastoplastic damage solids. Different approaches resulting from two complementary methodologies, i.e., discontinuities localized in an elastic solid and strain localization of an inelastic solid, are systematically investigated for the modeling of localized failure in softening medium.

In the first methodology, discontinuities are localized in elastic solids along a known orientation. It is assumed *a priori* that the bulk material remains elastic during the whole deformation process and all inelastic behavior is localized within the discontinuity (band). That is, strain localization always occurs with a continuous stress field. A traction-based failure criterion can be introduced to characterize the discontinuity (band). However, the discontinuity orientation cannot be determined uniquely unless some additional assumptions, e.g., Mohr's maximization postulate considered in this work, are made. With respect to the strategies dealing with the traction continuity condition between the bulk stresses and tractions across the discontinuity (band), two approaches can be identified. If the traction continuity condition is enforced in weak (average) form, the strong/regularized discontinuity approaches follow. In this approach, the displacement jumps (or equivalently, the inelastic deformations) are retained as independent variables, and constitutive models for both the bulk and discontinuity (band) should be fed. Alternatively, being enforced in strong (point-wise) form, the traction continuity condition coincides with the classical static constraint. This property allows eliminating the kinematic unknowns (i.e., displacement jumps or inelastic deformations) associated with the discontinuity (band) from the governing equations. In the resulting embedded/smeared discontinuity approaches, an overall inelastic constitutive model fulfilling the static constraint suffices.

In order to check whether above strain localization can occur and identify its consequences on the resulting approaches, the second methodology is considered. The kinematic constraint guaranteeing stress boundedness/continuity upon strain localization is established for general inelastic softening solids. It is then applied to a unified elastoplastic damage model with the inelastic evolution laws characterized by a dissipative flow tensor. For the discontinuity kinematics to be reproduced in an appropriate manner, the tensorial components of the dissipative flow tensor in the directions orthogonal to the discontinuity orientation have to vanish upon strain localization. Satisfaction of this kinematic constraint allows introducing a traction-based failure criterion and developing a localized cohesive model for the discontinuity (band), justifying the first methodology. Dependent on the strategies dealing with the discontinuity orientation and failure criterion, two dual (formally identical) but not necessarily equivalent approaches are identified. For a given traction-based failure criterion and a known discontinuity orientation, the resulting elastoplastic damage model is equivalent to the embedded/smeared discontinuity models discussed before. Alternatively, for a given stress-based failure criterion, the discontinuity orientation and associated traction-based counterpart are consistently determined from the kinematic constraint, resulting in the projected discontinuity model.

The *bi-directional* connections between the aforementioned traction- and stress-based approaches are explored in general 3D cases. Particularly, the equivalence between Mohr's maximization postulate for a traction-based failure criterion and the kinematic constraint for a stress-based one is established. This equivalence makes it possible to bridge the gap between traction- and stress-based approaches. In the plane stress condition, the discontinuity orientation and the corresponding stress-/traction-based failure criteria are explicitly given in closed form. The classical Rankine, Mohr-Coulomb, von Mises and Drucker-Prager criteria are analyzed as the illustrative examples. A generic stress-based failure criterion is then considered in a unified manner. Depending on the involved parameters, the projected traction-based failure criterion can be either an ellipse, a parabola, a hyperbola or the product of two straight lines, recovering most of those adopted in the literature as particular cases. In particular, a traction-based failure criterion of hyperbolic type, widely adopted for the modeling of mixed mode localized failure in quasi-brittler materials, is obtained naturally. More importantly, owing to the established equivalence, the involved model parameters can be identified from available standard experimental data, so that the deficiency hindering its application in practice is largely removed.

Only localized models with associated evolution laws are investigated in this work, though the stress boundedness/continuity condition and the resulting kinematic constraint also apply for non-associated cases. However, they are no longer equivalent to Mohr's maximization postulate, but to Roscoe's zero-extension postulate [47, 52]. Extension of the current work to localized models with non-associated evolution laws will be addressed in the future.

Acknowledgments

Support from the National Natural Science Foundation of China (51222811, 51008130) and the Fundamental Research Funds for the Central University (2014XZZX003-13) to the first author (J.Y. Wu) is acknowledged. Sup-

port from the Spanish Ministry of Econimy and Competitivity under the project Enhanced Accuracy Computational Framework for Strain Localization and Failure Mechanisms (EACY) – is acknowledged by the second author (M. Cervera).

Appendix A. Characteristic angles of the discontinuity (band)

To characterize the discontinuity orientation, let us consider the spectral decomposition of the stress tensor $\boldsymbol{\sigma}$ and the coaxial dissipative flow tensor $\boldsymbol{\Lambda} := \partial\mathcal{F}/\partial\boldsymbol{\sigma}$ [23], i.e.,

$$\boldsymbol{\sigma} = \sum_{i=1}^{3} \sigma_i \boldsymbol{v}_i \otimes \boldsymbol{v}_i, \qquad \boldsymbol{\Lambda} = \sum_{i=1}^{3} \Lambda_i \boldsymbol{v}_i \otimes \boldsymbol{v}_i \tag{A.1}$$

where σ_i and $\Lambda_i = \partial\mathcal{F}/\partial\sigma_i$ denote the i-th principal values, with $\boldsymbol{v}_i$ being the corresponding principal vector and satisfying the orthogonal property $\boldsymbol{v}_i \cdot \boldsymbol{v}_j = \delta_{ij}$ for $i, j = 1, 2, 3$.

For general 3D cases, a local orthogonal base $(\boldsymbol{n}, \boldsymbol{m}, \boldsymbol{p})$ is introduced, with vectors $\boldsymbol{m}$ and $\boldsymbol{p}$ perpendicular to the normal vector $\boldsymbol{n}$ and tangent to the discontinuity $\mathcal{S}$. In the coordinate system of the principal stresses, the base vectors $(\boldsymbol{n}, \boldsymbol{m}, \boldsymbol{p})$ can be expressed in terms of a set of characteristic angles $\boldsymbol{\theta} := \{\theta_1, \theta_2, \vartheta_1, \vartheta_2\}^{\mathrm{T}}$

$$\boldsymbol{n}(\boldsymbol{\theta}) = \Big\{ \sin\vartheta_1 \cos\theta_1,\ \sin\vartheta_1 \sin\theta_1,\ \cos\vartheta_1 \Big\}^{\mathrm{T}} \tag{A.2a}$$

$$\boldsymbol{m}(\boldsymbol{\theta}) = \Big\{ \sin\vartheta_2 \cos\theta_2,\ \sin\vartheta_2 \sin\theta_2,\ \cos\vartheta_2 \Big\}^{\mathrm{T}} \tag{A.2b}$$

$$\boldsymbol{p}(\boldsymbol{\theta}) = \boldsymbol{n}(\boldsymbol{\theta}) \times \boldsymbol{m}(\boldsymbol{\theta}) \tag{A.2c}$$

constrained by

$$C(\boldsymbol{\theta}) := \boldsymbol{n}(\boldsymbol{\theta}) \cdot \boldsymbol{m}(\boldsymbol{\theta}) = \sin\vartheta_1 \sin\vartheta_2 \cos\big(\theta_1 - \theta_2\big) + \cos\vartheta_1 \cos\vartheta_2 = 0 \tag{A.2d}$$

where (θ_1, θ_2) and $(\vartheta_1, \vartheta_2)$ denote the spherical azimuth and polar angles, respectively; the operator "$\times$" denotes the Gibbs' vector product (the right hand rule is followed). Note that only three of the characteristic angles $(\theta_1, \theta_2, \vartheta_1, \vartheta_2)$ are independent variables, and the constraint (A.2d) can be readily handled by the Lagrangian multiplier method.

The tractions $\boldsymbol{t}$ acting on the surface with normal vector $\boldsymbol{n}(\boldsymbol{\theta})$ are given by

$$\boldsymbol{t} := \boldsymbol{\sigma} \cdot \boldsymbol{n} = t_n \boldsymbol{n} + t_m \boldsymbol{m} + t_p \boldsymbol{p} \tag{A.3}$$

where the traction components (t_n, t_m, t_p) are expressed as

$$t_n = \sigma_{nn} = \big(\boldsymbol{n} \otimes \boldsymbol{n}\big) : \boldsymbol{\sigma}, \qquad t_m = \sigma_{nm} = \big(\boldsymbol{n} \otimes \boldsymbol{m}\big)^{\mathrm{sym}} : \boldsymbol{\sigma}, \qquad t_p = \sigma_{np} = \big(\boldsymbol{n} \otimes \boldsymbol{p}\big)^{\mathrm{sym}} : \boldsymbol{\sigma} \tag{A.4}$$

Being coaxial to the stress $\boldsymbol{\sigma}$, the dissipative flow tensor $\boldsymbol{\Lambda}$ can also be expanded in the local orthogonal system $(\boldsymbol{n}, \boldsymbol{m}, \boldsymbol{p})$ as

$$\begin{aligned} \boldsymbol{\Lambda} = {} & \Lambda_{nn} \boldsymbol{n} \otimes \boldsymbol{n} + 2\Lambda_{nm} \big(\boldsymbol{n} \otimes \boldsymbol{m}\big)^{\mathrm{sym}} + 2\Lambda_{np} \big(\boldsymbol{n} \otimes \boldsymbol{p}\big)^{\mathrm{sym}} \\ & + \Lambda_{mm} \boldsymbol{m} \otimes \boldsymbol{m} + \Lambda_{pp} \boldsymbol{p} \otimes \boldsymbol{p} + 2\Lambda_{mp} \big(\boldsymbol{m} \otimes \boldsymbol{p}\big)^{\mathrm{sym}} \end{aligned} \tag{A.5}$$

with the following tensorial components

$$\Lambda_{nn} = \big(\boldsymbol{n}\otimes\boldsymbol{n}\big) : \boldsymbol{\Lambda}, \qquad \Lambda_{nm} = \big(\boldsymbol{n}\otimes\boldsymbol{m}\big)^{\text{sym}} : \boldsymbol{\Lambda}, \qquad \Lambda_{np} = \big(\boldsymbol{n}\otimes\boldsymbol{p}\big)^{\text{sym}} : \boldsymbol{\Lambda} \tag{A.6a}$$

$$\Lambda_{mm} = \big(\boldsymbol{m}\otimes\boldsymbol{m}\big) : \boldsymbol{\Lambda}, \qquad \Lambda_{pp} = \big(\boldsymbol{p}\otimes\boldsymbol{p}\big) : \boldsymbol{\Lambda}, \qquad \Lambda_{mp} = \big(\boldsymbol{m}\otimes\boldsymbol{p}\big)^{\text{sym}} : \boldsymbol{\Lambda} \tag{A.6b}$$

With the spectral decomposition (A.1) and the base vectors (A.2), the above traction vectorial and dissipative flow tensorial components can be expressed in terms of their principal values and the characteristic angles $\boldsymbol{\theta}$.

For the simpler 2D case shown in Fig. 8, the characteristic angles $\boldsymbol{\theta} := \big\{\theta_1, \theta_2, \vartheta_1, \vartheta_2\big\}^{\text{T}}$ of the discontinuity (band) are given by

$$\theta_1 = \theta, \qquad \theta_2 = \theta - \pi/2, \qquad \vartheta_1 = \vartheta_2 = \pi/2 \tag{A.7}$$

where $\theta \in [-\pi/2, \pi/2]$ denotes the inclination angle (anti-clockwise) between the normal vector $\boldsymbol{n}$ and the principal vector $\boldsymbol{v}_1$ of the stress tensor. It then follows that

$$\boldsymbol{n}(\theta) = \big\{\cos\theta, \sin\theta, 0\big\}^{\text{T}}, \qquad \boldsymbol{m}(\theta) = \big\{\sin\theta, -\cos\theta, 0\big\}^{\text{T}} \tag{A.8}$$

together with the other tangential vector $\boldsymbol{p} = \big\{0, 0, -1\big\}^{\text{T}}$ perpendicular to the plane of interest.

Accordingly, the tractions (t_n, t_m, t_p) acting on the surface with orientation $\boldsymbol{n}(\theta)$ are expressed as

$$t_n = \sigma_{nn} = \sigma_1 \cos^2\theta + \sigma_2 \sin^2\theta = \frac{\sigma_1 + \sigma_2}{2} + \frac{\sigma_1 - \sigma_2}{2}\cos(2\theta) \tag{A.9a}$$

$$t_m = \sigma_{nm} = \big(\sigma_1 - \sigma_2\big)\sin\theta\cos\theta = \frac{\sigma_1 - \sigma_2}{2}\sin(2\theta) \tag{A.9b}$$

and $t_p = \sigma_{np} = 0$. Similarly, Eqs. (A.6) give the following in-plane components Λ_{nn}, Λ_{mm} and $\Lambda_{nm} = \Lambda_{mn}$

$$\Lambda_{nn} = \Lambda_1 - \big(\Lambda_1 - \Lambda_2\big)\sin^2\theta = \frac{\Lambda_1 + \Lambda_2}{2} + \frac{\Lambda_1 - \Lambda_2}{2}\cos(2\theta) \tag{A.10a}$$

$$\Lambda_{mm} = \big(\Lambda_1 - \Lambda_2\big)\sin^2\theta + \Lambda_2 = \frac{\Lambda_1 + \Lambda_2}{2} - \frac{\Lambda_1 - \Lambda_2}{2}\cos(2\theta) \tag{A.10b}$$

$$\Lambda_{nm} = \big(\Lambda_1 - \Lambda_2\big)\cos\theta\sin\theta = \frac{\Lambda_1 - \Lambda_2}{2}\sin(2\theta) \tag{A.10c}$$

together with the remaining out-of-plane components

$$\Lambda_{pp} = \Lambda_3, \qquad \Lambda_{np} = 0, \qquad \Lambda_{mp} = 0 \tag{A.10d}$$

for the in-plane principal values $\Lambda_1 := \partial\mathcal{F}/\partial\sigma_1$ and $\Lambda_2 := \partial\mathcal{F}/\partial\sigma_2$ as well as the out-of-plane one $\Lambda_3 := \partial\mathcal{F}/\partial\sigma_3$. It is assumed that the relation $\Lambda_1 \geq \Lambda_2$ is satisfied so that the identity $\text{sign}(\Lambda_{nm}) = \text{sign}(\sigma_{nm})$ holds. Note that in the plane stress condition all the out-of-plane components of tensors $\boldsymbol{\sigma}$ and $\boldsymbol{\Lambda}$ vanish, i.e., $\sigma_{pp} = \sigma_{np} = \sigma_{mp} = 0$ and $\Lambda_{pp} = \Lambda_{np} = \Lambda_{mp} = 0$.

Appendix B. Derivation of the traction-based failure criterion for the Drucker-Prager criterion

In the case of plane stress, for the discontinuity angle (6.39) it follows from Eqs. (A.9) that

$$t_n = \frac{2}{3}\Big[\alpha\big(1+\alpha\big)q + \big(1-\alpha^2\big)\big(\sigma_1+\sigma_2\big)\Big] \tag{B.1a}$$

$$t_m^2 = -\Big(\sqrt{2/3}\,\alpha\|\boldsymbol{s}\| + s_1\Big)\Big(\sqrt{2/3}\,\alpha\|\boldsymbol{s}\| + s_2\Big) \tag{B.1b}$$

Accordingly, the normal and tangential components (γ_n, γ_m) in Eq. (6.6) become

$$\gamma_n = \frac{1}{\big(1+\alpha\big)\sqrt{2/3}\,\|\boldsymbol{s}\|}\,\frac{\big(1-4\alpha^2\big)t_n + 2\alpha\big(1+\alpha\big)q}{2\big(1-\alpha^2\big)} \tag{B.2a}$$

$$\gamma_m = \frac{1}{\big(1+\alpha\big)\sqrt{2/3}\,\|\boldsymbol{s}\|}\,2t_m \tag{B.2b}$$

where the norm $\|\boldsymbol{s}\|$ is evaluated from Eq. (6.37) as

$$\sqrt{\frac{2}{3}}\,\|\boldsymbol{s}\| = \frac{1}{1-\alpha^2}\Big[\frac{2}{3}\big(1+\alpha\big)q - \alpha t_n\Big] \geq 0 \tag{B.3}$$

Therefore, the definition (6.7) gives the following traction-based failure function

$$\frac{2}{\big(1+\alpha\big)\sqrt{2/3}\,\|\boldsymbol{s}\|}\Big[t_m^2 - \frac{4\alpha^2-1}{4\big(1-\alpha^2\big)}t_n^2 + \frac{\alpha}{1-\alpha}q\,t_n - \frac{1+\alpha}{3\big(1-\alpha\big)}q^2\Big] \leq 0 \tag{B.4}$$

which can be transformed into the homogeneous failure function (6.40) of degree $M = 2$.

In the case of plane strain, the discontinuity angle (6.49) leads to the following normal traction t_n

$$t_n = \sigma_1 + \sigma_2 - \sigma_3 = \frac{\big(1-4\alpha^2\big)\big(\sigma_1+\sigma_2\big) + 2\alpha\big(1+\alpha\big)q}{2\big(1-\alpha^2\big)} \tag{B.5}$$

which yields the following relations

$$\sigma_1 + \sigma_2 = \frac{2\big(1-\alpha^2\big)t_n - 2\alpha\big(1+\alpha\big)q}{1-4\alpha^2} \tag{B.6a}$$

$$\sigma_3 = \frac{\big(1+2\alpha^2\big)t_n - 2\alpha\big(1+\alpha\big)q}{1-4\alpha^2} \tag{B.6b}$$

Similarly, the square of the tangential traction t_m^2 is given by

$$t_m^2 = -\big(2s_1 + s_2\big)\big(s_1 + 2s_2\big) \tag{B.7}$$

Accordingly, the normal and tangential components (γ_n, γ_m) are evaluated from Eq. (6.6) as

$$\gamma_n = \frac{3\alpha}{1+\alpha}, \qquad \gamma_m = \frac{2\alpha}{1+\alpha}\cdot\frac{t_m}{s_1+s_2} \tag{B.8}$$

where the following relation applies

$$s_1 + s_2 = \frac{\sigma_1+\sigma_2-2\sigma_3}{3} = \frac{2\alpha}{3\big(1-4\alpha^2\big)}\Big[-3\alpha t_n + \big(1+\alpha\big)q\Big] \geq 0 \tag{B.9}$$

Note that, owing to the relation (6.48) the inequality $\big(1+\alpha\big)q - 3\alpha t_n > 0$ holds. Therefore, Eq. (6.7) gives the following traction-based failure criterion

$$f(\boldsymbol{t},q) = \frac{1}{1+\alpha}\left[\frac{3\big(1-4\alpha^2\big)}{\big(1+\alpha\big)q - 3\alpha t_n} t_m^2 - 3\alpha t_n + \big(1+\alpha\big)q\right] \leq 0 \tag{B.10}$$

which can be transformed into the form (6.52).

References

[1] Armero, F., 1999. Large-scale modeling of localized dissipative mechanisms in a local continuum: applications to the numerical simulation of strain localization in rate-dependent inelastic solids. *Mech. Cohes.-Frict. Mater.*, 4: 101-131.

[2] Armero, F. and Oller, S., 2000. A general framework for continuum damage models. I: Infinitesimal plastic damage models in stress space. *Int. J. Solids Structures*, 37: 7409-7464.

[3] Barenblatt, G.I., 1959. The formation of equilibrium cracks during brittle fracture. General ideas and hypotheses. Axially-symmetric cracks. *J. Applied Mathematics and Mechanics*, 23: 622-636.

[4] Barenblatt, G., 1962. The mathematical theory of equilibrium cracks in brittle fracture. *Adv. Appl. Mech.*, 7: 55-129.

[5] Bažant, Z.P. and Oh, B.H., 1983. Crack band theory for fracture of concrete. *Mater. Struct.* (RILEM, Paris), 16: 155–177.

[6] Camacho G.T. and Ortiz M., 1996. Computational modeling of impact damage in brittle materials. *Int. J. Solids Structures*, 33: 2899-2938.

[7] Carol, I., Prat, P., and López, C., 1997. Normal/shear cracking model: Application to discrete crack analysis. *J. Eng. Mech., ASCE*, 123(8): 765-773.

[8] Carol, I., Rizzi, E., Willam, K., 1994. A unified theory of elastic degradation and damage based on a loading surface. *Int. J. Solids Structures*, 31(20): 2835-2865.

[9] Cervera, M., 2008a. A smeared-embedded mesh-corrected damage model for tensile cracking. *Int. J. Numer. Meth. Engng.*, 76: 1930-1954.

[10] Cervera, M., 2008b. An othortropic mesh corrected model. *Comput. Methods Appl. Mech. Engrg.*, 197: 1603-1619.

[11] Cervera, M., Chiumenti, M. and Di Capua, D., 2012. Benchmarking on bifurcation and localization in J_2 plasticity for plane stress and plane strain conditions. *Comput. Methods Appl. Mech. Engrg.*, 241-244: 206-224.

[12] Cervera, M. and Chiumenti, 2006a. Smeared crack approach: back to the original track. *Int. J. Numer. Anal. Meth. Geomech.*, 30: 1173-1199.

[13] Cervera, M. and Chiumenti, 2006b. Mesh objective tensile cracking via a local continuum damage model and a crack tracking technique. *Comput. Methods Appl. Mech. Engrg.*, 196: 304-320.

[14] Cervenka, J., 1994. *Discrete Crack Modelling in Concrete Structures*. Ph.D. Thesis, University of Colorado, Boulder.

[15] Chen, W.F., 1994. *Constitutive Equations for Engineering Materials: Plasticity and Modeling*, vol. 2. Elsevier, Amsterdam.

[16] Comi, C. and Perego, U., 2001. Fracture energy based bi-dissipative damage model for concrete. *Int. J. Solids Structures*, 38: 6427-6454.

[17] Dugdale, D., 1960. Yielding of steel sheets containing slits. *J. Mech. Phys. Solids*, 8: 100-108.

[18] Golub, G.H. and van Loan, C.F., 1996. *Matrix computations*, third edition (page 50). The John Hopkins University Press, Baltimore.

[19] Govindjee, S.D, Kay, G.J. and Simò, J.C., 1995. Anisotropic modeling and numerical simulation of brittle damage in concrete.. *Int. J. Numer. Meth. Engng*, 38: 3611-3633.

[20] Hill, R., 1958. General theory of uniqueness and stability of elasto-plastic solids. *J. Mech. Phys. Solids*, 6: 236–249.

[21] Hill, R., 1962. Acceleration waves in solids. *J. Mech. Phys. Solids*, 10: 1–16.

[22] Hillerborg, A., Modeer, M. and Petersson, P.E., 1976. Analysis of crack formation and crack growth in concrete by means of fracture mechanics and finite elements. *Cement Concrete Res.*, 6: 773-782.

[23] Itskov, M., 2007. *Tensor algebra and tensor analysis for engineers: With applications to continuum mechanics*. Springer, Berlin.

[24] Jirásek, M. and Zimmermann, T., 2001. Embedded crack model. I: Basic formulation. *Internat. J. Numer. Methods Engrg.*, 50(6): 1269-1290.

[25] Krajcinovic, D., 2003. Damage Mechanics. Elsevier B.V., Netherlands.

[26] Kuhl, E., Ramm, E. and Willam, K., 2000. Failure analysis of elasto-plastic material models on different levels of observation. *Int. J. Numer. Meth. Engng*, 46: 1673-1698.

[27] Kupfer, H., Hilsdorf, H.K. and Rüsch, H., 1969. Behavior of concrete under biaxial stresses. *ACI J.*, 66(8): 656-666.

[28] Lee, S.K., Song, Y.C. and Han, S.H., 2003. Biaxial behavior of plain concrete of nuclear containment building. *Nucl. Eng. Des.* 227, 143153.

[29] Li, W.Z., Guo, Z.H., 1991. Experimental research for strength and deformation of concrete under biaxial tension-compression loading (in Chinese). *Journal of Hydraulic Engineering*, 8: 51-56.

[30] Malvern, L.E., 1969. Introduction to the mechanics of a continuous medium. Prentice-Hall International, New Jersey.

[31] Meschke, G, Lackner, R. and Mang, H.A., 1998. An anisotropic elastoplastic damage model for plain concrete. *Int. J. Numer. Meth. Engng.*, 42: 703-727.

[32] Mohr, O., 1900. Welche Umstände bedingen die Elastizitätsgrenze und den Bruch eines Materials? *Civilingenieur: Zeitschrift des Vereins deutscher Ingenieure*, VDI 44/45: 1524-1530; 1572-1577.

[33] Mosler, J., 2005. On advanced solution strategies to overcome locking effects in strong discontinuity approaches. *Int. J. Numer. Meth. Engng.*, 63: 1313-1341.

[34] Most, T. and Bucher, C., 2007. Energy-based simulation of concrete cracking using an improved mixed-mode cohesive crack model within a meshless discretization. *Int. J. Numer. Anal. Meth. Geomech.*, 31: 285-305

[35] Ngo, D., Scordelis, A.C., 1967. Finite element analysis of reinforced concrete beams, *ACI J.*, 64(14): 152-163.

[36] Ohlsson, U. and Olofsson, T., 1997. Mixed-mode fracture and anchor bolts in concrete analysis with inner softening bands. *J. Eng. Mech., ASCE*, 123: 1027-1033.

[37] Ohtani, Y. and Chen, W.F., 1988. Multple hardening plasticity for concrete material. *J. Eng. Mech., ASCE*, 114: 1890–1910.

[38] Oliver, J., 1989. A consistent characteristic length for smeared cracking models. *Int. J. Numer. Meth. Engng*, 28: 461-474.

[39] Oliver, J., 1996. Modeling strong discontinuities in solid mechanics via strain softening contitutive equations. Part I: Fundaments & Part II: Numerical simulation. *Int. J. Numer. Meth. Engng*, 39: 3575-3623.

[40] Oliver, J., Cervera, M. and Manzoli, O. 1998. On the use of strain-softening models for the simulation of strong discontinuities in solids. *Material instabilities in solids*: 107-123, Wiley.

[41] Oliver, J. Cervera, M. and Manzoli, O., 1999. Strong discontinuities and continuum plasticity models: the strong discontinuity approach. *Int. J. Plast.*, 15: 319-351.

[42] Oliver, J., 2000. On the discrete constitutive models induced by strong discontinuity kinematics and continuum constitutive equations. *Int. J. Solids Structures*, 37: 7207-7229.

[43] Oliver, J., Huespe, A.E., Pulido, M.D.G., Chaves, E., 2002. From continuum mechanics to fracture mechanics: the strong discontinuity approach. *Eng. Fract. Mech.*, 69: 113-136.

[44] Oliver, J., Huespe, A.E., Pulido, M.D.G., Blanco, S. and Linero, D., 2006. On the fracture models determined by the continuum-strong discontinuity approach. *Int. J. Fract.*, 137: 211-229.

[45] Oliver, J., Huespe, A.E. and Dias, I.F., 2012. Strain localization, strong discontinuities and material fracture: Matches and mismatches. *Comput. Methods Appl. Mech. Engrg.*, 241-244: 323-336.

[46] Ortiz., M., 1985. A constitutive theory for the inelastic behavior of concrete. *Mech. Mater.*, 4: 76-93.

[47] Ottosen, N. and Runesson, K., 1991. Discontinuous bifurcations in a non-associated Mohr material. *Mech. Mater.*, 12: 255-265.

[48] Pietruszczak, S., and Mroź, Z., 1981. Finite-element analysis of deformation of strain-softening materials. *Int. J. Numer. Methods Eng.*, 17: 327-334.

[49] Pandolfi, A., Krysl, P. and Ortiz, M., 1999. Finite element simulation of ring expansion and fragmentation: the capturing of length and time scales through cohesive models of fracture. *Int. J. Fracture*, 95: 279-297.

[50] Rashid, Y., 1968. Analysis of prestressed concrete pressure vessels. *Nucl. Eng. Des.*, 7: 334-344.

[51] Rice, J.R. and Rudnicki, J.W., 1980. A note on some features of the theory of localization of deformation. *Int. J. Solids Structures*, 16: 597-605.

[52] Roscoe, K.H., 1970. The influence of strains in soil mechanics, 10th Rankine Lecture. *Géotechnique*, 20: 129-180.

[53] Rosenthal, I. and Glucklich, J., 1970. Strength of plain concrete under biaxial stress. ACI Journal, 67: 903–914.

[54] Rots, J.G., et al., 1985. Smeared crack approach and fracture localization in concrete. *Heron*, 30: 1-47.

[55] Rots, J.G., 1988. Computational modeling of concrete fracture. *Doctoral Dissertation*, Delft University of Technology, Delft, The Netherlands.

[56] Rots, J.G., Blaauwendraad, J., 1989. Crack models for concrete: discrete or smeared? fixed, multi-directional or rotating? *Heron*, 34(1): 1-59.

[57] Rudnicki, J.W. and Rice, J.R., 1975. Conditions of the localization of deformation in pressure-sensitive dilatant material. *J. Mech. Phys. Solids*, 23: 371–394.

[58] Runesson, K., Ottosen, N.S. and Peric, D., 1991. Discontinuous bifurcations of elastic-plastic solutions at plane stress and plane strain. *Int. J. Plast.*, 7: 99-121.

[59] Simó, J.C. and Ju, J.W., 1987. Strain- and stress-based continuum damage models. I: Formulation; II: Computational aspects. *Int. J. Solids Structure*, 23(7): 821-869.

[60] Simó, J.C. and Oliver, J., 1994. A new approach to the analysis and simulation of strain softening in solids. In: Z.P. Bažant et al. (eds.), *Fracture and Damage in Quasibrittle Structures*, E & FN Spon: 25-39.

[61] Simó, J.C., Oliver, J. and Armero, F., 1993. An analysis of strong discontinuities induced by strain-softening in rate-independent inelastic solids. *Comput. Mech.* , 12: 277-296.

[62] Stankowski, T., Runesson, K., Sture, S., 1993. Fracture and slip of interfaces in cementitious composites. I: Characteristics, II: Implementation. *J. Engrg. Mech., ASCE*, 90: 845-867.

[63] Steinmann, P., Willam, K., 1991. Localization within the framework of micropolar elastoplasticity. *Advances in Continuum Mechanics*, VI: 296-313.

[64] Thomas, T.Y., 1961. *Plastic Flow and Fracture of Solids*. Academic Press, New York.

[65] Vrech, S.M. and Etse, G., 2006. Geometrical localization analysis of gradient-dependent parabolic Drucker-Prager elasto-plasticity. *International Journal of Plasticity*, 22: 943-964.

[66] Weihe, S., Kröplin, B. and de Borst R., 1997. Classification of smeared crack models based on material and structural properties. *Int. J. Solids Structures*, 35(5): 467-484.

[67] Wu, J. Y., 2011. Unified analysis of enriched finite elements for modeling cohesive cracks. *Comput. Methods Appl. Mech. Engrg.*, 200(45-46): 3031-3050.

[68] Wu, J. Y., Cervera, M., 2013. Strain localization in elastoplastic damage solids. In: *Proceeding of International Symposium on Innovation & Sustainability of Structures in Civil Engineering (ISISS-2013)*, Harbin, China.

[69] Wu, J. Y., Cervera, M., 2014. On the stress continuity condition for strain localization in softening solids. In: *Proceeding of 11th World Congress On Computational Mechanics (WCCM-2014)*, Barcelona, Spain.

[70] Wu, J.Y. and Xu, S.L., 2011. An augmented multicrack elastoplastic damage model for tensile cracking. *Int. J. Solids Structures*, 48: 2511-2528.

[71] Wu, J.Y. and Xu, S.L., 2013. Reconsideration on the elastic damage/degradation theory for the modeling of microcrack closure-reopening (MCR) effects. *Int. J. Solids Structures*, 50(5): 795-805.